Master Thesis

Porous Si_3N_4-based Support Materials with tailored Gas Permeability

Technische Universität WIEN
Institute of Chemical Technologies and Analytics
Getreidemarkt 9/164-CT
A - 1060 Wien

under supervision of Univ.Ass Dr. Thomas Konegger
and Ao.Univ.Prof. Dipl.-Ing. Dr.techn. Roland Haubner

Thomas Prochaska
Gersthoferstraße 150/3/4
1180 Vienna

Vienna, 29.11.2017 Signature

ACKNOWLEDGEMENTS

I would first like to thank my thesis supervisors Dr. Thomas Konegger and Dr. Roland Haubner. Whenever I ran into trouble they had a possible solution I hadn't tried yet at hand. Not only did I learn a lot from them, it also was a pleasure to work for and with them.

I would also like to thank the HLK working group. Especially the PhD student Christina Drechsel who always listened to my problems and gave valuable input that helped me view them from another angle.

Furthermore, I would like to acknowledge all the students and post docs on the second floor for all the fun lunch and coffee breaks, as well as the support and advice. If something went south everyone tried to help and had an ear whenever it was needed. The work environment I found myself in on the Institute, was a very pleasant and inspiring one.

I am also grateful for the financial support received through the Austrian Science Fund FWF. (Project number P29058)

Last but definitely not least, I must express my endless gratitude to my parents and to my partner Julia for providing me with unweary support and omnipresent encouragement through the process of writing this thesis and the study as a whole.

I couldn't have done it without them.
Thank you.

ABSTRACT

The objective of this work was an investigation of the influence of various processing parameters on the permeability behaviour of porous silicon nitride tubes generated via slip casting. These tubes have a potential application as support for high temperature membranes, for example for steam reforming of hydrocarbons or coal/biomass gasifications.

Three silicon nitride sources with different particle sizes and α – Si_3N_4 to β – Si_3N_4 ratio were used. Furthermore, different sintering temperatures ranging from 1500 °C to 1750 °C were investigated. The variation of the sintering aids, Al_2O_3 and Y_2O_3, ranged from 0.2 % to 2.5 % with respect to the mass of silicon nitride. Finally, the holding time at sintering temperature was varied between 2 h and 5 h. The hollow tubes were generated via slip casting. The moulds were made from plaster, as a positive form a Teflon halfcylinder was used.

To generate the slurry, water, dispersing agent, sintering aids and Si_3N_4 were mixed together followed by ball milling and degassing. After casting in the mould, the samples were dried at 105 °C for 24 h followed by sintering in a Si_3N_4/BN bed at 1500 °C – 1750 °C for 2 h – 5 h.

As methods of investigation mercury porosimetry, helium pycnometry, water immersion, scanning electron microscopy and an air flow test bench were used. With these methods the porosity, density, median pore diameter, characteristic strength and air permeability were measured. The results showed that an increase in particle size of the powder increased the permeability and the median pore diameter. The samples with a higher β – Si_3N_4 percentage showed a different behaviour than the samples made of only α – Si_3N_4. For samples made from solely α – Si_3N_4 with increasing temperature the porosity, median pore diameter and the permeability decreased and the characteristic strength increased. An increase in holding time from 2 h to 5 h led to densification and so permeability, median pore diameter and porosity decreased while the characteristic strength increased. For samples with a higher β – Si_3N_4 percentage, a temperature increase decreased the porosity whereas permeability didn't change significantly in the beginning and started to increase only above 1600 °C. The same is true for median pore diameter. The characteristic strength increased with higher sintering temperature. The holding time increase from 2 h to 5 h led to a decrease in porosity and an increase in median pore diameter while permeability and characteristic strength remained. A reduction of sintering aids yielded in an increased pore diameter, permeability and porosity and a decrease in characteristic strength for both α/β ratios. Compared to the starting point of the work an improvement in all characteristics was possible. Further improvement of the permeability may be possible with decreasing the sintering aid contents even more or increasing the pore diameter with the use of sacrificial fillers.

KURZFASSUNG

Das Ziel der Arbeit war die Untersuchung des Einflusses der verschiedenen Prozessparameter auf die Permeabilität von über Schlickerguss erzeugtem porösen Siliziumnitridröhren. Diese Röhren haben potentielle Anwendungen als Träger für Hochtemperaturmembranen, beispielsweise bei der Dampfreformierung von Kohlenwasserstoffen oder der Kohle/Biomasse Vergasung.[1, 2]

Dabei wurden drei Siliziumnitridquellen mit unterschiedlicher Partikelgröße und unterschiedlichen α – Si_3N_4 und β – Si_3N_4 Gehalt verwendet. Des Weiteren wurden unterschiedliche Sintertemperaturen im Bereich von 1500 °C und 1750 °C untersucht. Die Sinterhilfsmittel Al_2O_3 und Y_2O_3 wurden von 0.2 % bis 2.5 % variiert. Als letzte Prozessgröße wurde weiters die Haltezeit der Sintertemperatur zwischen 2 h und 5 h variiert. Die Röhren wurden mittels Schlickerguss hergestellt. Die Formen bestanden aus Gips, als Positivform für die Röhren diente ein Halbzylinder aus Teflon. Für die Herstellung des Schlickers wurde Wasser, Dispergiermittel, Sinterhilfsmittel und Siliziumnitrid gemischt und mittels Kugelmühlen vermahlen. Vor dem Guss wurde der Schlicker noch entgast. Nach dem Guss wurden die Proben bei 105 °C über Nacht getrocknet, gefolgt von der Sinterung zwischen 1500 °C und 1750 °C für 2 h bis 5 h. Als Untersuchungsmethoden wurden Quecksilberporosimetrie, Helium pyknometrie, Wasser- Immersionsverfahren, Elektronenmikroskopie und Luftdurchfluss gewählt. Mit diesen Methoden wurden die Porosität, die Dichte, der mediane Porendurchmesser, die Festigkeit und die Permeabilität gemessen. Die Ergebnisse zeigten, dass ein höherer β – Si_3N_4 Anteil zu einem unterschiedlichen Ergebnis führte als Proben, die nur aus α – Si_3N_4 bestanden. Für reine α – Si_3N_4 Proben verringerten sich die Porosität, der mediane Porendurchmesser und die Permeabilität, während die Festigkeit mit erhöhter Sintertemperatur stieg. Die Erhöhung der Haltezeit von 2 h auf 5 h führte zu einer Verdichtung und damit zu einer Verringerung der Permeabilität, des medianen Porendurchmessers und der Porosität, während die Festigkeit stieg. Proben mit einem höheren β – Si_3N_4 Anteil zeigten bei einer erhöhten Sintertemperatur eine Verringerung der Porosität, wohingegen sich die Permeabilität am Anfang nicht signifikant veränderte und ab 1600 °C anstieg. Die Festigkeit stieg mit erhöhter Sintertemperatur. Mit Erhöhung der Haltezeit von 2 h auf 5 h wurde die Porosität verringert und der mediane Porendurchmesser erhöht, während die Permeabilität und die Festigkeit auf demselben Level blieben. Für beide β – Si_3N_4 Gehalte führte eine Verringerung der Sinterhilfsmittel zu einer Erhöhung des medianen Porendurchmessers, der Permeabilität und Porosität und zu einer Verringerung der Festigkeit. Ausgehend vom Startpunkt konnten alle untersuchten Eigenschaften verbessert werden. Eine Erhöhung der Permeabilität könnte durch eine weitere Verringerung der Sinterhilfsmittel oder durch eine Erhöhung des Porendurchmessers mittels Opferfüllstoffen gelingen.

Index

1. INTRODUCTION

Motivation

With demanding membrane separation applications like steam reforming or biomass gasification more and more durable thermal stable membranes are needed.[1, 2]

Membranes for such applications are often built up of layers with different porosities. The porosity ranged from macroporosity for the support structure over a mesoporosity as intermediated layer and microporosity for the separation layer. It is aimed to reduce the thickness of the separation layer; therefore the mechanical stability is provided by the support structure.[3]

Silicon nitride with its high thermal and chemical properties is well suited as a material for the support structure under demanding circumstances.[4, 5]
The potential of silicon nitride in the desired application was already shown in the work of T. Konegger et al. [6] In their work they produced an asymmetric membrane completely built up of Si_3N_4.

It is possible to produce complex structures in form of a tubular shape accomplished via slip casting and gelcasting. These support structures achieved a permeability up to $9 \cdot 10^{-16}$ m^2 and a total porosity between 32 and 41 %.[7]

For the application as a separation membrane a higher permeability of the support structure would be desirable. It's also important not to disregard stability as it is important for the desired application.

2. THEORETICAL BACKGROUND

2.1. Gas separation – an overview

With increasing challenges to the membrane separation processes, the field of porous ceramics as such is getting more and more attention. High temperature membrane applications are for instance the steam reforming of hydrocarbons or coal/biomass gasification. [1, 2]
Typical materials for these extreme conditions are ceramics, for example Al_2O_3, [8] SiC [9] and Si_3N_4.[10]
These membranes are usually built up in an asymmetric manner, with a microporous support, macro/mesoporous intermediate layers and microporous selective layer.(See Figure 1) The pore diameter is, according to IUPAC, classified in three categories: macroporous ($Ø_p$ > 50 nm), mesoporous (2 nm < $Ø_p$ < 50 nm) & microporous ($Ø_p$ < 2nm).[3]

There are different approaches to produce such a membrane. For example a thin SiC layer can be achieved by coating a polycarbosilane on an Al_2O_3 tube, exposing it to electron beam irradiation followed by a pyrolysis. Another approach, which also involves Al_2O_3 and SiC is the application via CVD techniques.[11] A possible microporous layer can be obtained via polymer derived ceramics. Thereby a thermal decomposition of a silicon based polymer is initiated. Possible are polycarbosilanes or polyorganosilanzes which decompose with temperature to SiC or $Si_xC_yN_z$, respectively.[12]

The diffusion is limited because of the microporous structure of the top layer. To reduce this effect it is tried to reduce the thickness of the top layer to around 30 nm. A separation layer of this thickness cannot withstand the pressure present for example in the gas separation and therefore relies completely on the support structure.[13]
It is essential that the support structure has a high mechanical strength, but also a high flux to maintain the throughput. Additionally the support structure needs to be resistant to corrosive atmosphere, as well resistant to high temperature and pressure (e.g. H_2 production).[11]

For the support structure porosity can be achieved via sacrificial fillers like starch[14] or UHMW Polyethylene.[6] An alternative is partial sintering achieved for example via pressureless sintering of silicon nitride.[7] Possible manufacturing methods of the support structure are dry – pressing, pasteprocessing and the subsequent sintering of ceramic powder.[13]

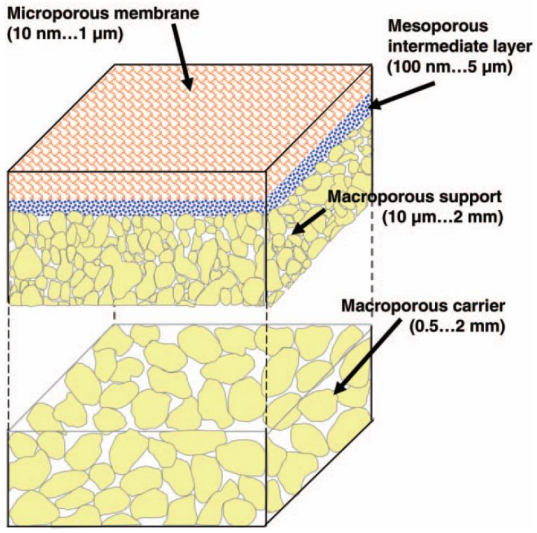

Figure 1: Scheme of a supported membrane structure with different pore sizes.[3] (reprinted with permission by Cambridge University Press)

2.2. Silicon Nitride

Silicon nitride is a non-oxide ceramic; it comes in four modifications: α, β, γ and δ. Only α and β are stable at room temperature with β being the most stable configuration. γ and δ are only meta stable at high temperatures.[4]

α and β are both hexagonal structures (P31c and $P6_3$). The structure is built up of tetrahedrons. As seen in Figure 2 in α all the tetrahedrons are looking in the same direction, in β they change in every second row.[5]

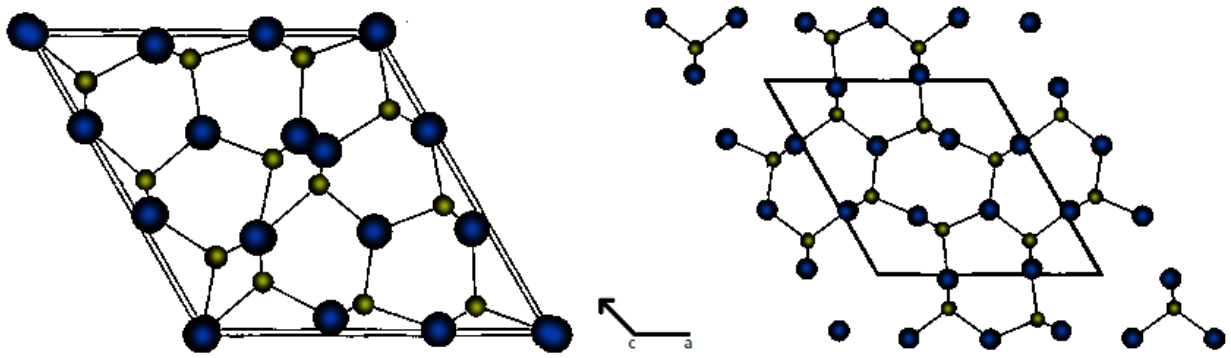

Figure 2: Projection of crystal structure of Si_3N_4, left: α – Si_3N_4 P31c, right: β – Si_3N_4 $P6_3$ after [5]

Silicon nitride has remarkable properties [4], which are:

- **Density** ranges in reliance to the modification. While the α phase ranges from 3.167 – 3.19 g/cm^3, the β phase differs less and has around ~3.192 g/cm^3.
- **Mean elastic modulus (Young modulus)** is around 30 – 300 GPa,
- **Fracture toughness (K_{ic})** commercially sintered Si_3N_4 ranges from 5 to 8 MPa m$^{1/2}$
- **Low Thermal expansivity** of 3.6 MK^{-1} (In a range of 25 – 1000 °C). This is slightly smaller than silicon carbide, which is why silicon nitride is considered to be resistant to thermal shock.
- **Low Thermal conductivity**. For polycrystalline materials: 15 – 30 Wm^{-1}K^{-1} at 25 °C. The value decreases as the temperature rises. The thermal conductivity is around 10 % of silicon Carbide.
- **Electrical conductivity.** With 10^{-14} Sm^{-1} silicon nitride is a good electrical isolator. The reason for this is the large gap between valence and conduction band of around ~5.5eV.
- High **chemical and thermal stability** at high temperature. Because of the liquid phase formed on the surface silicon nitride, it can be used up to a temperature of 1400 °C for a long time.

Because of different manufacturing techniques, different percentages of sintering aids and the different modifications, the values found in literature for silicon nitride differ.

2.2.1. Sintering aids

Silicon Nitride has a strong covalent bonding and a low diffusivity. For this reason Si_3N_4 cannot be densified by solid - state sintering. Liquid-forming additives are necessary to sinter silicon nitride. Without them Si_3N_4 would decompose at higher temperature, depending on the N_2 partial pressure. The additives react with SiO_2 on the surface to a silicate phase. At sintering temperature, this phase is molten. Metal oxides like MgO, CaO, Al_2O_3, ZrO_2, Y_2O_3, Eu_2O_3 and Lu_2O_3 are commonly used as sintering aids. Supplemental non-oxides like AlN, ZrN and Mg_3N_2 can be added. [5]

Many different combinations like Y_2O_3/MgO/CaO [15], Y_2O_3/Al_2O_3 [16] and CaO/Sm_2O_3 [17] are used in literature.

Most of the time the sintering aids combinations are developed empirically. There are although two requirements for a good additive. First of all it should not react with Si_3N_4 under sintering conditions to SiO_2 and the corresponding nitride. The ΔG^0 of the reaction

$$Si_3N_4 + 3\ Me_xO_2 \leftrightarrow 3\ SiO_2 + 3\ xMeN_y + (2 - 1.5yx)N_2$$

must be positive, if this is not the case Si_3N_4 decomposes. The second requirement is that Si_3N_4 is not allowed to react with oxides or nitrides to form metals or silicides. Therefore the reaction

$$Si_3N_4 + 3\ Me_xO_2 \leftrightarrow 3\ SiO_2 + 3\ xMe + 2N_2$$

must have a large ΔG^0. Figure 3 shows suitable sintering additives which meet both requirements in the grey area.[5]

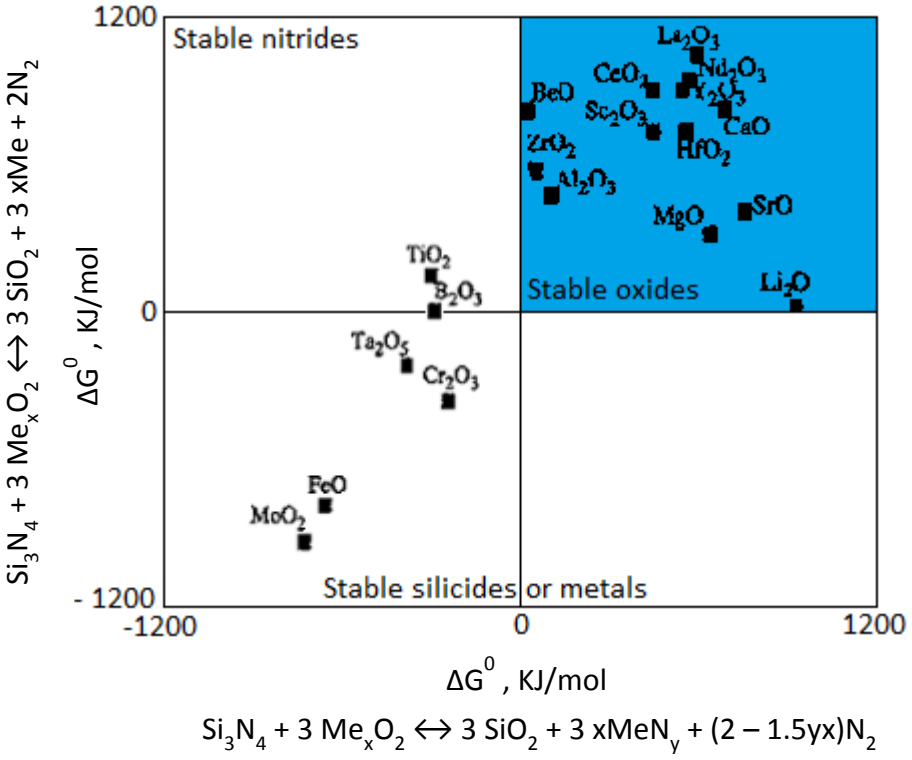

Figure 3: Plot of both requirement reactions. Grey area are stable oxides at sintering conditions and therefore possible sintering aids after [5]

The phase diagram of a complex system like Si_3N_4 with sintering aids Y_2O_3 and Al_2O_3 gets quite complicated. One possible way to visualize it, is the Jänecke prism shown on the left side in Figure 4. It shows the quasi quaternary subsystem Si_3N_4-AlN-Al_2O_3-SiO_2-Y_2O_3-YN. It consists of three quasi ternary salt systems on the square planes namely Si_3N_4 – AlN – Al_2O_3 – SiO_2, Si_3N_4 – YN – Y_2O_3 – SiO_2 and AlN – Al_2O_3 – Y_2O_3 – YN and two ternary systems on the triangular faces namely Si_3N_4 – AlN – YN and Al_2O_3 – Y_2O_3 – SiO_2. This makes the diagram look simpler but does not make it accessible. Detailed information can be obtained with further restriction on the system which lead to an accessible three phase system, shown in Figure 4 on the right side.[5]

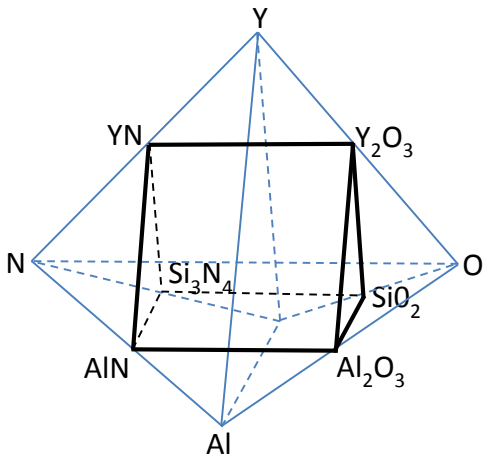

Figure 4: left: The system Si-N-O-Al-Y (Jänecke prism) after [5]

2.2.2. Densification

The densification of Si_3N_4 is influenced by the starting powder, the sintering additives, the sintering temperature, the holding time and the atmosphere. Increasing the sintering temperature and holding time favours the densification. The most important factor are the sintering aids because, without them, densification is not possible.[5]

When the eutectic melt forms, the densification starts. This happens between 1200 – 1300 °C. After the process the β – phase embedded in an amorphous phase remains. With a devitrification treatment the amorphous phase can be reduced, but a small part always remains in the product. This treatment is carried out just below the eutectic temperature.[5]

Suttor et al. looked at the densification of an α - Si_3N_4 powder with Y_2O_3 and Al_2O_3 as sintering aids. Figure 5 shows the densification behaviour of the system. Close to the formation of the liquid phase, the densification starts at 1350 °C. This goes with the ternary eutectic of SiO_2 – Al_2O_3 – Y_2O_3 at 1345 °C.[18]

The transformation from α to β starts at 1550 °C and plays a major part in the densification. With the advanced transformation from α to β the densification rate decreases at 1650 °C.[18]

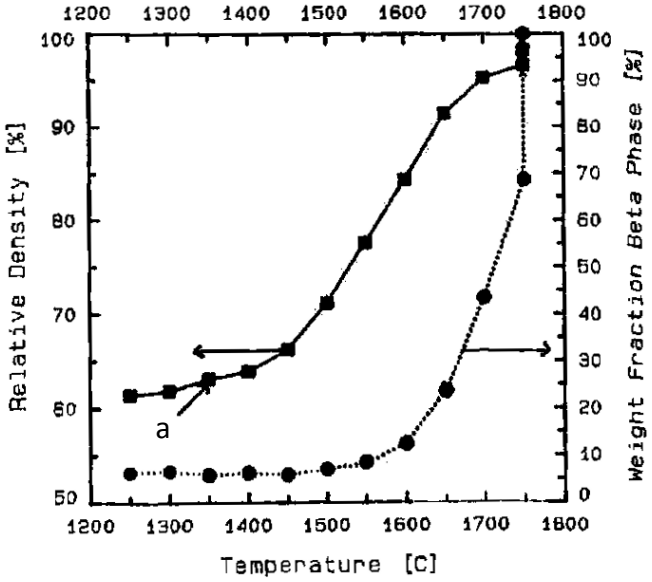

Figure 5: Plot of relative density and weight fraction of beta phase versus temperature, a: start of the densification [18] (reprinted with permission by Cambridge University Press)

2.2.3. Microstructure

Silicon nitride can exhibit different microstructures depending on the α/β ratio in the starting powder, the sintering temperature and the sintering aids. The microstructure is important for the properties of the final product, for example it is the microstructure that gives Si_3N_4 its high characteristic strength.[4] The key part here are the rod-like elongated grains of β - Si_3N_4, they form because of the hexagonal crystal system, which favours the c axis.[19]
β - Si_3N_3 is thermodynamically more stable, nevertheless α – Si_3N_4 is formed at a sintering temperature of 1300 – 1400 °C. At higher temperatures it transforms to the more stable β – Si_3N_4. A reversed transformation has never been observed. [4]

F. F. Lange showed the influence of the α/β ratio on the grain shape and size. He tested compositions ranging from a high α - Si_3N_4 (85 % α, 15 % β) content to a high β - Si_3N_4 content (26 % α, 74 % β).
For materials with a high α – Si_3N_4 percentage, he observed a fibrous fracture and a higher fracture toughness. Since he was interested in dense silicon nitride, his sintering method was hot-pressing.[20]

Topates et.al showed in their work, that the microstructure is as important for porous silicon nitride as it is for solid silicon nitride. In their work they compared two powders, one with a α - Si_3N_4 content of 80 % and one with a β - Si_3N_4 content of 90 %. As sintering aid $CaCO_3$ was used. The samples were uniaxially pressed and, after the removal of the binder, sintered at 1750 °C. This yielded microstructures shown in Figure 7. [21]
Topates et.al saw two possible reasons for the different behaviour. The first possibility they mentioned is the “location of precipitation”. Hereby α - Si_3N_4 dissolves and precipitates as β - Si_3N_4. If the starting powder has a high α - Si_3N_4 content these β grains can precipitate on newly formed β - particles and generate the anisotropic grains. If the starting powder has a high β- Si_3N_4 content the β - grains precipitate on existing β – particles, which yields a coarser, more equiaxed microstructure. The second possibility is the grain impingement effect. Hereby the initial number of β – particles influences the microstructure. If the starting powder has a low content of β grains, new grains find more space to grow without impingement effect. In their

study the samples made from > 80 % α - Si_3N_4 yielded a higher permeability of porous samples.[21]

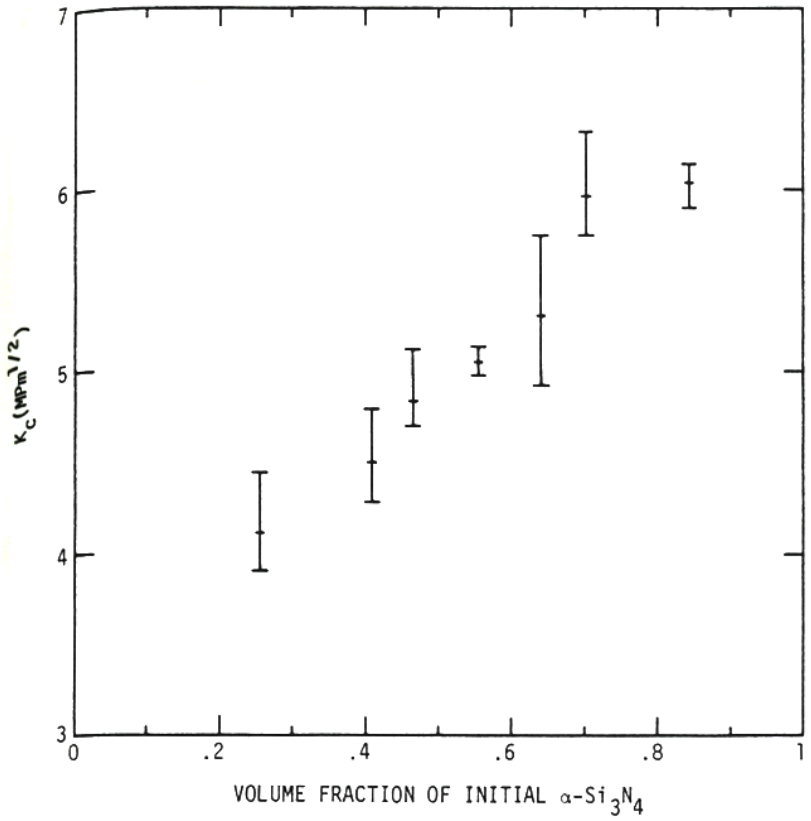

Figure 6: Graph used by Lange to show the dependence of the volume fraction of α – Si_3N_4 on the critical stress intensity factor[20] (reprinted with permission by Cambridge University Press)

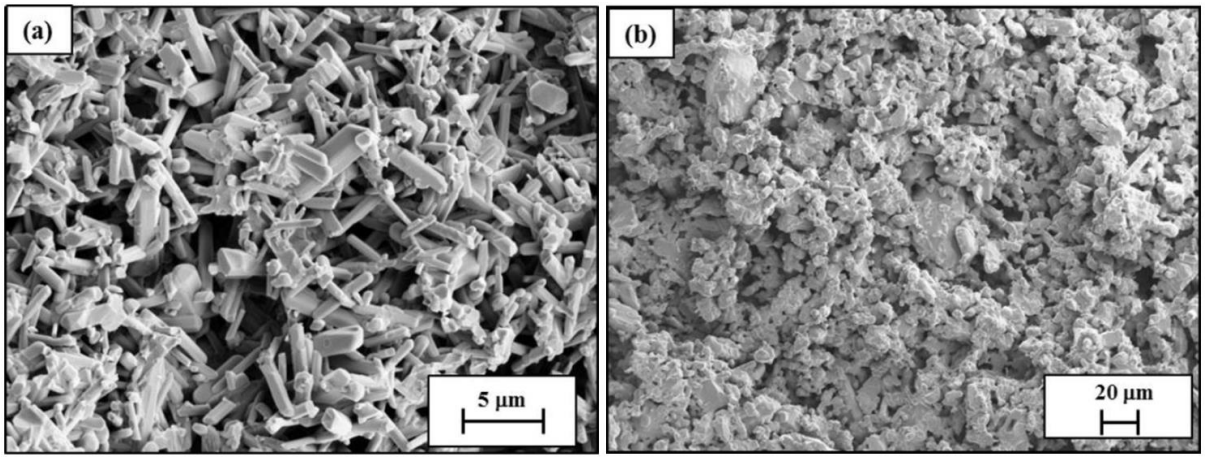

Figure 7: Porous microstructures achieved by Topates et. al., left: with a starting powder α – Si_3N_4 > 80%, right: with a starting powder β – Si_3N_4 > 90% [21] (reprinted with permission by Cambridge University Press)

2.3. Slip casting

Slip casting is a cheap and easy way for shaping green bodies. In slip casting a watery suspension is filled in a porous mold. The water is removed by the mould and a thin ceramic layer is formed. After waiting for a certain amount of time, the excess slurry is removed, and the sample is dried. In the last step the mould is opened and the sample removed. With this method very complex structures can be created. [22, 23]

An alternative for generating green bodies would be uniaxial pressing like it is used by Topates et. al.[21] This shaping technique only works for simple shapes. For more complex shapes, such as tubular structurers slip casting is the more viable technique. With greater effort it is possible to generate similar results with gelcasting.[7]

In the work of Mori et al. [10], porous silicon nitride is cast into gypsum moulds. They used a slurry with a solid content of 35 vol%. As dispersant, 1 wt% triethanolamine was used. To homogenise the slurry they milled it in the ball mill for 16 h. They were able to achieve a Si_3N_4 support structure with a porosity of 42 % and a pore diameter between 0.4 and 0.52 µm. The support structure had the shape of a flat cylinder and achieved a He permeation of $\geq 5.3 \cdot 10^{-6}$ mol m^{-2} s^{-1} Pa^{-1}. They were also able to apply a separation layer on top.

Hotasa et al. showed that slip casting is a cost effective method for the production of silicon nitride parts. They described the use of many different dispersing agents with $\alpha - Si_3N_4$ powder ($\beta < 10$ %, d_{50} = 0.6 µm) and measured the zeta potential and the rheology. They didn't use sintering aids; instead they relied on the amorphous silica on the grain surface. The deflocculants differed in their chemical base. Among them were amino alcohol (Dolapix A88), sodium lignosulphonate (Vanisperse CB) and sodium salt of an acrlic copolymer (Duramax D–3007).

The zeta potential measurement showed that nearly all of the tested dispersing agents can be used to stabilize the silicon nitride slurries. The zeta potential of the suitable candidates reached a slowly decreasing plateau with increasing amount of dispersing agent. The rheological analysis showed that all tested slurries were non-Newtonian fluids. For their compositions they recommend Vanisperse CB [24].

For this work Dolapix A88 was chosen, in Hotasa et al. work they were able to load the slurry up to 30 vol% of solid. Additionally, Dolapix A88 is the recommend dispersant agent for silicon nitride of the company Zschimmer & Schwarz.[25]

3. AIMS

The main aim of this work was to manufacture porous ceramic support structures for prospective membrane applications with controlled porosity. The porosity was achieved via partial sintering. As material silicon nitride was chosen. This structure should be used as a support material for silicon nitride layers with a finer porosity.

The goals were:

- The structure should be tubular in shape.
  L = 60 mm, OD = 6 - 10 mm, wall thickness 1 - 2 mm
- The membrane should have an open porosity of 30 to 40 percent.
- The characteristic strength should be sufficiently high for the application as membrane support.
- The influence of various processing parameters on the permeability, the porosity, characteristic strength and the pore diameter should be investigated.

4. EXPERIMENTAL PROCEDURES

Different parameters of interest were varied. Three different Si_3N_4 sources with different α/β ratio and particle size were used. The sintering temperature and holding time were varied between 1500 °C – 1750 °C and 2 h - 5 h. The amount of sintering aids of Al_2O_3 and Y_2O_3 was varied between 0.2 % and 2.5 %.

For each composition and parameter setting three to four samples were prepared.

4.1. Materials

Name	Formula	Company	Batch Number	specification
Silicon Nitride	Si_3N_4	UBE	SN-E03, Lot No. B165313	SSA: 3.1m^2/g
Silicon Nitride	Si_3N_4	UBE	SN-E10, Lot No. A166610	SSA: 11.1 m^2/g
Silicon Nitride	Si_3N_4	UBE	SN-XP06, Lot No. Z166210	SSA: 6.2 m^2/g
Boron Nitride	BN	ESK	BN – S1, Komm. Nr 312182	-
Alumina	Al_2O_3	Almatis	CT3000SG, Lot. Nr.1 103323490 0	d_{50} = 0.4 –0.5 µm
Yttria Grade C	Y_2O_3	C. Starck	AB134554, Lot 09061/06	d_{50} = 0.8 µm
Dolapix A88	Amino alcohol	Zschimmer & Schwarz	251804	
Supraduro Plaster		Lehrer Töpferbedarf		

4.2. Characterisation of Si_3N_4 starting materials

Three different powders were used as a silicon nitride source. They differ in α/β ratio and in particle size. The particle size was determined via laser diffraction analysis (Mastersizer 2000, Malvern). The α/β ratio was determined using powder XRD measurement (X'Pert Pro, PANalytical). The angle 2Θ between 5° and 100° was measured within 19 minutes with rotation.

4.3. Preparation of the plaster moulds

To achieve the desired shape, a split mould was necessary. For the first half of the mould a Polytetrafluorethylene (PTFE) half cylinder and two PTFE cones were glued on a clean glass plate. They were surrounded with a plastic frame, which was also glued to the surface. To hold it in place, old moulds were placed on each side to prevent moving.

Next 220 g water was filled in a beaker. Afterwards 330 g plaster was added and sat for 90 seconds followed by 110 seconds stirring. The beaker was then tabbed 10 times on the table to remove the bubbles.

Afterwards the plaster mould was slowly cast into the plastic frame. To remove bubbles from the PTFE half cylinder the table next to the mould was knocked. On the next day the plastic frame was removed. The PTFE parts were carefully removed and the PTFE half cylinder was replaced with a full cylinder.

Excess plaster was removed so that the plastic frame fitted on top of it. With a brush the whole surface and the inner wall of the plastic, with the exception of the PTFE cylinder was covered with separating emulsion (W165). Afterwards the plaster mould was prepared a second time and was cast on top of the first half. Again, the table next to mould was knocked, to remove the air bubbles from the PTFE cylinder through the vibration of the table.

On the next day the two halves were separated. An opening on both sides was carved with a knife. They then were placed in the drying oven over night at 50 °C.

4.4. Preparation of the Slurry

For the slip casting it was necessary to create a waterbased slurry. It contained Si_3N_4, powder, sintering aids, a dispersing agent and water. As silicon nitride source three powders SN-E10, SN-E03 and SN-XP06 were used. As sintering aids Al_2O_3 and Y_2O_3 and as dispersing agent Dolapix A88 was used. An overview of slurry compositions can be found in Table 1.

In the beginning the liquid components, distilled water and the dispersing agents (Dolapix A88), were filled a 250 mL polyethylene bottle. The Dolapix mass was fixed to 1 % of the used mass of Si_3N_4 powder. Afterwards the sintering aids Y_2O_3 and Al_2O_3 were added. To achieve a homogeneous mixture, 18 grinding balls with 1 cm diameter made of Si_3N_4 were added and afterwards mixed on the milling table for 30 min. Si_3N_4 was added in two steps. After the addition of Si_3N_4 the bottle was shaken until a homogeneous dispersion had formed.

Finally the slurry was rotated for 24 h on the milling table at a low rotation. After that period the grinding balls were removed. In the last step the slurry was degassed. Therefore the bottle was placed on the rotation table without grinding balls for three days.

After two months the procedure was changed and a planetary centrifugal mixer (Thinky ARE 250) was used for degassing. The used degassing program was set to 20 min at 800 rpm.

The exact starting values can be found in Table 1. To increase the output of samples it was necessary to cast more samples at once, therefore the total volume of the slip was increased. The new values can be found in Table 2. It was important that the volumes percentage stayed the same. With the increase of the mass, 22 grinding balls were used.

After the ball grinding three slips were combined. This yielded in more samples with exactly the same composition.

Table 1: Starting percentages and mass of the slurry

	mass [g]	rel. m % calculated with respect to Si_3N_4 mass	Abs. Vol.%
Si_3N_4	50		35
Y_2O_3	1.25	2.5	0.56
Al_2O_3	1.25	2.5	0.71
H_2O	28.36		63.73
Dolapix A88	0.5	1	
sum	80.86		100
Sum solid components	52.5		36.27

Table 2: Percentages and mass of the slurry after all changes

	mass [g]	rel. m % calculated with respect to Si_3N_4 mass	Abs. Vol.%
Si_3N_4	60		35
Y_2O_3	1.5	2.5	0.56
Al_2O_3	1.5	2.5	0.71
H_2O	34.04		63.73
Dolapix A88	0.6	1	
sum	97.04		100
Sum solid components	63		36.27

4.5. Slip casting

4.5.1. Determination of the layer formation rate

To determine the layer formation rate, four samples with different dwelling periods were prepared. The wall thickness was determined using a calipes.

The determination the layer formation rate was calculated after following formula[22]:

$$const. = \frac{x^2}{t} \quad \textbf{(1)}$$

x … wall thickness [mm]
t … dwelling period [s]

It is important to note that the method to stop the timer changed over the course of this work. For the determination of the layer formation rate the time was measured when the slurry was filled in. Later it was started before the slurry was filled in. The difference in these two methods adds 10 s and is already taken into account in 4.5.2.

4.5.2. Preparation of the Samples

To ensure a constant and reproducible moulding behaviour, the moulds were dried over night at 50 °C before every use. The dried plaster moulds were equipped with a Teflon disk, and closed and sealed with two rubber bands. For every cast, 5 plaster moulds were prepared.

The time was stopped using a stopwatch, the measurement was started and the mould was filled with slurry up to one centimetre under the rim. The slurry bottle was immediately closed to prevent drying out. Afterwards the mould was turned around to equally distribute the slurry. After 70 seconds the excess slurry was removed by turning the mould upside down while it still was turned around. The excess slip was collected in a beaker for later use in the sintering process (See 4.6).

On the next day the sample was demoulded (Figure 9). The tube was carefully removed. Most of the time the sprue broke off on its own, if not it was removed by tipping it with the spatula.

The tubes were dried over night at 110 °C. On the next day the length, radius, wall thickness and weight were measured with a calliper. The whole process of the slip casting is illustrated in Figure 8. Figure 9 shows a picture of the mould after opening.

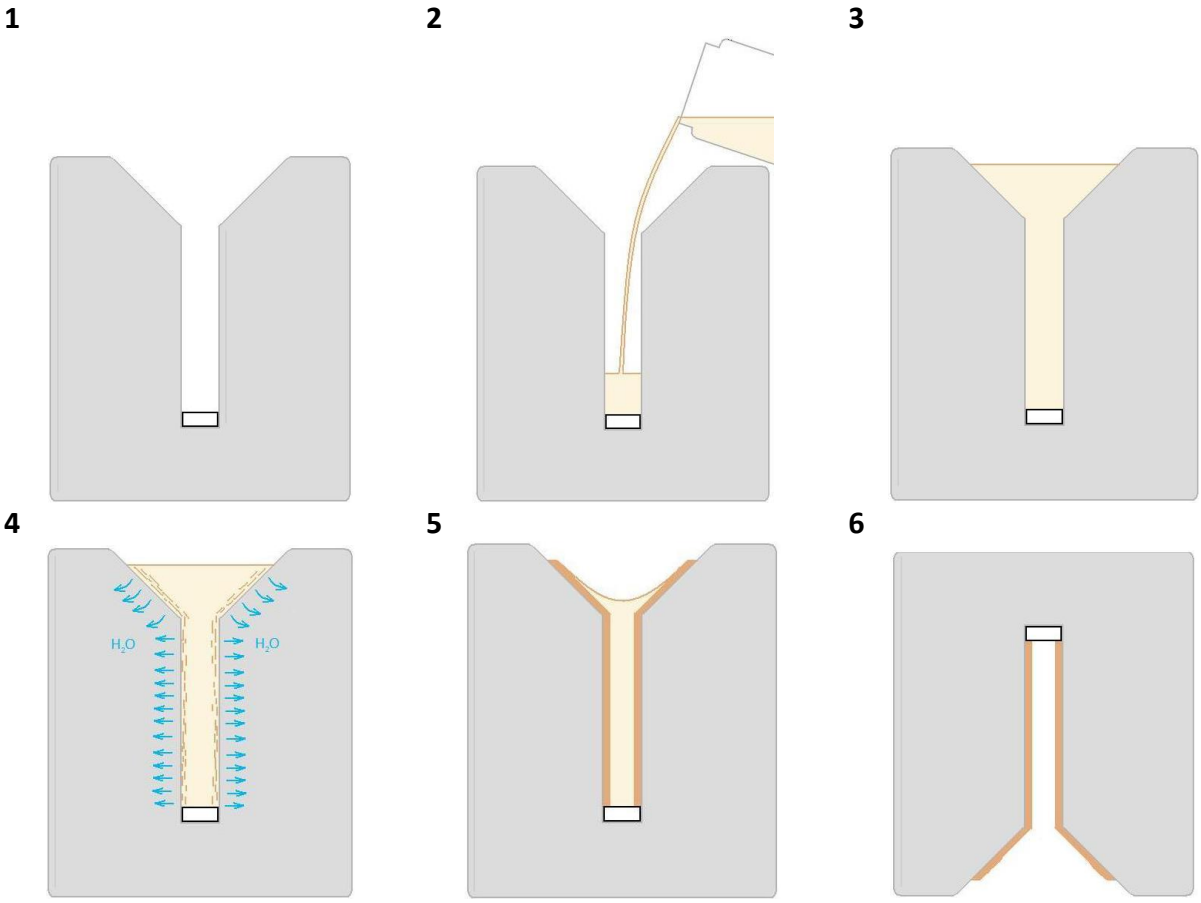

Figure 8: Slip casting process in detail, 1. Mould equipped with Teflon disk, 2. Filling the mould with the slurry, 3. Formation of the shards, 4. Removal of the excess slurry, 5. Drying and shrinkage of the sample, 6. Demoulding

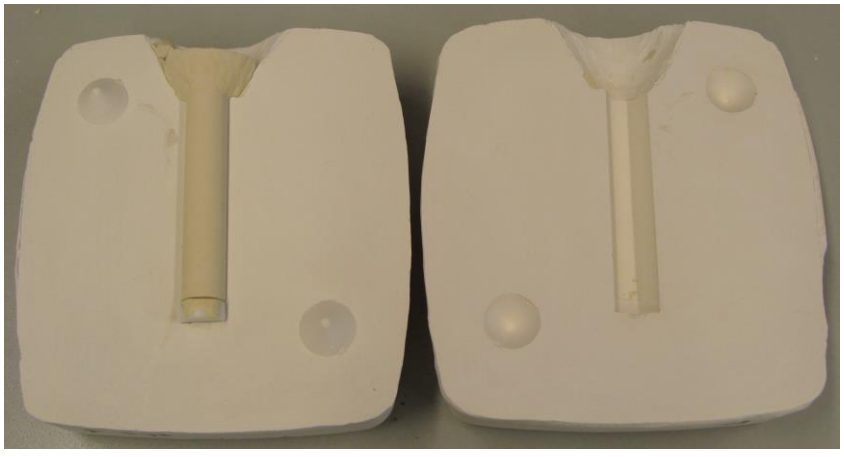

Figure 9: Sample after opening of the mould, still with sprue on top

4.6. Sintering

The samples were sintered at ambient pressure under N_2 (≥99.999 %) atmosphere in a hot press (FCT HPW 150/200-2200-100-LA). In each run four to six samples were sintered. All samples for one composition were sintered in one run.

The furnace was heated with carbon heating elements. The inside insulation consists of graphite. The Si_3N_4 tubes were sintered in a graphite crucible and were placed in a powder bed of Si_3N_4 and BN on top of a Si_3N_4 shard. The powder was a 50:50 mixture of Si_3N_4 and BN. The shards were generated through the excess slurry described in 4.5. For several runs, in the middle of the crucible a process temperature control ring (PTCR-HTH, 1450 – 1750 °C, Ferro) was placed. The PTCR served as a separated temperature control. The sample openings were also closed with a Si_3N_4 shard and afterwards covered in the Si_3N_4/BN powder mixture. The Si_3N_4 shards prevented the surrounding powder bed from filling up the tubes. This could lead to cracks in the sample when the sample shrinks due to the sintering process. It's important that the colour of the powder bed is always controlled and should always be white or at least light grey. The arrangement of the samples can be seen in Figure 10. The crucible was closed and surrounded with a graphite coat for equal heat distribution, and afterwards placed in the hot press.

The hot press was closed and sealed and vacuum was applied for 5 min. Afterwards it was filled with N_2, before again vacuum was applied for 5 min. This process was repeated one time. Still under vacuum the program was started. Program started with three purging steps with N_2, for the first two it ended at 450 mbar, the last ended at 1050 mbar. After the last purging step the N_2 flow was reduced to 0.4 L/min. Then the heating started.

The heating rate stayed the same of 10 K/min over all experiments. Until the temperature reached 650 °C the heating power was fixed at 4 kW, and after that point switched to pyrometer controlled until the desired temperature was reached. The temperature then was held for 2 h or 5 h depending on the composition. Afterwards it was cooled down with 10 K/min.

To ensure that the samples and the setup were at room temperature, the hot press was opened on the next day.

Reproducible sintering at higher temperatures proved to be challenging, further information can be found in Appendix A1.

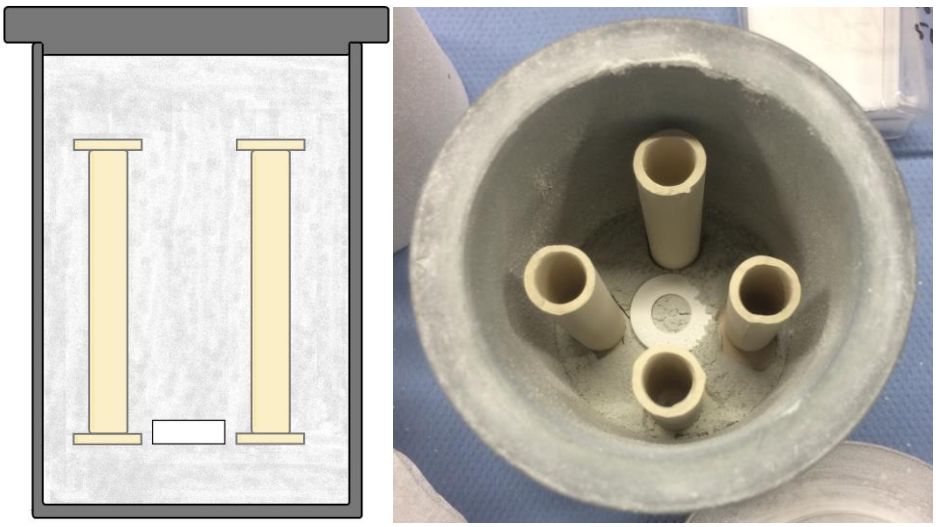

Figure 10: Typical arrangement of the samples in the graphite crucible with PTCR-HTH in the middle left: cross-sectioned view up front, right: View from above

Figure 11: Comparison of the sample before sintering (left) and after sintering at 1700 °C for 5 h (right)

4.7. Shape finishing of the tubes

The edges of the samples were different from the body. On the top, the surface bottom was uneven because of the fracture surface due to the removal of the sprue. On the bottom undercut was present due to the Teflon disk in the casting process. For the permeability measurement it was necessary to remove the edges with a cutting machine (Uniprec) with a diamond cut-off wheel. In Figure 12 the shape finished samples can be seen.

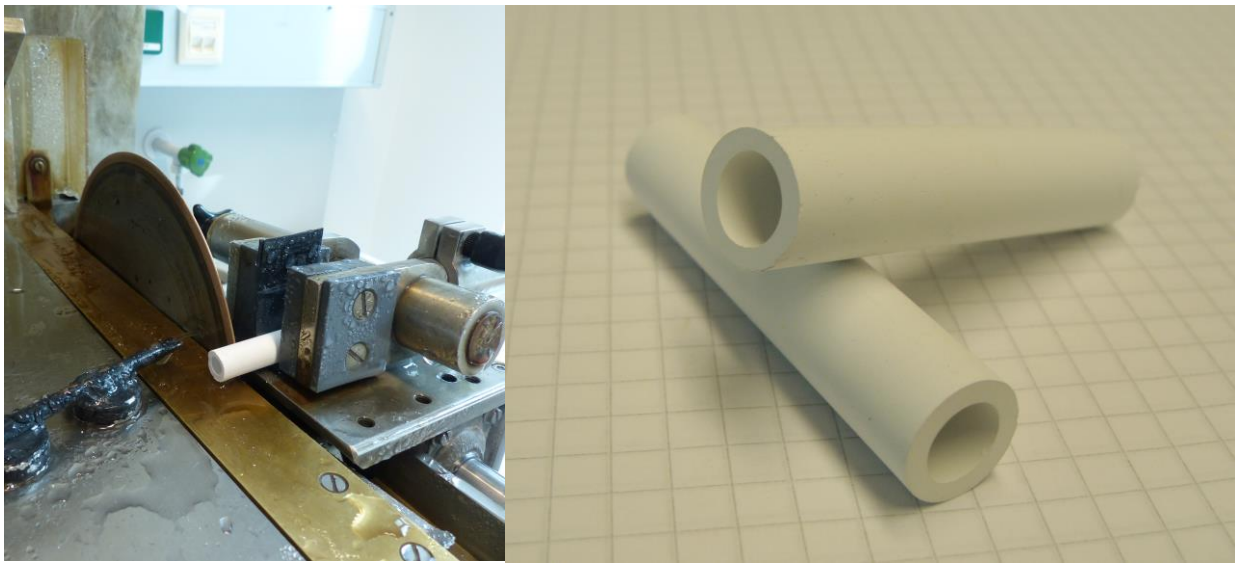

Figure 12: Sample placement in the cutting machine (left), Samples after shape finishing (right)

4.8. Characterization of the samples

For sample characterization the methods mercury porosimetry, He pycnometry, water intrusion, scanning electron microscopy, and an air flow work bench were used. With these methods the porosity, density, median pore diameter, characteristic strength and air permeability were measured.

4.8.1. Permeability

The gas permeability was measured on a test rig designed based on a European standard for permeability testing of planar samples (DIN EN ISO 4022).

The samples were dried at 100 °C before the measurement. To prevent leakage the samples were equipped with two rubber O – rings on each side. After the first two rings were placed on the sample the screw fitting was pulled over them and screwed together. Then the second screw fitting followed with the final two O-rings. The tube was placed in the permeability test rig. On the outside 0.2 bar of relative pressure was applied which was slowly increased to 3 bar of compressed air were applied to ensure that the sample can take the pressure. Afterwards the pressure was reduced to 0.2 and the air flow measured. The air passes through the support and enters a soap bubble flowmeter. The time it takes the bubble to pass through a known volume is measured. For a reproducible value this should take the bubble at least 8 seconds. Since the volume of the flowmeter was limited it took the samples with higher permeability only 2 – 3 seconds to pass through. For some samples it was not possible to measure at higher pressures.

Nine relative pressures were chosen (0.2, 0.4, 0.6, 0.8, 1, 1.5, 2, 2.5, 3 bar) each of them was measured seven times.

For calculation, Forchheimer's equation [26] for compressible fluids was used.[27] k_1 the Darcian permeability, (related to viscous flow) and k_2, the non-Darcian permeability (related to inertial force), characterise the behaviour of the fluid in porous medias. The focus was mainly on the Darcian permeability. With the least-squares method a quadratic function was fitted to ($p_i^2 - p_0^2/2p_0l$) versus Q/A. Out of this fit k_1 and k_2 were calculated. [26]

The aim was to reach $k_1 = 10^{-14}$ m^2. The starting composition achieved $k_1 = 10^{-16}$ m^2.

$$\frac{p_i^{\,2} - p_0^{\,2}}{2p_o \cdot l} = \frac{\eta}{k_1}\frac{Q}{A} + \frac{\rho}{k_2}\left(\frac{Q}{A}\right)^2 \qquad \textbf{(2)}$$

η	…	viscosity of air ($18.43 \cdot 10^{-6}$ Pa·s) [28]
ρ	…	density (1.15 km/m^3) [28]
k_1	…	Darcian permeability (m^2)
k_2	…	Non-Darcian permeability (m^2)
Q	…	mass flow (cm^3/s)
A	…	cross-sectional area of flow (cm^2)
p_i	…	absolute pressure at inlet (bar)
p_o	…	absolute pressure at outlet (bar)
l	…	thickness along flow direction (cm)

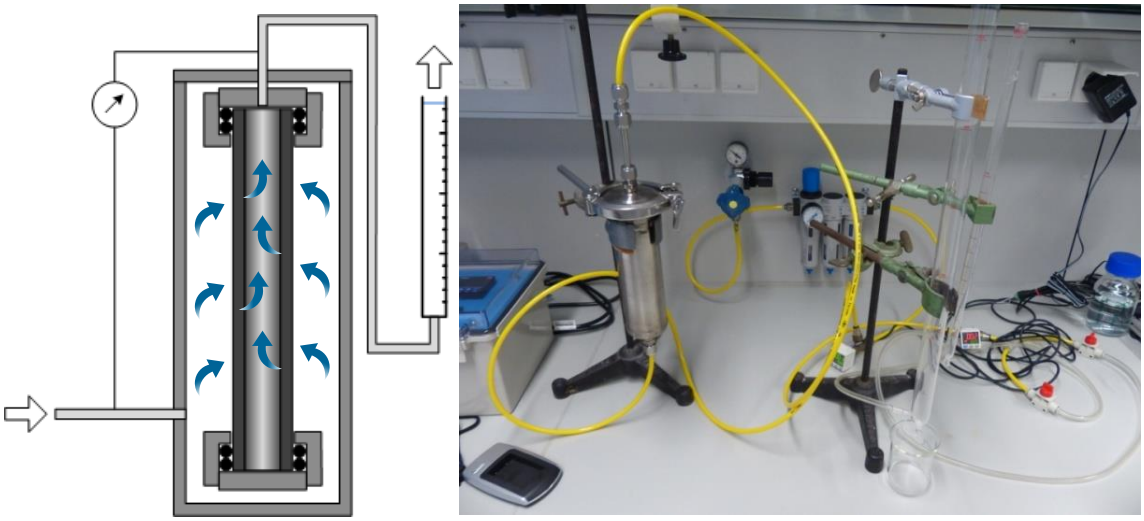

Figure 13: left: Working scheme of the permeability work bench[29]; right: Permeability work bench setup

4.8.2. Density according to helium pycnometry

Since the density of the samples varies depending on the Si_3N_4 source used, the skeleton density was determined for a sample made up of each of the three powders. Each sample was sintered at 1600 °C for 2 h and contained 2.5 % of each sintering aid.
They were measured at the pycnometer (Ultrapycnometer 1000, Quantachrome Instruments) equipped with the microcell. Each sample was measured two times. Each measurement yielded 10 values. Only the last 5 values of each measurement were used to calculate the mean value and the standard deviation. The mean values were used as the initial value for the mercury porosity.

4.8.3. Density and porosity measurement via water immersion according to standard EN 623-6

Because of cost and time reasons an alternative measurement for density and porosity was necessary. For that an arrangement according to European standard EN 623 - 2 was used.[30]
With this method three values were determined, the mass under air, the mass under water and the mass of the sample infiltrated with water.

The tubes were dried at 110 °C overnight and weighed in air on the next morning. A desiccator was equipped with a funnel and a valve on top. The samples were placed on a rack in a crystallisation dish to ensure that the opening of all tubes was above ground level. This made it easy for the air bubble to leave the structure. The lid was closed and vacuum was applied until 25 mbar was reached. This pressure was applied for at least 30 minutes.
Afterwards the funnel on top of the desiccator was filled with water and the valve opened. The funnel was not allowed to get empty. If the water level sank too far, water was added to the funnel.
Water was filled in until the water level in the crystallizing dish was roughly 1 cm above the highest point of the samples. After that, vacuum was applied until 25 mbar was reached. This pressure was applied for 30 minutes. In the meantime, the setting for the scale was prepared. The setting reassembles the setting for Archimedes density. For the removal of excess water a wet paper towel was prepared.

After the expiration of the period, the samples were removed. Each sample was weighed three times under water and three times infiltrated with water. Before the measurement with the infiltrated water was made, the excess water was removed from the surface.

The densities were calculated according to the following formulae:

Geometric bulk density

$$\rho_b = \frac{m_1}{m_3 - m_2} \cdot \rho_L \quad \textbf{(3)}$$

m_1	…	Mass of the dried sample [g]
m_2	…	Apparent mass of the sample underwater [g]
m_3	…	Sample mass infiltrated with water [g]
ρ_L	…	Density of the infiltration liquid water [g/mL]

Apparent density

$$\rho_s = \frac{m_1}{m_1 - m_2} \cdot \rho_L \quad \textbf{(4)}$$

Apparent porosity

$$\Pi_a = \frac{m_3 - m_1}{m_3 - m_2} \cdot 100 \quad \textbf{(5)}$$

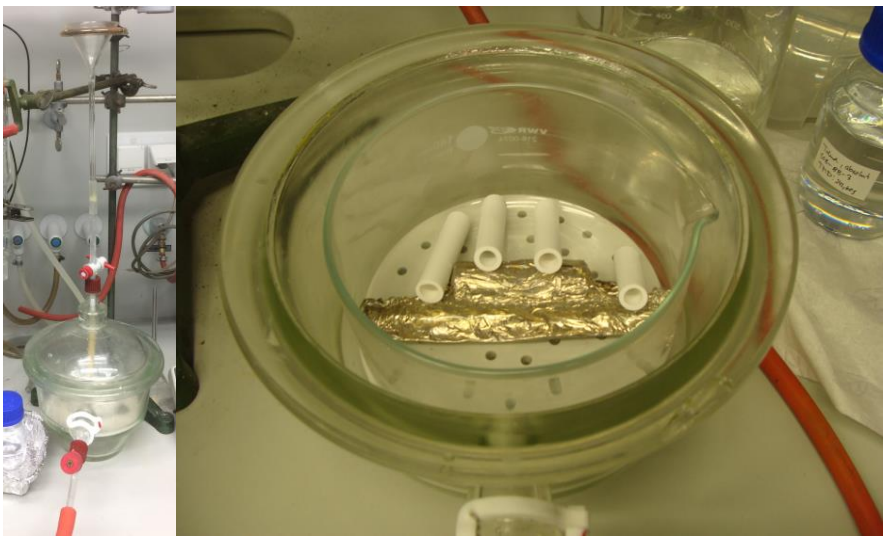

Figure 14: left: Finished setting for the infiltration ready to use; right: position of the samples on the rack in the desiccator

4.8.4. Mercury porosimetry

In advance of the mercury porosity measurement the skeleton density and the porosity were measured using the density and porosity measurement described in 4.8.2 and 4.8.3.
With the porosity values from the other measurement techniques the necessary mass of sample was calculated. This was important because the porosimeter had a limited pore volume of 400 mm^3. The ideal pore volume should be at around 200 mm^3 and so the sample mass was calculated to reach that value.
The samples were measured used a two-step porosimetry method (Pascal 140/440, Porotec).

For the mercury measurement the sample was crushed into pieces. The pieces needed to be smaller than 1 cm to fit into the bottleneck of the dilatometer. The exact weight was noted and filled in the dilatometer. To prevent sample bits from sticking to the dilatometer neck, it was covered with a weighing paper which also served as a funnel.
The joint of the capillary of the dilatometer was covered in grease and closed tightly. The cap was placed on top and the shell was pulled over the capillary. The dilatometer then was placed in the Pascal 140 which served as a filling unit and a pressure of 400 kPa was applied. After the run the dilatometer was then moved to the high pressure unit Pascal 440, where pressure up to 400 MPa was applied. With this set up pores with a diameter between 4 nm and 150 µm could be measured.

4.8.5. Scanning electron microscopy

As imaging technique scanning electron microscopy (Quanta 200, FEI) was used. Pictures of the starting powder and the sintered samples were made.
The powders were prepared by spreading them thin on a piece of carbon tape. For the sintered samples a slice of the tube was cut down and broken. The broken parts were arranged on the carbon tape as shown in Figure 15. The arrows show the three locations where, pictures were taken. As conductive coating gold was sputtered on. It was applied with 10 mA for duration of 50 s. In the beginning the pictures were taken using the high vacuum setting. After a few measurements the setting was changed to low vacuum.
For one sample (XP06, 1700 °C, 2.5% SA, 5h) an EDX scans were recorded to look at the distribution of the sintering aids.

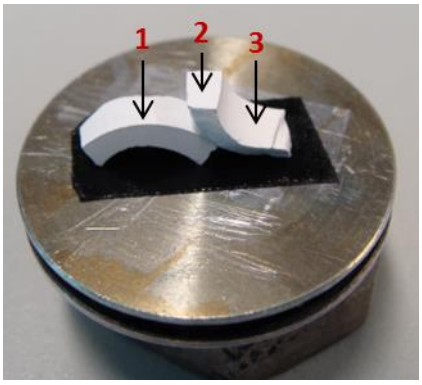

Figure 15: Placement of the broken sample for the SEM measurement, the arrows indicate the measured spots 1: outside wall surface; 2: fracture surface, 3: inside wall surface

4.8.6. Compressive strength measurement of sintered samples

To measure the compressive strength the samples were cut with a diamond cut-off wheel (Uniprec, unique precision) into 5 mm thick slices. Afterwards a piece of the ring was cut out so that the sample ended up in the shape of a C. To get a statistic relevant value, the aim was to produce 20 samples for each composition.

The compressive strength was calculated according to equation 6 [31]:

$$\sigma_C = \frac{F}{B \cdot t} \cdot \left(\frac{(r_0 - 0.5 \cdot t) \cdot (r_0 - L)}{r_0 \cdot (r - L)} \right) - 1 \quad \text{(6)}$$

with

$$L = \frac{t}{ln\left(\frac{r_0}{r_i}\right)}$$

σ_c	…	failure strength [MPa]
F	…	load of failure [N]
B	…	specimen length [mm]
t	…	wall thickness of the ring at the fracture surface [mm]
r_0	…	outside radius of the ring [mm]
r	…	mean radius of the Ring (with $r = (r_0 + r_i)/2$) [mm]
r_i	…	inner radius of the ring [mm]

The 1 kN measurement cell was used on the electromechanical testing machine (Zwick). The ring was placed in the setup (Figure 16). In addition to the applied pressure the setup applied an additional force of 5.29 N, which was added to the result. The results were validated using the probability distribution after Weibull using the maximum-likelihood-method

according to European standard EN 843-5. Also according to European standard the confidence interval was calculated. [32]

For some measurements the 100 kN measurement cell was used, these values are marked with a *.

Figure 16: Setup used for compressive strength testing with a built-in C-Ring sample

4.8.7. XRD of the sintered samples

The XRD measurements were made on a powder diffractometer (X'Pert Pro, PANalytical). After the compressive strength measurement, one piece of the broken sample for every composition was chosen and partly grounded on the surface. Afterwards, in order to achieve a flat surface, it was placed on a piece of putty and pressed in with a plate made of glass. The angle 2 Θ between 5 and 100° was measured in 19 minutes with rotation. The phases were analysed using Rietveld refinement, using the program Highscore.

5. RESULTS & DISCUSSION

5.1. Determination of the layer formation rate

In Table 3 the results for the layer formation rate are shown. The dwelling period of 60 s yielded the desired wall thickness and was never changed. With the changing of the time measurement the dwelling period of 60 s equals the 70 s mentioned in 4.5.2..

Table 3: Layer formation rate and wall thickness at different dwelling time

	dwelling period [s]	mean wall thickness [mm]	layer formation rate c [mm^2/s]
A1	50	1.95	0.076
B1	60	2.43	0.098
C1	70	2.49	0.089
D1,1	80	2.76	0.095

5.2. Density according to helium pycnometry

The results gained through the helium pycnometry are found in Table 4. All samples were prepared with the same parameters except for the Si_3N_4 source. They were sintered at 1600 °C for 2 h with sintering aid content of 2.5 %. Si_3N_4 E10 and Si_3N_4 E03 yielded a very similar density, which was to be expected since they only differ in particle size of the powder. The sample with XP06 as Si_3N_4 source achieved a higher density.

Table 4: Mean value and standard deviation of the density according to Helium Pycnometry

Si_3N_4 source	density [g/cm^3]
E10	3.171 ± 0.021
E03	3.187 ± 0.009
XP06	3.246 ± 0.043

5.3. Parameter variation for Si_3N_4 - E10

The starting parameters of the work was Si_3N_4 powder type E10 with a sintering aids content of 2.5%, a sintering temperature of 1600 °C and 2 h holding time. With E10 powder as silicon nitride source the influence of the sintering aids percentage was observed.

5.3.1. Starting powder SN – E10

SN – E10 was the starting powder. The X-Ray measurement showed that the powder consists mostly out of alpha silicon nitride.

The SEM picture suggests that the powder consist of a fraction of equiaxed grains surrounded by a fine fraction of the same powder. In the laser diffraction analysis only one fraction is shown. The determined particle size d_{50} is 1.1 µm. According to XRD results seen in Figure 18, the β percentage is in the declared range.

Table 5: Specifications and measured values for powder SN - E10

	Specifications (UBE Industries)	Datasheet Value (UBE Industries)	measured
β - Si_3N_4 (wt %)	<5	<5	0.6
N (wt %)	>38.0	>38.0	-
O (wt %)	< 2.0	1.31	-
Crystallinity	>99	>99.5	-
d(0.5) (µm)	-	-	1.1

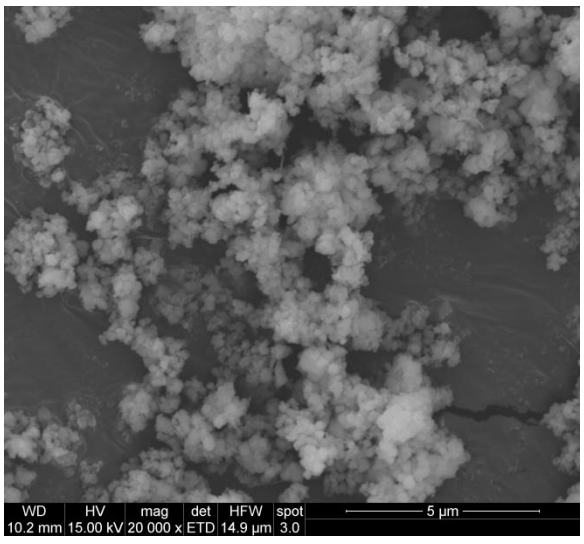

Figure 17: SEM Picture of Si_3N_4 Powder SN - E10

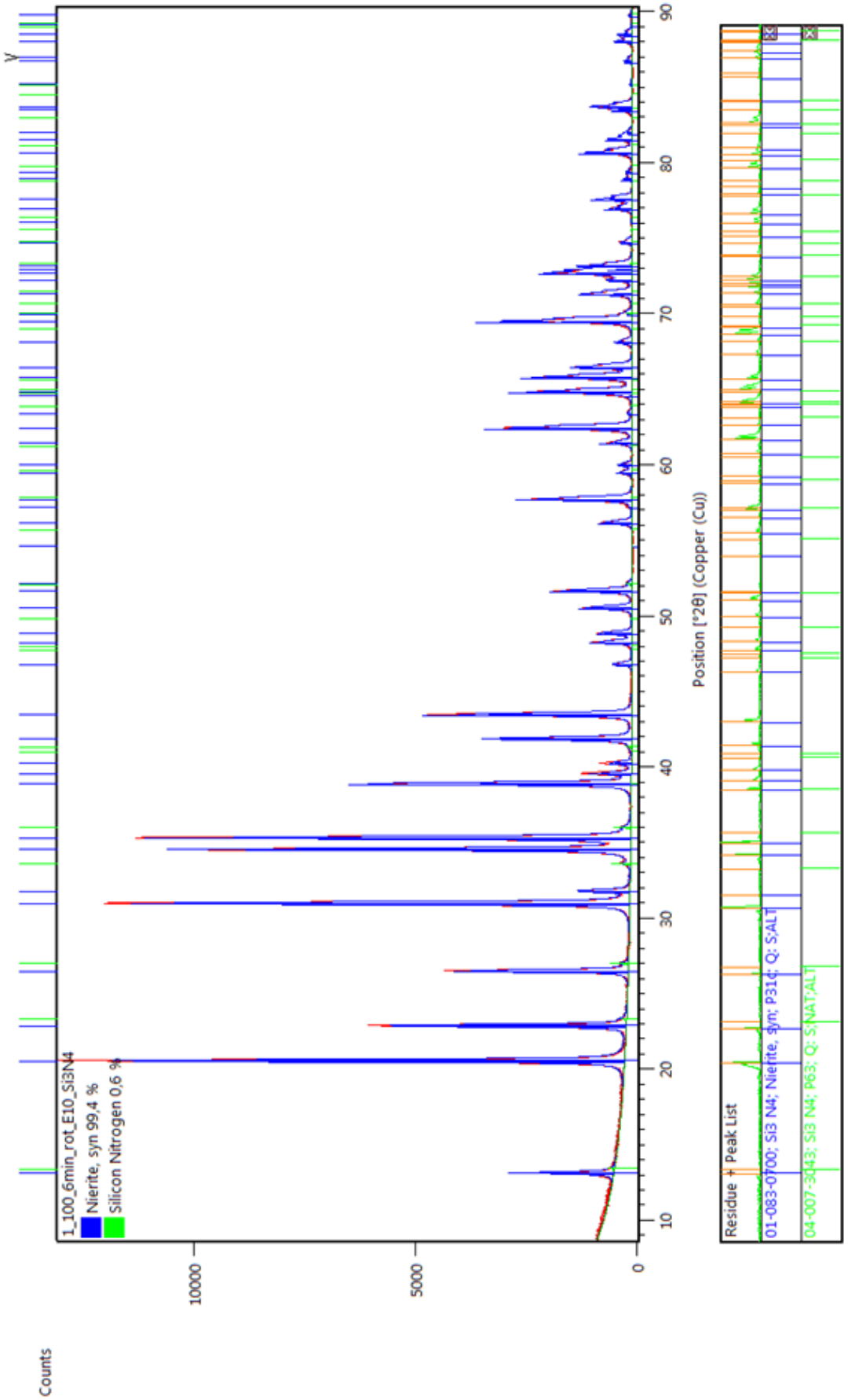

Figure 18: XRD of Powder SN-E10, blue: α-Si_3N_4, green:β-Si_3N_4

5.3.2. Porosity, density and microstructure of E10 specimens

An increase of sintering aids leads to a decrease in porosity, shown in Figure 19. The density on the other hand stays nearly the same for all compositions. The mean value and the standard deviation were calculated from three samples. The pore diameter was measured only for two samples. The exact values can be found in Table 6.

Since the reproducibility of the permeability of the sample E10, 0.2 %, 1600 °C, 2 h and E10, 0.5 %, 1600 °C, 2 h was low no mercury intrusion measurements were made, therefore no pore diameter data are known for these samples.

The mercury porosimetry shows that the median pore diameter increases from 0.168 µm at 2.5 % to 0.216 µm at 1.0 % sintering aids. The inaccessible porosity was under 2 % for both samples.

In Figure 20 SEM pictures of all samples with E10 as Si_3N_4 source can be seen. There is no significant change in microstructure visible in the SEM picture between 0.2 % and 0.5 % sintering aid content. The shape of the grains on the fracture surface resemble the shape of the starting powder seen in Figure 17. At 1.0 % sintering aids visible necks between the grains begin to form. With 2.5 % sintering aids the fracture surface gets rougher and the necks are connected. The grains grew in size.

Table 6: Porosity and density by water intrusion and median pore diameter by mercury porosity values for E10

	$\rho_{s\varnothing}$ g/cm³	$\Pi_{a\varnothing}$ %	median pore diameter, µm
E10, 0.2 %, 1600 °C, 2 h	3.205 ± 0.049	50.2 ± 0.8	-
E10, 0.5 %, 1600 °C, 2 h	3.199 ± 0.006	45.7 ± 1.1	-
E10, 1.0 %, 1600 °C, 2 h	3.192 ± 0.020	40.6 ± 1.2	0.2145
E10, 2.5 %, 1600 °C, 2 h	3.207 ± 0.010	28.9 ± 0.6	0.1684

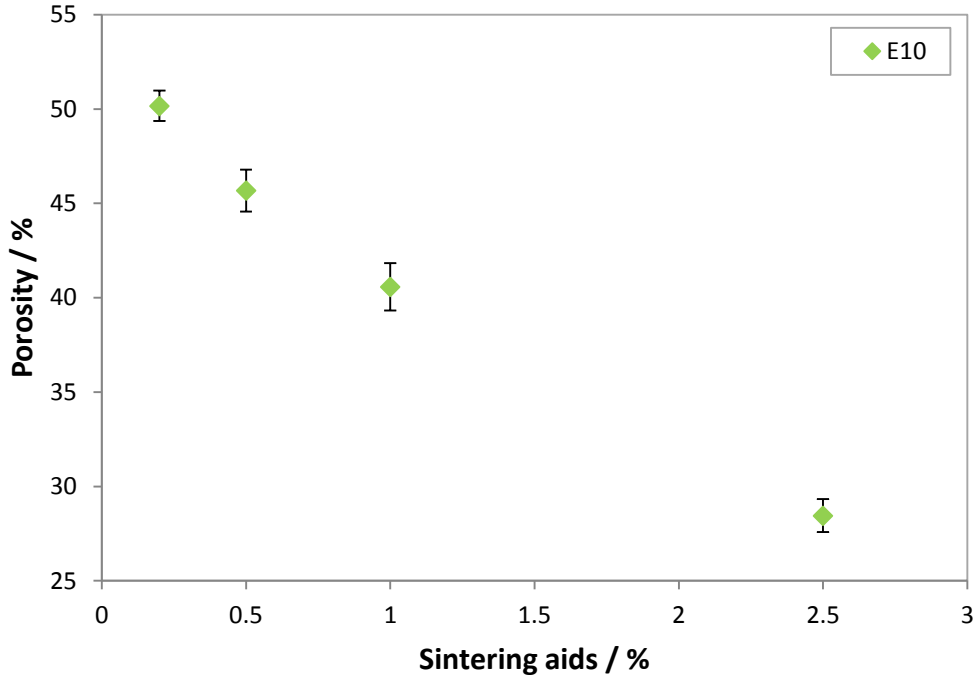

Figure 19: Influence of sintering aids on the porosity of E10 –samples sintered at 1600 °C for 2 h

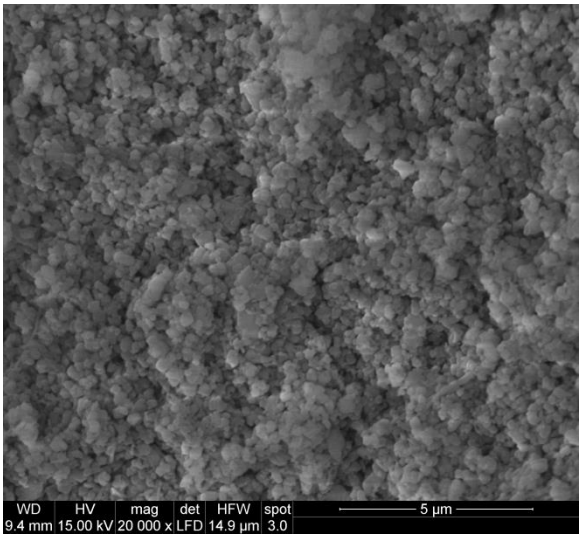

0.2 % SA, 5C5

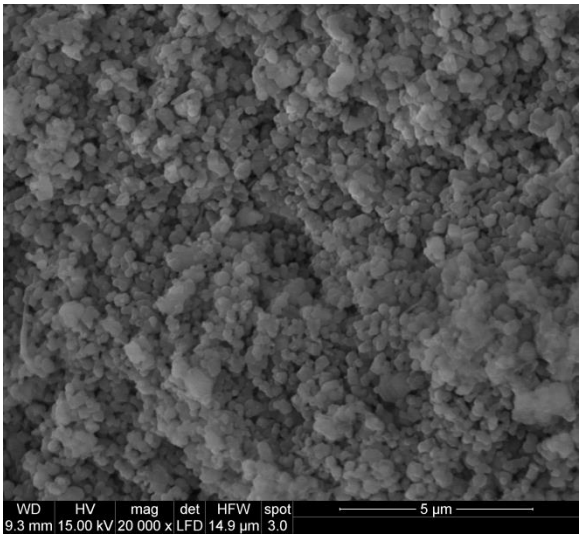

0.5 % SA, 4D4

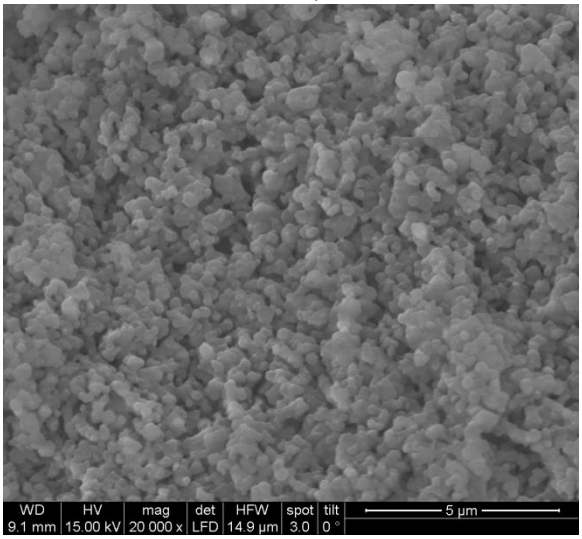

1.0 % SA, 3A3

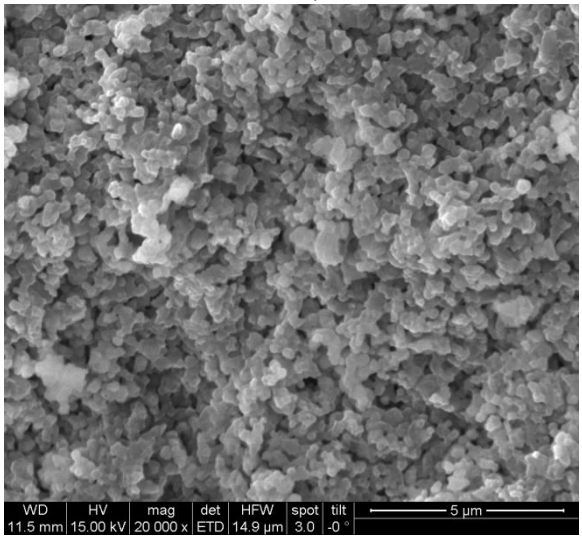

2.5 % SA, 2B2

Figure 20: SEM pictures of E10 Samples with different sintering aids content sintered at 1600 °C for 2 h

5.3.3. Crystalline composition of E10 specimens

The E10 starting powder consisted mainly of α-Si_3N_4. With an increasing amount of sintering aids the content of β-Si_3N_4 increases in the sintered samples. In Figure 21 the α/β ratios of all samples made of E10 determined by Rietveld refinement of the XRD data can be found.

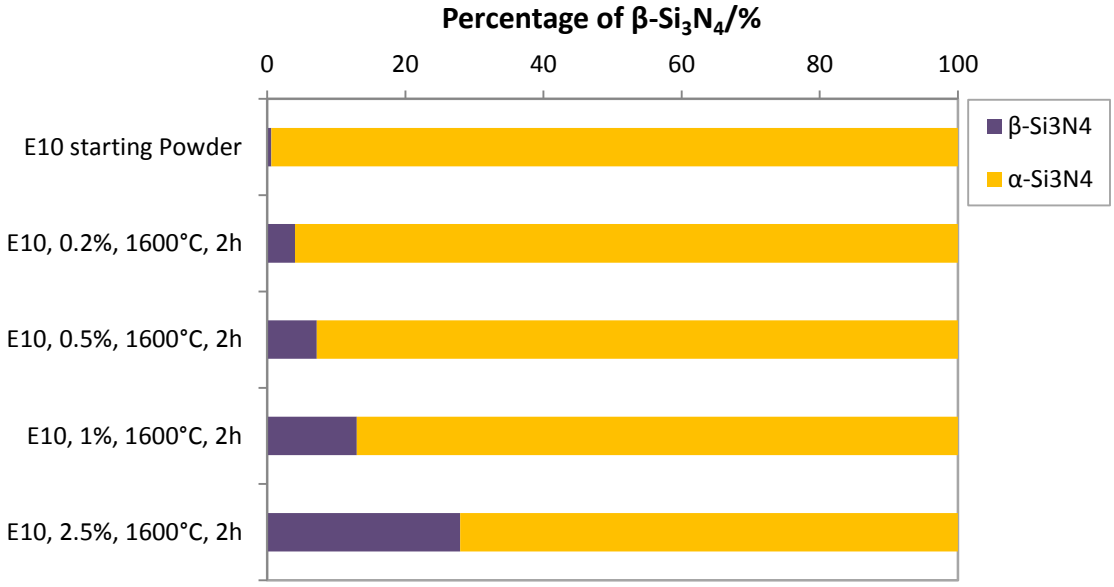

Figure 21: Percentage of α – Si_3N_4 and β - Si_3N_4 in the starting powder and the different samples made of E10

5.3.4. Permeability of E10 specimens

Figure 22 shows the influence of sintering aid content on the permeability of sintered samples. The exact values can be seen in Table 7. With the decrease of sintering aid content from 2.5 % to 1 % the permeability increased. Further reduction leads to a higher standard deviation with lower reproducibility.

The mean value and the standard deviation were calculated with at least three samples.

Table 7: Permeability values for E10 sample with different SA

Sample	$k_{1ø}$ m^2	$k_{2ø}$ m^2
E10, 0.2 %, 1600 °C, 2 h	1.07E-15 ± 6.42E-16	2.02E-12 ± 2.33E-12
E10, 0.5 %, 1600 °C, 2 h	1.38E-15 ± 1.10E-15	4.01E-12 ± 4.79E-12
E10, 1.0 %, 1600 °C, 2 h	1.23E-15 ± 8.71E-17	2.40E-12 ± 5.34E-13
E10, 2.5 %, 1600 °C, 2 h	3.43E-16 ± 1.40E-16	1.23E-13 ± 3.14E-14

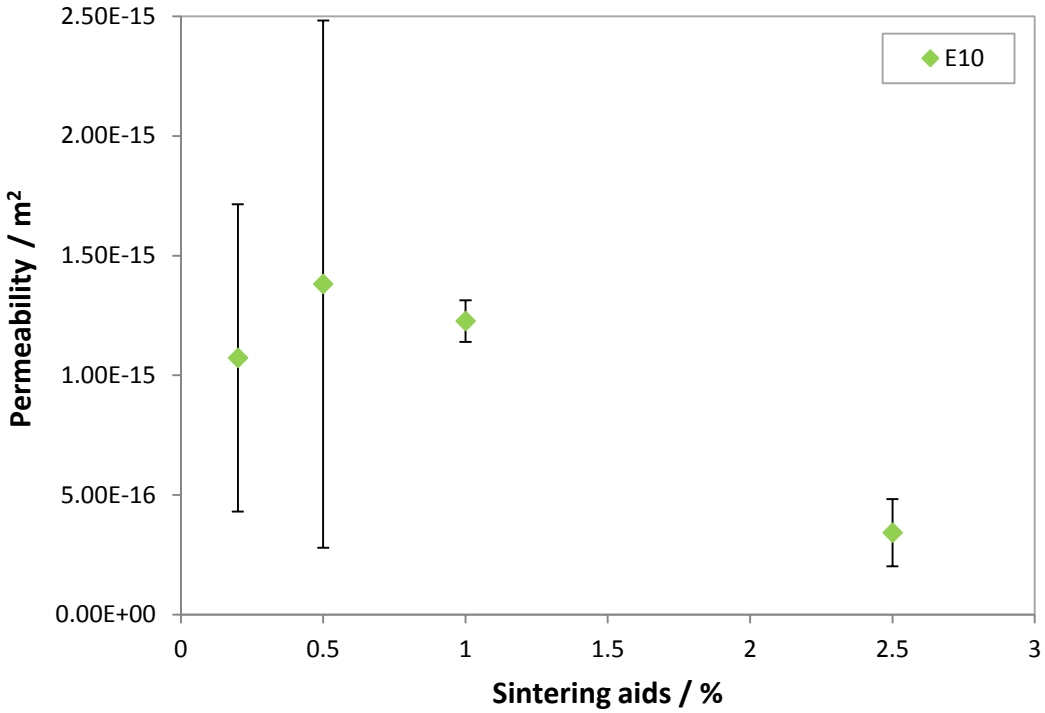

Figure 22: Influence of sintering aid content on the permeability of E10 –samples

5.3.5. Characteristic strength of E10 samples

Figure 23 shows an increase in the characteristic strength with an increasing amount of sintering aids. In Table 8 the exact values can be found.

The samples with 0.2 % and 0.5 % were very fragile which lead to difficulties in the preparation progress. They often broke prior to the measurement under the pressure applied by the construction. This is the reason why less than the desired 20 samples were measured.

Table 8: Characteristic strength and Weibull parameter for E10 with varied sintering aid content, (bracketed values represent the confidence interval for 95 %)

sample	n	Weibull $\hat{m}$ (D_l – D_u)	σ_0 (C_l – C_u)
E10, 0.2 %, 1600 °C, 2 h*	7	2.2 (0.8 – 3.4)	27.7 (16.6 – 48.0)
E10, 0.5 %, 1600 °C, 2 h*	18	3.2 (1.9 – 4.3)	50.4 (41.9 – 60.5)
E10, 1.0 %, 1600 °C, 2 h	21	3.4 (2.2 – 4.5)	102.4 (87.4 – 119.7)
E10, 2.5 %, 1600 °C, 2 h	23	3.2 (2.1 – 4.3)	153.2 (131.0 – 178.4)

** measured with the 100 kN cell used*

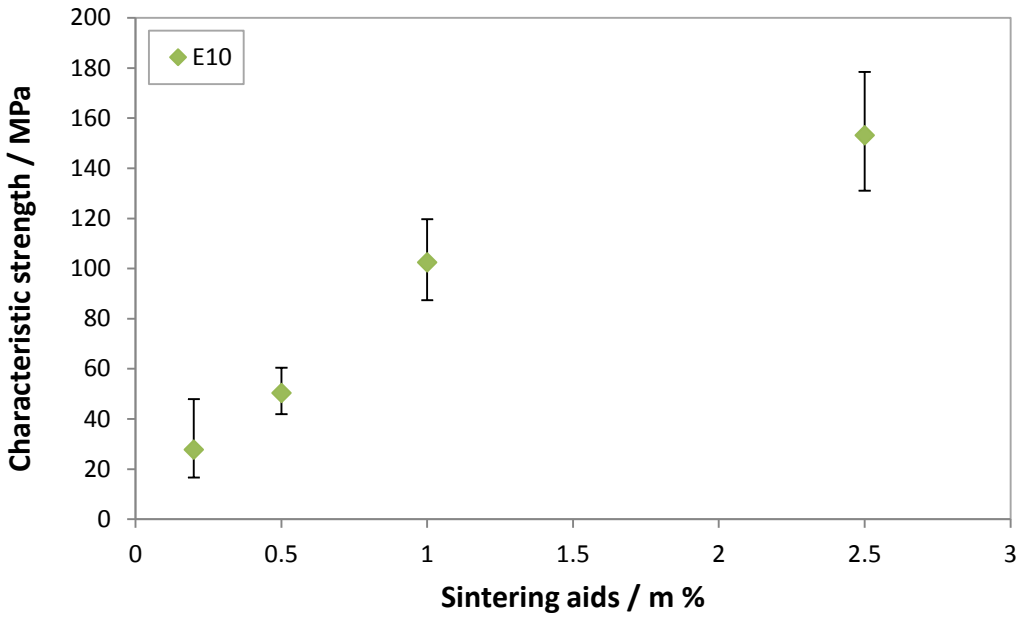

Figure 23: Influence of sintering aids on the characteristic strength with confidence intervall of E10 –samples

5.3.6. Discussion of results for E10 specimens

Influence of sintering aid content

Figure 24 shows that an increasing percentage of sintering aids leads to a decrease of the porosity along with the permeability. The values for the reproducibility of the permeability for 0.2 % and 0.5 % sintering aids are too low for a representative statement. The samples for 1.0 % and 2.5 % sintering aids had a higher reproducibility.

The porosity of the same samples had a high reproducibility throughout the whole range of sintering aids.

The permeability is further increased by an increase in median pore diameter observed for 1 % to 2.5 % sintering aids. As expected this leads to a decrease in porosity and to an increase of the characteristic strength.

Figure 25 shows that the increase in sintering aids also leads to an increase in the content of β-Si_3N_4 in the final materials. The reason for the different β- Si_3N_4 percentage at 0.5% SA is not known at this point.

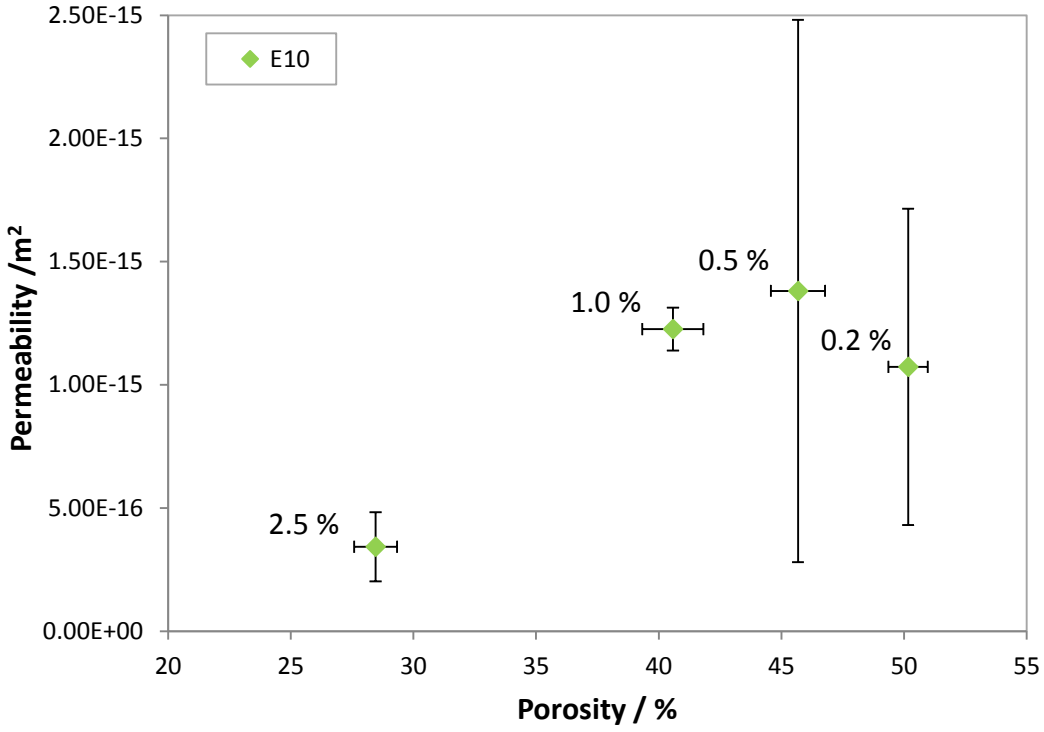

Figure 24: Influence of sintering aid content on the permeability and the porosity of E10 –samples with varied sintering aids

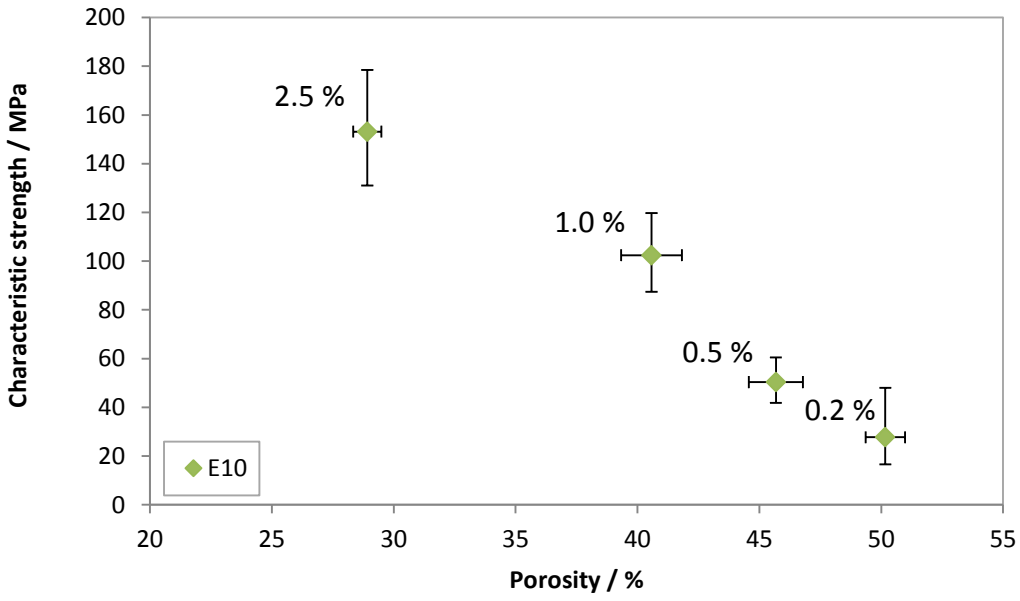

Figure 25: Influence of sintering aid content on the characteristic strength and porosity of E10 –samples

5.4. Parameter variation for Si_3N_4 - E03

With the compositions using E03 as a Si_3N_4 source the influence of sintering temperature and holding time on the desired parameters was determined. For the first experiment the influence of the sintering temperature was determined. Afterwards the holding time was increased.

5.4.1. Starting powder SN – E03

The second starting powder used was SN – E03. Table 9 shows the specifications according to UBE Industries and the measured values. E03 had a higher mean diameter of 1.6 µm compared to E10. The SEM picture in Figure 26 shows that the powder has equiaxed grains and no visible small fraction. The XRD measurement in Figure 27 shows that SN – E03 mainly consists of α –Si_3N_4 (99.9 %).

Table 9: Specifications and measured values for powder SN – E03

	Specifications (UBE Industries)	Datasheet Value (UBE Industries)	measured
β - Si_3N_4 (wt %)	<5	<5	0.1 %
N (wt %)	>38.0	>38	-
O (wt %)	<2.0	0.67	-
Crystallinity	>99	>99.5	-
d(0.5) (µm)	-	-	1.6

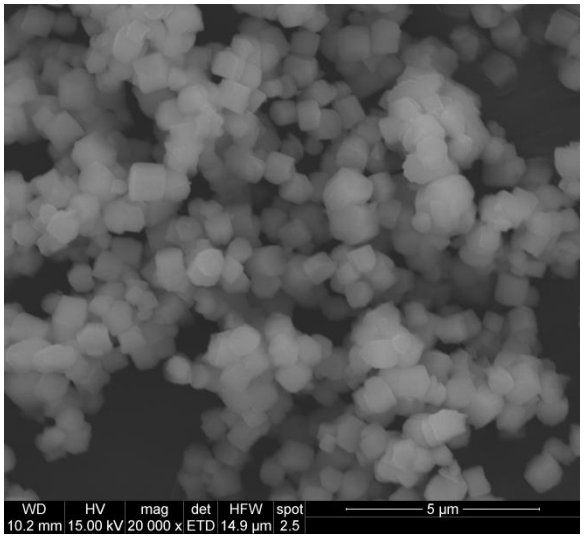

Figure 26: SEM Picture of Si_3N_4 Powder SN – E03

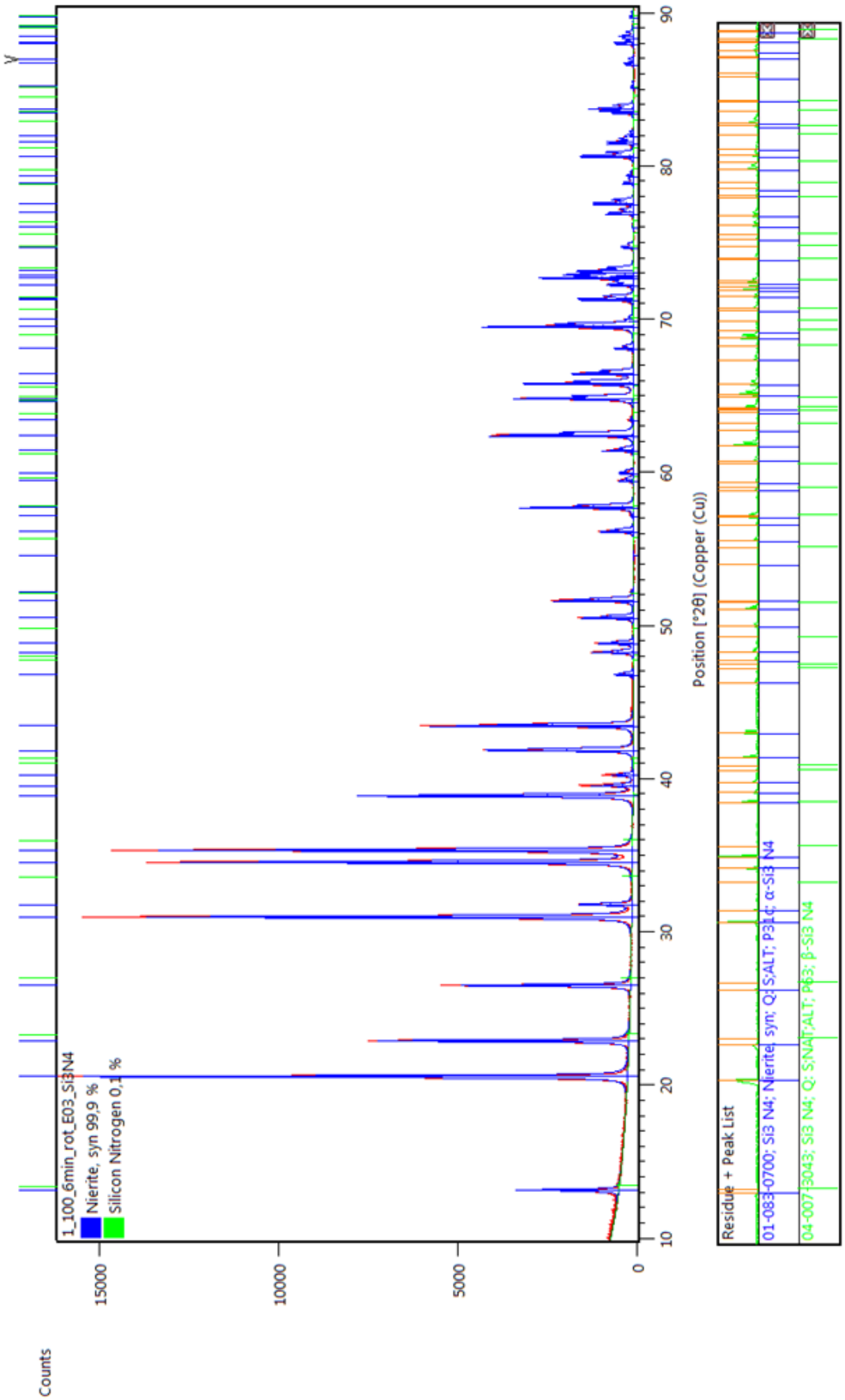

Figure 27: XRD measurement of Powder SN-E03; blue: α-Si_3N_4, green: β-Si_3N_4

5.4.2. Porosity, density and microstructure of E03 specimens

Figure 28 shows the dependency of porosity with respect to sintering temperature. Table 10 shows the exact values. Decreasing temperatures lead to an increase in porosity. The density stays the same for 1500 °C and 1500 °C and slightly decreases at a sintering temperature of 1600 °C. If the holding time at 1600 °C is extended from 2 h to 5 h, the porosity heavily decreases from 30.50 % to 5.98 %. This also goes along with a decrease in the density from 3.208 g/cm^3 to 2.903 g/cm^3.

With increasing temperature, the pore diameter decreases slightly. Increasing the holding time at 1600 °C from 2 h to 5 h reduces the pore diameter further. The mean value and the standard deviation were calculated out of at least three samples.

The pore diameter was measured only for one sample per composition.

Table 10: Porosity and density by water intrusion and median pore diameter by mercury porosity values for E03

	$\rho_{s\varnothing}$ g/cm^3	$\Pi_{a\varnothing}$ %	median pore diameter µm
E03, 2.5 %, 1500 °C, 2 h	3.211 ± 0.004	41.00 ± 0.59	0.3450
E03, 2.5 %, 1550 °C, 2 h	3.212 ± 0.000	38.14 ± 0.63	0.3361
E03, 2.5 %, 1600 °C, 2 h	3.208 ± 0.001	30.50 ± 0.50	0.2988
E03, 2.5 %, 1600 °C, 5 h	2.903 ± 0.040	5.98 ± 1.95	0.2779

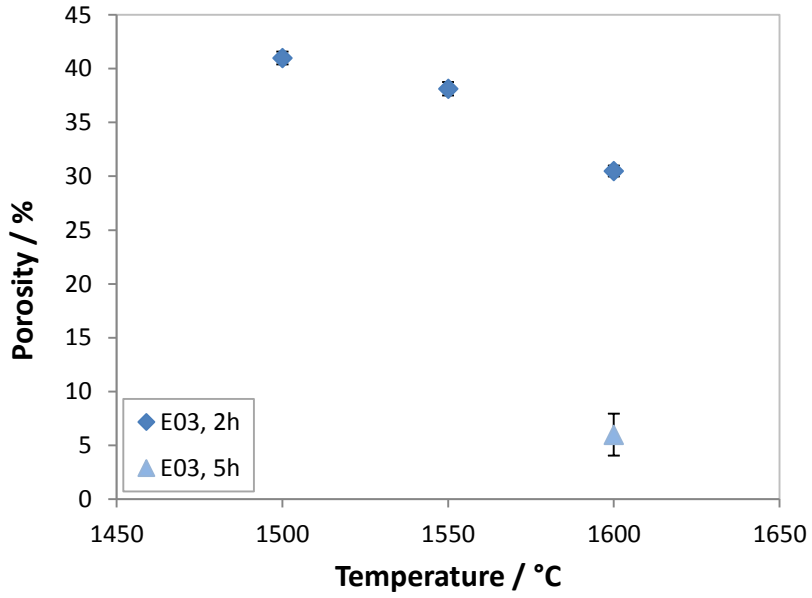

Figure 28 Influence of the sintering temperature on the porosity of E03 – samples with different holding time and 2.5 % SA

Figure 29 shows the SEM pictures of all E03 samples. For a holding time of 2 h, the grain shape of the fracture surface resembles the shape of the powder, at all temperatures. The grains are equiaxed. The fracture surfaces of grains in samples sintered at 1500 °C and 1550 °C look very similar. At 1600 °C, the fracture surface look more interconnected, and the surface appears rougher.

An increase of the sintering time to 5 h at 1600 °C completely changes the fracture surface. The surface seems to be sintered together, it also looks much denser. Also anisotropic rod-like grains begin to form. These grains are much bigger than the equiaxed grains previously observed.

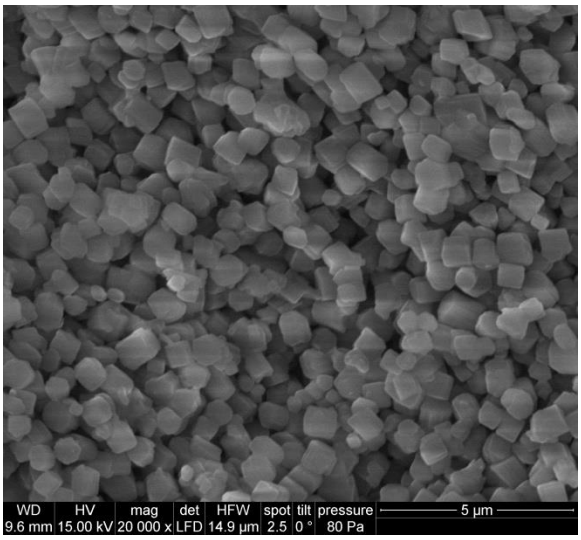

1500 °C, 2 h, 7E7

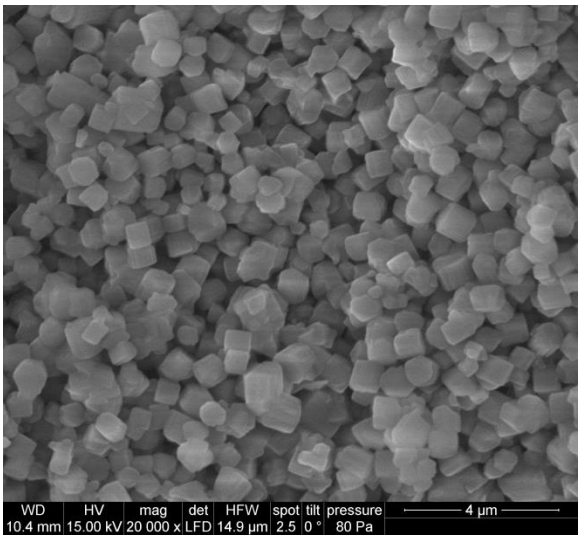

1550 °C, 2 h, 10B12

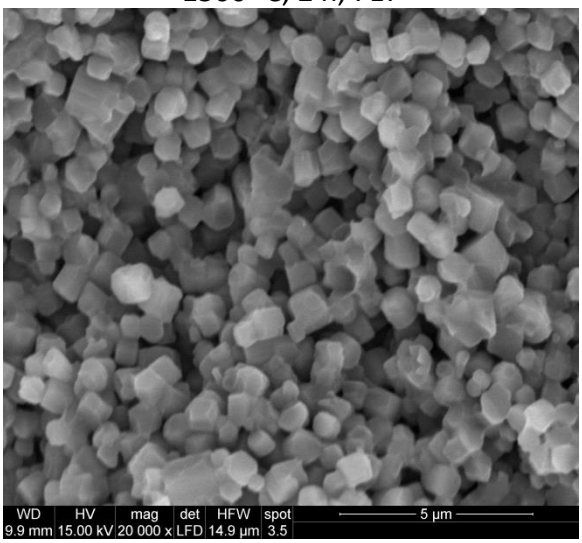

1600 °C, 2 h, 7A7

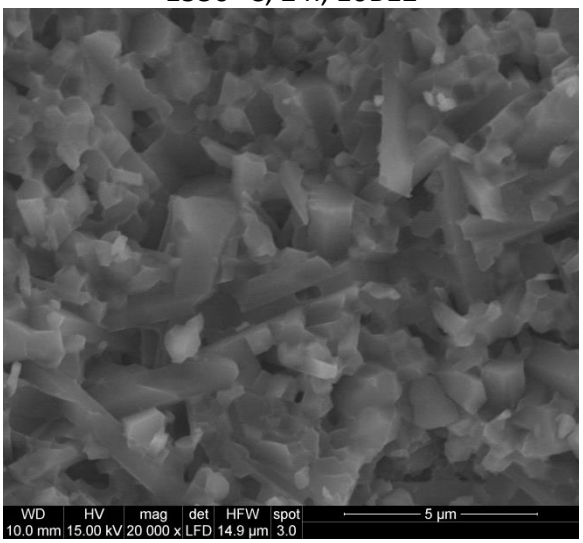

1600 °C, 5 h, 10E10

Figure 29: E03 samples with 2.5 % SA, with varying sintering temperature and holding time

5.4.3. Crystalline composition of E03 specimens

The starting powder SN-E03 consists nearly exclusively of α – Si_3N_4 (β- Si_3N_4 = 0.1 %). After sintering at 1500 °C, 1550 °C and 1600 °C the percentage of β- Si_3N_4 increases but stays around the same level for the whole range of sintering temperatures. Increasing the holding time from 2 h to 5 h leads to a β- Si_3N_4 percentage of 43.5 %. In Figure 30 the α/β ratios of all samples made out of E03 determined by Rietveld refinement of the XRD data can be found.

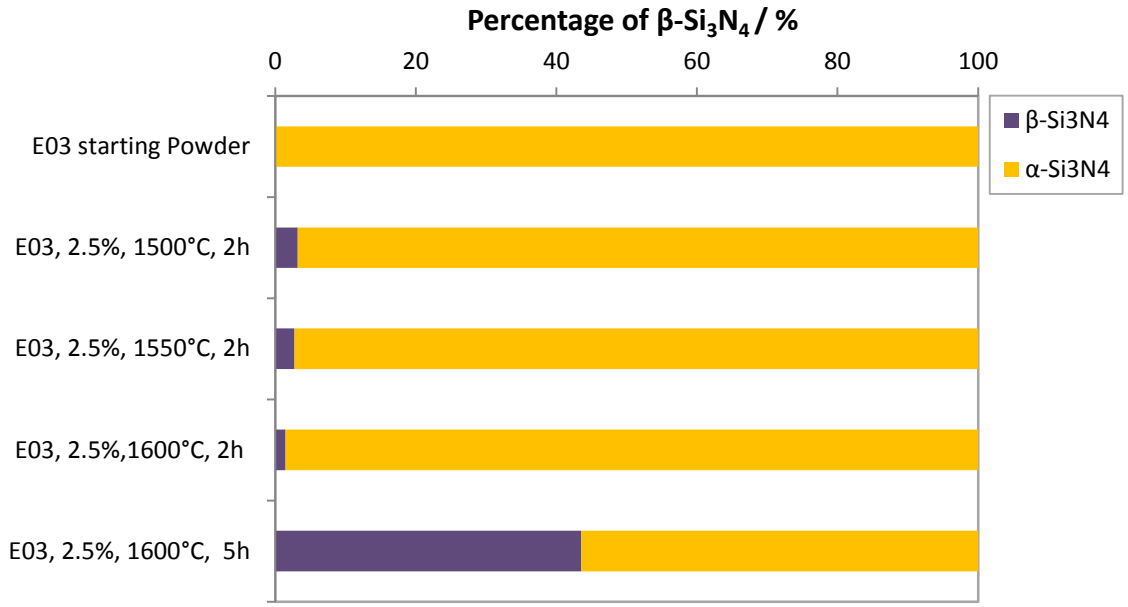

Figure 30: Percentage of α – Si_3N_4 and β- Si_3N_4 in the starting powder and the different samples made of E03

5.4.4. Permeability of E03 specimens

Figure 31 shows the influence of different sintering temperatures and different holding times on the permeability of E03 samples. The exact values can be taken from Table 11. With increasing temperature, the permeability decreases. At 1600 °C, increasing the holding time from 2 h to 5 h leads to a strong decrease in the permeability.

The mean value and the standard deviation were calculated with at least three samples.

Table 11: Permeability values for E03 – samples with different sintering temperature and holding time

Sample	$k_{1ø}$ m^2	$k_{2ø}$ m^2
E03, 2.5 %, 1500 °C, 2 h	1.88E-15 ± 6.41E-17	5.61E-12 ± 1.08E-12
E03, 2.5 %, 1550 °C, 2 h	1.47E-15 ± 7.78E-17	3.66E-12 ± 1.01E-12
E03, 2.5 %, 1600 °C, 2 h	8.82E-16 ± 8.76E-17	8.56E-13 ± 8.58E-14
E03, 2.5 %, 1600 °C, 5 h	5.99E-17 ± 3.94E-17	1.17E-14 ± 9.59E-15

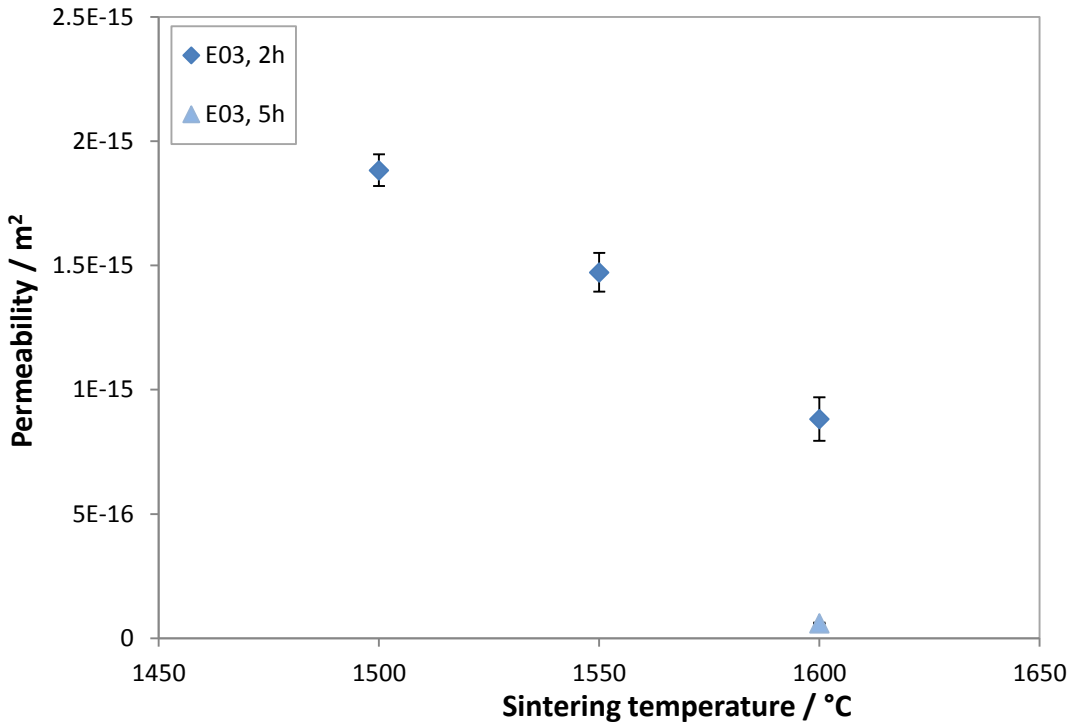

Figure 31 Influence of sintering temperature on the permeability of E03 –samples at different holding times (2.5 % SA)

5.4.5. Characteristic strength of E03 samples

As shown in Figure 32, a higher sintering temperature leads to a higher characteristic strength. Between 1500 °C and 1550 °C the characteristic strength increases slightly from 26.0 MPa to 39.4 MPa. Further increase of the sintering temperature to 1600 °C leads to an increase to 172.1 MPa.

Changing the holding time from 2 h to 5 h at 1600 °C increases the characteristic strength even further to 374.9 MPa. In this case, due to difficulties in the sample preparation, only four samples were measured. This number is too small to calculate the confidence interval according to European standard EN 843-5, which is why there are no values shown in Table 12 for the confidence interval for sample E03, 2.5 %, 1600 °C, 5 h.

Table 12: Characteristic strength and Weibull parameters for E03 samples at varying sintering temperature and holding time, bracket values represent the confidence interval for 95 % (#sample number too small)

Sample	n	Weibull $\hat{m}$ (D_l – D_u)	σ_0 (C_l – C_u) MPa
E03, 2.5 %, 1500 °C, 2 h	21	3.8 (2.5 – 5.1)	26.0 (22.6 – 29.8)
E03, 2.5 %, 1550 °C, 2 h	22	3.5 (2.3 – 4.6)	39.4 (33.9 – 45.6)
E03, 2.5 %, 1600 °C, 2 h	20	4.3 (2.7 – 5.8)	172.1 (151.6 – 195.1)
E03, 2.5 %, 1600 °C, 5 h*	4#	2.3 (-)	374.9 (-)

** measured with the 100 kN cell used*

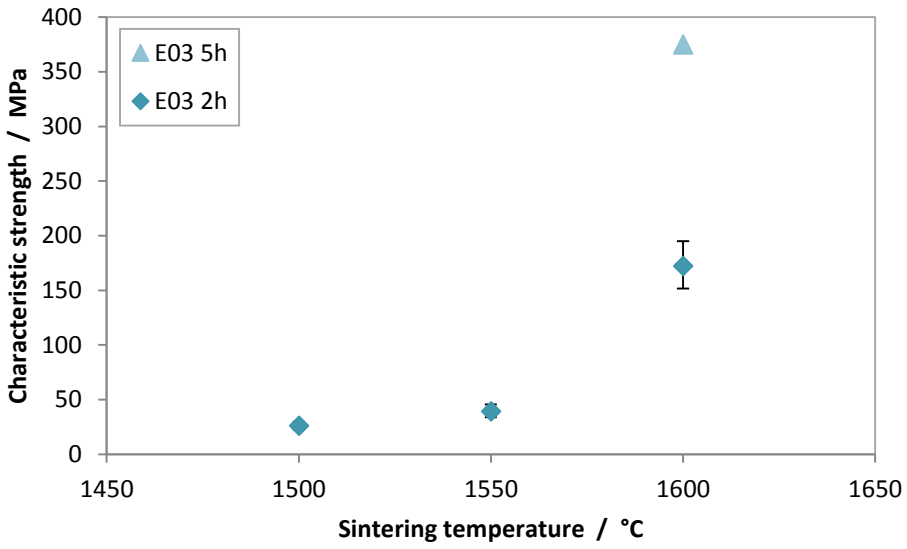

Figure 32: Influence of sintering temperature and holding time on the characteristic strength of E03 – samples

5.4.6. Discussion of results for E03 specimens

Figure 33 gives an overview of all data for compositions with E03 as Si_3N_4 source. Going from 1500 °C to 1550 °C, the porosity, median pore diameter and the permeability change to slightly lower values, and the characteristic strength increases. The SEM pictures complement the data available because in the pictures for 1500 °C to 1550 °C no change is visible.

By changing the sintering temperature from 1550 °C to 1600 °C, differences can be observed in the SEM images. The sintered area visible in the SEM images (Figure 29) suggests a higher characteristic strength which again complements the data. However, porosity, pore diameter and permeability decrease further.

Sintering for 5 h at 1600 °C yields a much denser sample, both shown in the data. In the SEM picture, anisotropic rod-like grains are visible. These rods are usually seen in β - Si_3N_4.[4] This fits to the observation of the XRD measurement, shown in Figure 30, with an increase of β – Si_3N_4 content to 43.5 %.

This, together with the low porosity, could be an explanation for the high increase in the characteristic strength and decrease in permeability and pore diameter.

Although the samples sintered at 1500 °C had the highest permeability, their low characteristic strength renders them it too fragile for the intended purpose. The same holds true for the samples sintered at 1550 °C. The samples sintered at 1600 °C for 5 h exhibit a low porosity and therefore a low permeability, also not suitable for the prospective application.

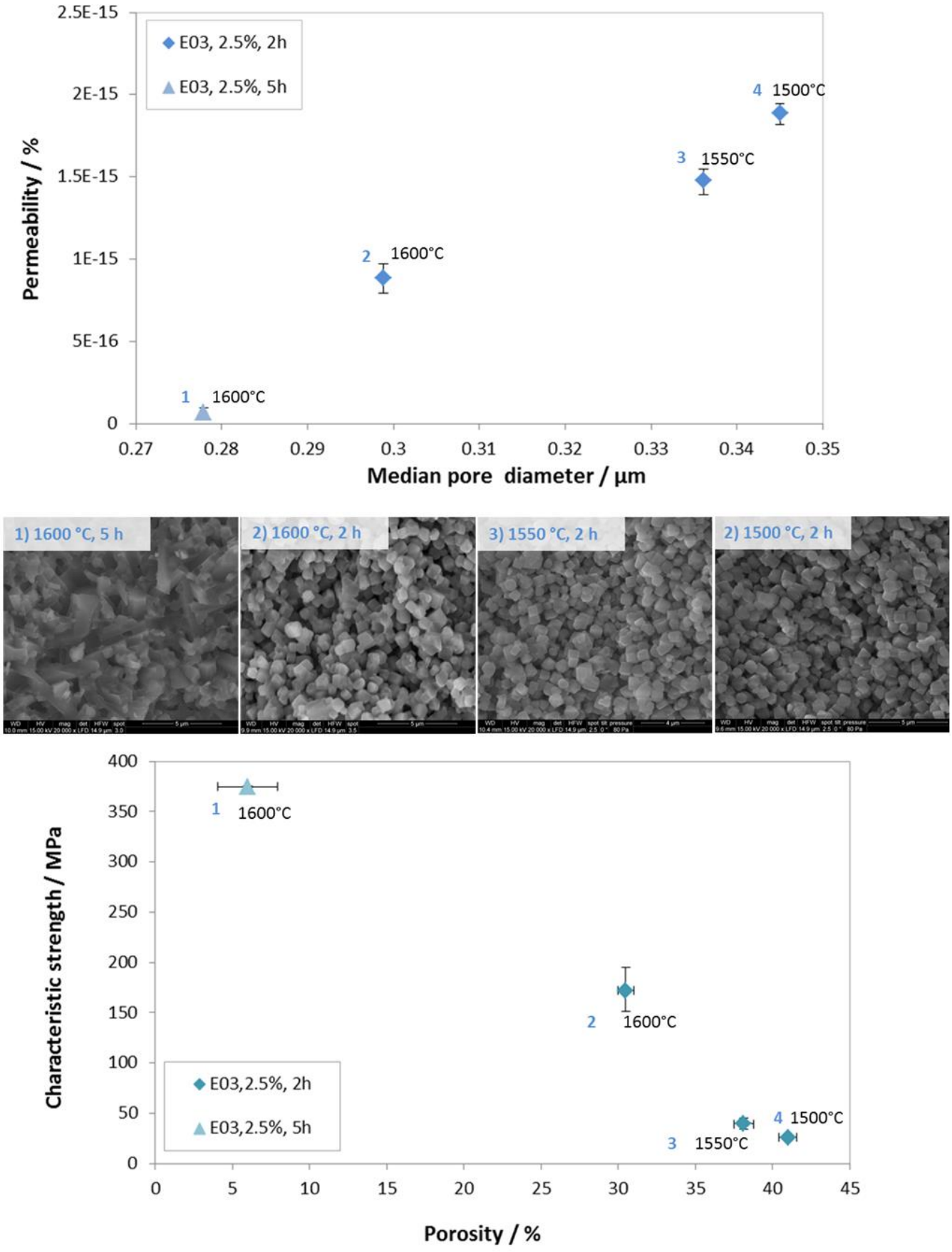

Figure 33: Influence of sintering aids on the permeability and characteristic strength (bottom) and porosity and characteristic strength (top) of E03 –samples

5.5. Parameter variation for Si_3N_4 XP06

With the compositions containing XP06 powder the influence of sintering temperature, sintering aid content and holding time on the desired parameters were investigated, using a starting powder with a higher initial β – Si_3N_4 content.

During the first experiments the influence of the sintering temperature was observed. Afterwards the holding time was increased. The final two compositions were made with the previous experiments in mind and were a combination of the previous parameter changes.

5.5.1. Starting powder SN – XP06

The third powder investigated was XP06. It has a higher β – Si_3N_4 to α – Si_3N_4 ratio. The mean particle diameter was close to the one of E03.

Table 13 shows the specifications and datasheet values according to UBE Industries and the measured values. The XRD measurement in Figure 35 shows that the powder consists of 11.7 % β – Si_3N_4. Two fractions can be seen in the SEM picture, a bigger one in the range of the measured value, and a smaller around it. The laser diffraction analysis shows only one fraction.

Table 13: Specifications and measured values for powder SN – XP06

	Specifications (UBE Industries)	Datasheet Value (UBE Industries)	measured
β – Si_3N_4 (wt %)	≤ 30	< 30	11.7
N (wt %)	≥ 38.0	>38	-
O (wt %)	≤ 1.0	0.61	-
Crystallinity	≥ 99	≥ 99.5	-
d(0.5) µm	Reference Value	1.22	1.4

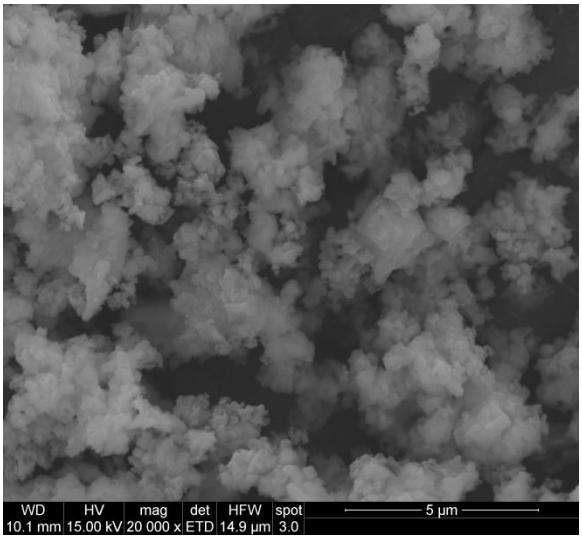

Figure 34: SEM Picture of the Si_3N_4 powder SN - XP06

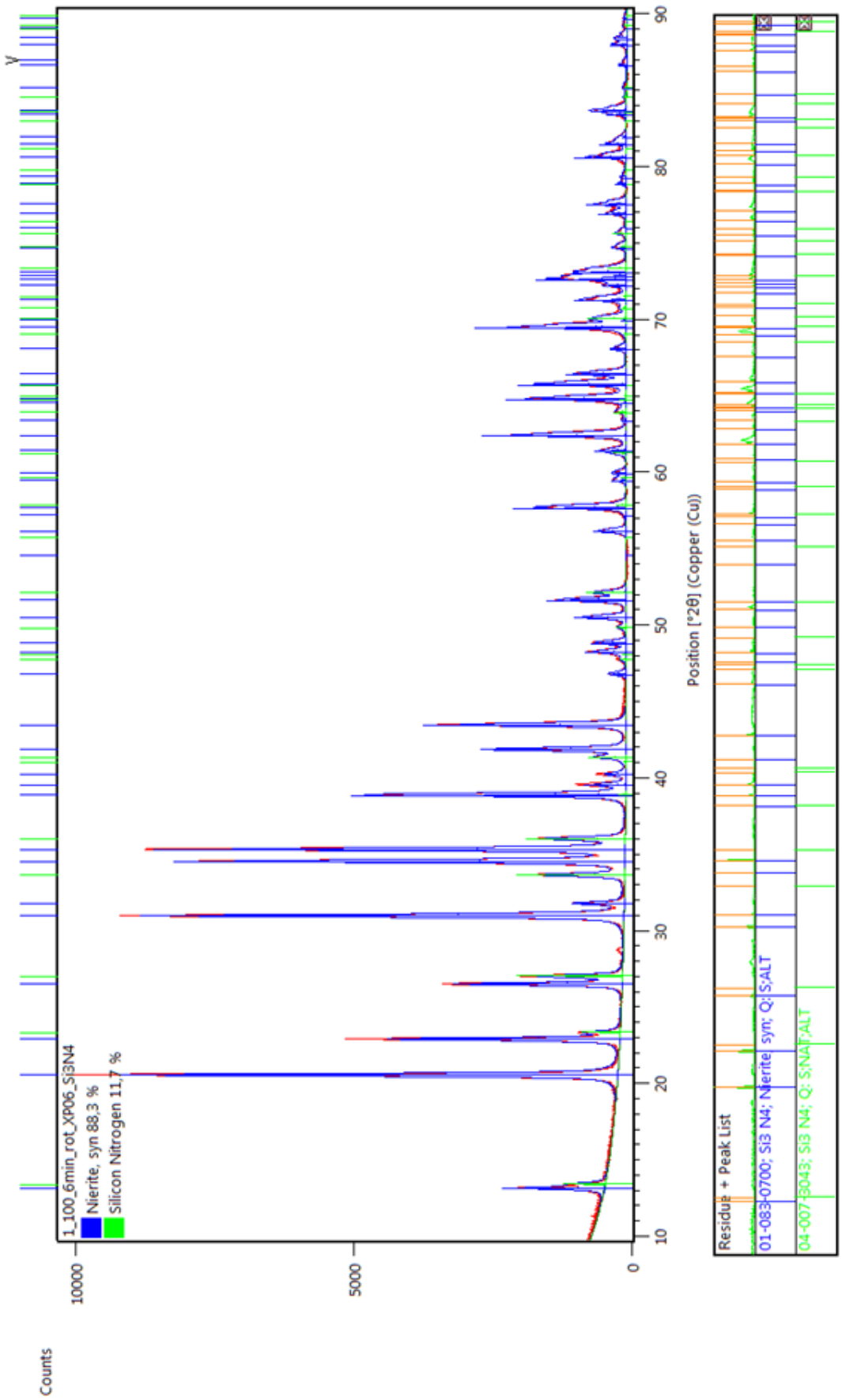

Figure 35: XRD of Powder SN-XP06; blue: α-Si_3N_4, green: β-Si_3N_4

5.5.2. Porosity, density and microstructure of XP06 specimens

Figure 28 shows the variation of porosity due to changing sintering temperature, holding time and sintering aid content. The according values can be found in Table 14.

The increase of the sintering temperature with unchanged holding time and SA content, leads to a decrease in porosity. The density stays the same between 1500 °C and 1550 °C and increases slightly at 1600 °C. The median pore diameter remains at the same level for 1500 °C and 1550 °C, but nearly doubles at 1600 °C.

At 1600 °C with 2.5 % SA and 5 h holding time, the porosity drops by nearly 8 % and the density decreases, the median pore diameter on the other hand increases further. If the SA contents in this composition were reduced to 1 %, the porosity and the density goes up to a level of the composition sintered at 1500 with 2.5 % SA for 2 h. However, the pore diameter more than doubled, reaching 0.63 µm.

With the next temperature change to 1700 °C with 1.0 % and 5 h holding time the porosity decreases again. The pore diameter further increases to 0.83 µm. Heating the sample to 1750 °C with 1.0 % SA content for 5 h leads to the same level of density and porosity. With the beginning disintegration in mind the pore diameter with 2 µm seems unlikely.

In Figure 38, SEM images of all compositions of XP06 specimens are seen. The first compositions contained 2.5 % sintering aids. At a sintering temperature of 1500 °C and 2 h holding time, the fracture surface looks like the powder shown in Figure 34. As before, two grain size fractions are visible. The SEM picture of 1550 °C and 2 holding time shows no visible change. The fracture surface changes a lot at a sintering temperature of 1600 °C for 2 h. The grain shape changes to mostly anisotropic rod-like. The pore structure looks much wider than before.

With a longer holding time of 5 h, the grain size and the pore size increased. The fracture surface appears to consist almost solely of anisotropic rod-like grains.

At the same sintering temperature and holding time, but with only 1.0 % sintering aid content, the fracture surface looks very similar to the one described for 2.5 % SA content, but with a larger pore size. The grain size appears smaller than before.

At 1700 °C for 5 h and with 1.0 % sintering aids, anisotropic rod-like grains grew again. The pore volume appeared to grow too. At 1750 °C the fracture surface looks denser and the grain size smaller.

Table 14: Porosity and density values for XP06 -samples

	$\rho_{s\varnothing}$ g/cm³	$\Pi_{a\varnothing}$ %	median pore diameter µm
XP06, 2.5 %, 1500 °C, 2 h	3.206 ± 0.003	46.32 ± 0.20	0.26
XP06, 2.5 %, 1550 °C, 2 h	3.207 ± 0.001	44.61 ± 0.27	0.27
XP06, 2.5 %, 1600 °C, 2 h	3.220 ± 0.005	39.13 ± 0.43	0.48
XP06, 2.5 %, 1600 °C, 5 h	3.072 ± 0.009	32.28 ± 0.53	0.54
XP06, 1.0 %, 1600 °C, 5 h	3.200 ± 0.003	44.49 ± 0.31	0.63
XP06, 1.0 %, 1700 °C, 5 h	3.141 ± 0.032	41.13 ± 0.20	0.83
XP06, 1.0 %, 1750 °C, 5 h	3.176 ± 0.008	40.47 ± 0.73	2.00*

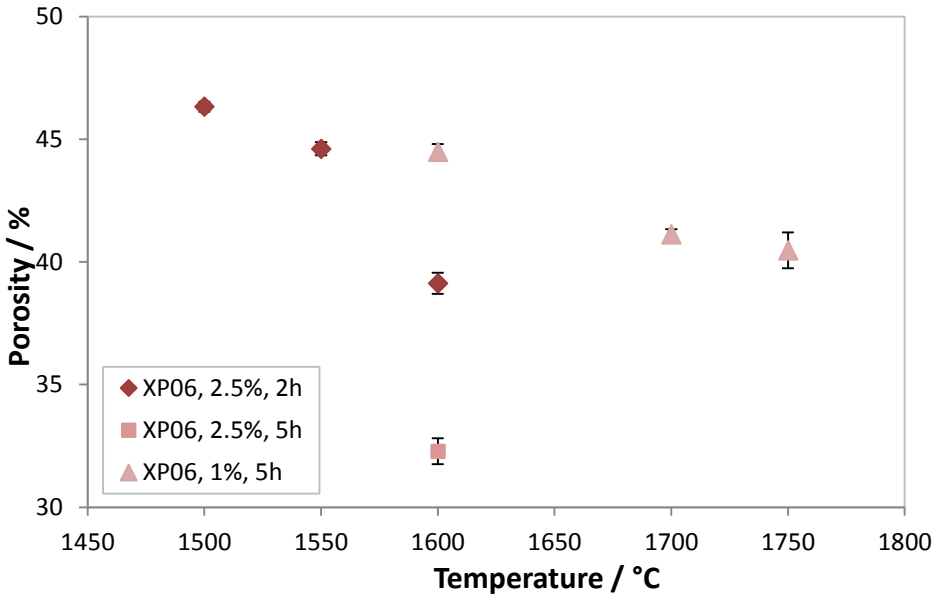

Figure 36: Influence of sintering temperature, sintering aid content and holding time on the porosity of XP06 -samples

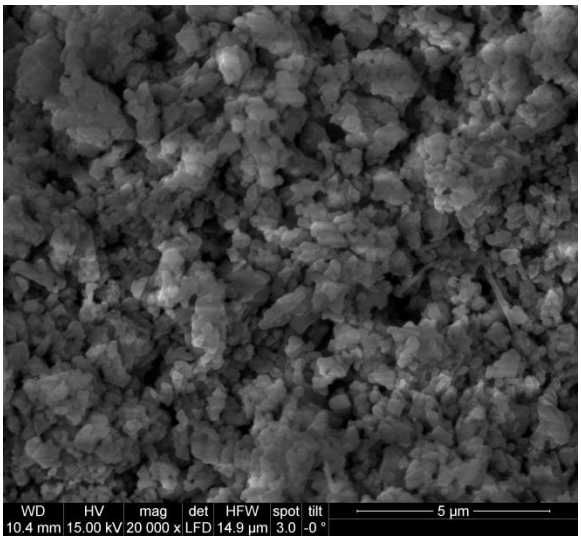

2.5 % SA, 1500 °C, 2 h, 9E10

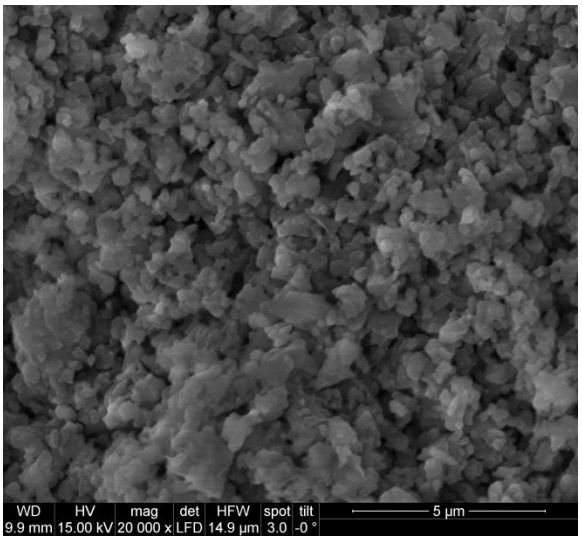

2.5 % SA, 1550 °C, 2 h, 9D9

Figure 37 : Fracture surface of XP06 samples with varying sintering temperature and sintering aid content and holding time (part1)

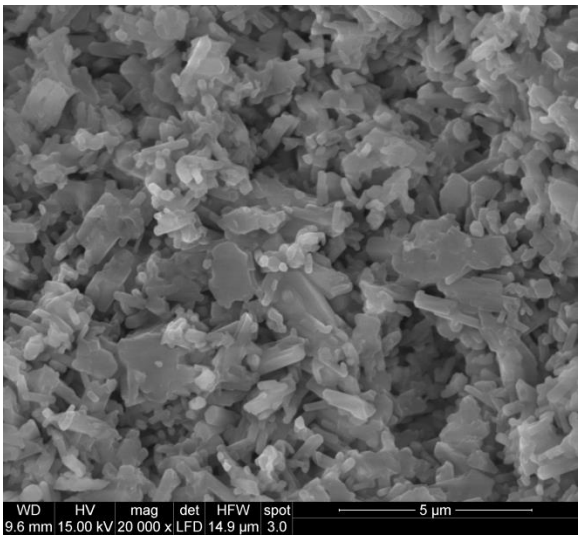

2.5 % SA, 1600 °C, 2 h, 6B6

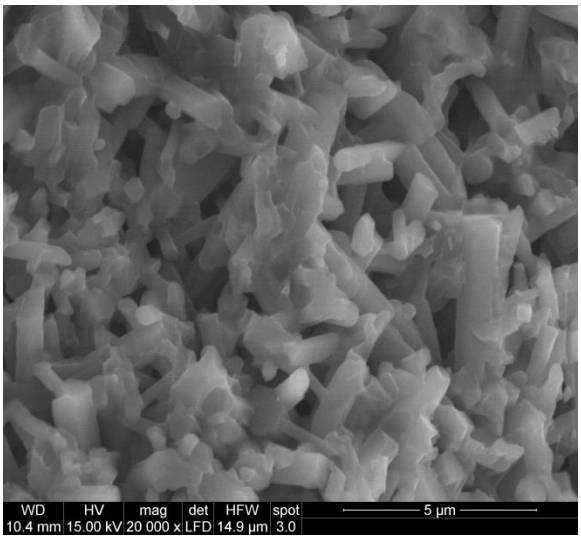

2.5 % SA, 1600 °C, 5 h, 9A11

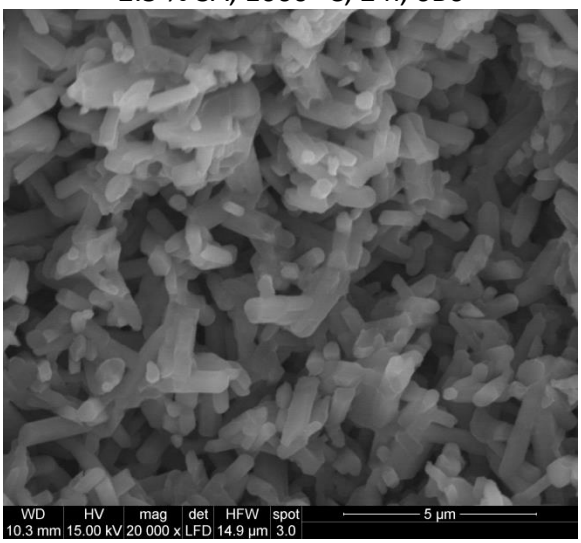

1 % SA, 1600 °C, 5 h, 11A14

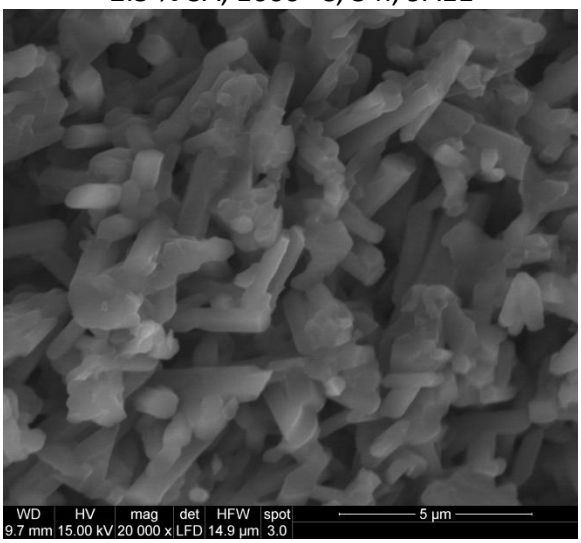

1 % SA, 1700 °C, 5 h, 11B15

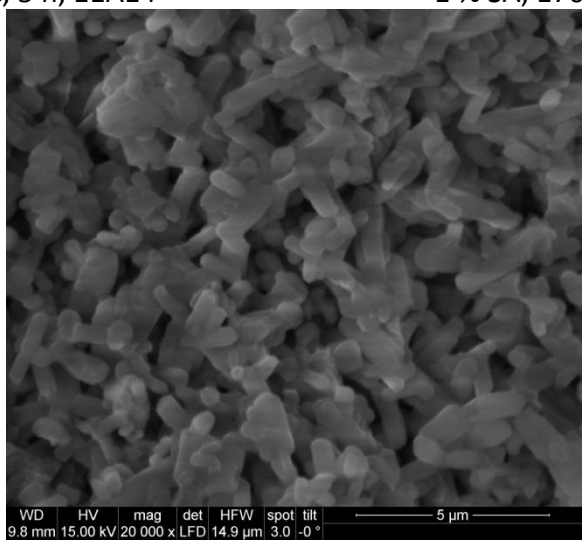

1 % SA, 1750 °C, 5 h, 14F2

Figure 38 : Fracture surface of XP06 samples with varying sintering temperature and sintering aid content and holding time (part2)

EDX analysis of XP06 1700 °C/1 %/5 h:

The samples sintered at 1700 °C with 1 % sintering aid content and 5 h holding time developed a second phase, made visible through a change in colour, from white to grey. This second phase is not visible in XRD measurements. In Figure 46 the polished surface in different magnifications is shown. EDX analyses were made of both areas. The results are shown in Figure 40 and Figure 41. The element distribution was as expected, except for the fact that yttrium wasn't found in any of the areas. There is no significant difference between the elemental distribution within the two areas.

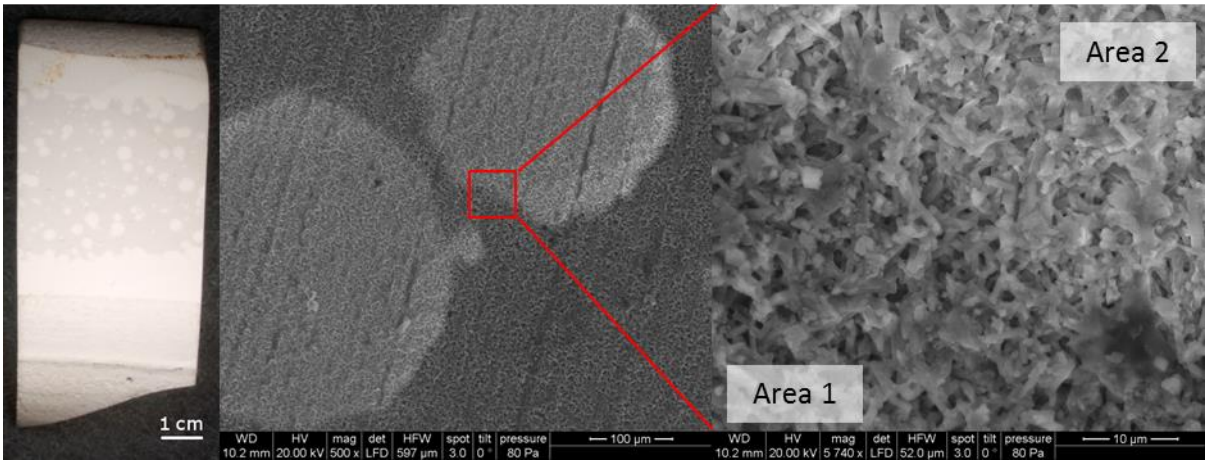

Figure 39: Different phases with different magnifications of the composition 1700 °C with 2.5 % at 5 h

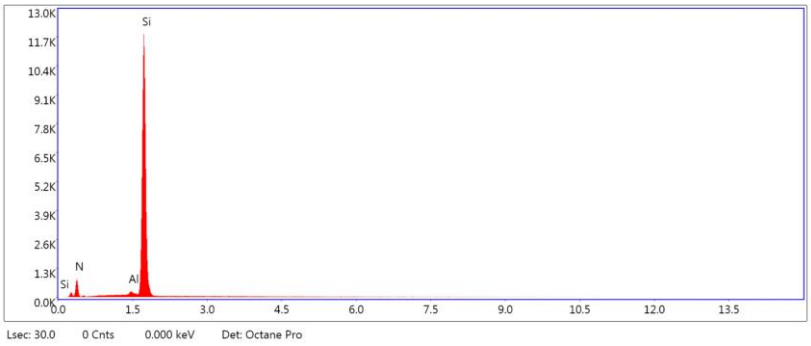

Element	Weight %	Atomic %	Net Int.	Error %	Kratio	Z	A	F
N K	38.28	55.41	189.22	10.64	0.0901	1.0772	0.2187	1.0000
AlK	1.23	0.92	65.20	7.51	0.0104	0.9296	0.8996	1.0143
SiK	60.50	43.67	3228.67	2.19	0.5439	0.9488	0.9474	1.0004

Figure 40: Results of Area 1, the grey phase (15kV acceleration voltage)

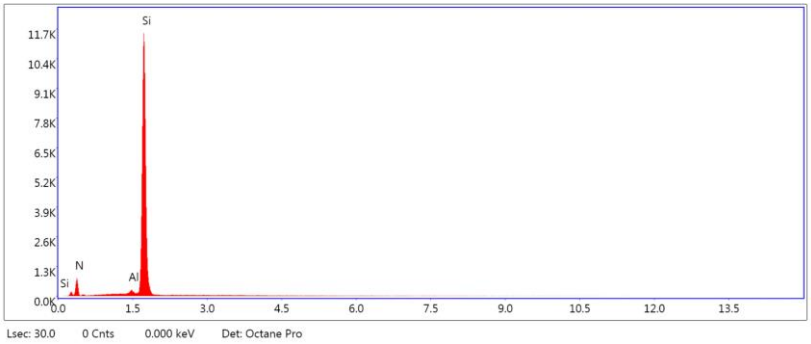

Element	Weight %	Atomic %	Net Int.	Error %	Kratio	Z	A	F
N K	37.82	54.93	182.40	10.68	0.0885	1.0779	0.2172	1.0000
AlK	1.18	0.89	61.52	7.49	0.0100	0.9302	0.9004	1.0143
SiK	61.01	44.19	3201.69	2.18	0.5493	0.9494	0.9483	1.0004

Figure 41: Results for Area 2, white phase: (15kV acceleration voltage)

5.5.3. Crystalline composition of XP06 specimens

As shown in Figure 35 the XP06 powder has a β - Si_3N_4 content of 11.7 %. In Figure 42 α to β - ratios of all XP06 compositions and the starting powder can be seen. The first two temperatures lead to a small increase of β - Si_3N_4. A sintering temperature of 1600 °C or above always leads to a high β - Si_3N_4 percentage. A small residue of α - Si_3N_4 is always left.

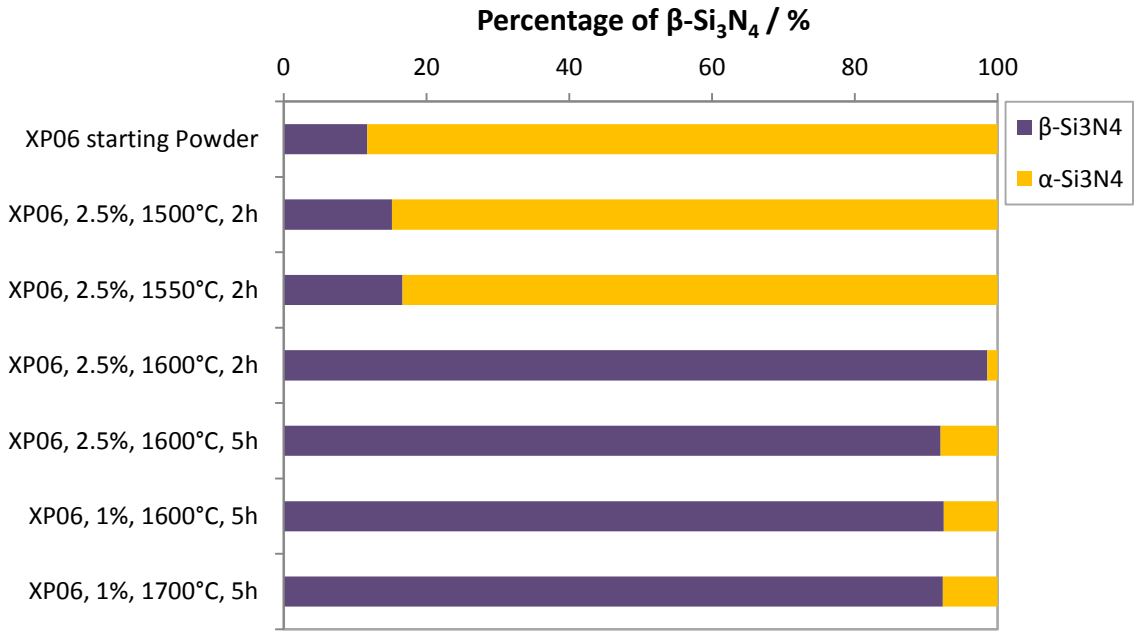

Figure 42: Percentage of α – Si_3N_4 and β- Si_3N_4 in the starting powder and the different samples made of XP06

5.5.4. Permeability of XP06 specimens

Figure 44 shows the influence of different sintering temperatures, sintering aid content and different holding times on the permeability of XP06 samples. The exact values can be taken from Table 15. For sintering temperatures 1500 °C and 1550 °C with 2.5 % sintering aids and 2 h holding time, the reproducibility is low. At 1600 °C with 2.5 % sintering aids and 2 h holding time the reproducibility is much higher, with a permeability that lies in the range of the two previous compositions.

Staying at 1600 °C and 2.5 % sintering aids but increasing the holding time to 5 h leads to a very similar result with a slightly higher standard deviation. The reduction of the sintering aids to 1 % leads to an increase in permeability. Sintering at 1700 °C with 1 % sintering aids and 5 h holding time increases the permeability further. Since the samples started to decompose at 1750 °C (see Figure 43) only one sample was measured for 1750 °C with 1% SA and 5 h holding time. The value lies in the standard deviation of the composition 1700 °C with 1 % SA and 5 h holding time.

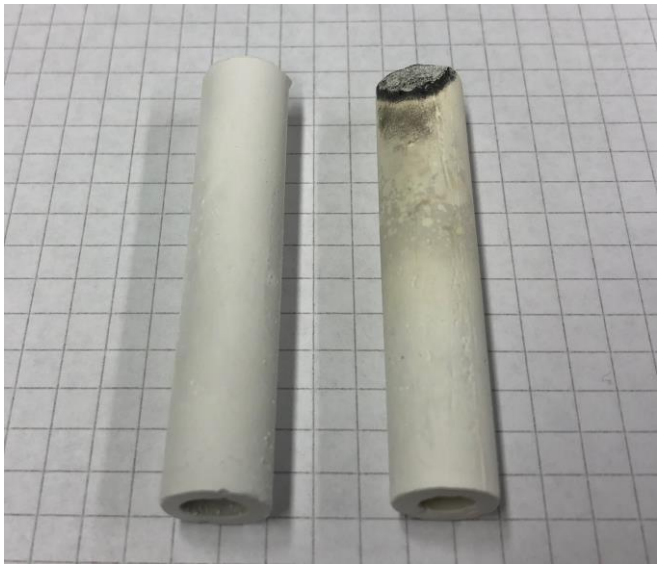

Figure 43: Comparison of a two XP06 samples with 1.0 % SA content and 5 h holding time, left: sintered at 1700 °C, right: sintered at 1750 °C with beginning decomposition

Table 15: Permeability values for XP06 – samples (* only one sample tested)

Sample	$k_{1ø}$ m^2	$k_{2ø}$ m^2
XP06, 2.5 %, 1500 °C, 2 h	2.59E-15 ± 1.50E-15	3.34E-12 ± 5.03E-13
XP06, 2.5 %, 1550 °C, 2 h	1.51E-15 ± 9.12E-16	2.60E-12 ± 1.49E-12
XP06, 2.5 %, 1600 °C, 2 h	1.76E-15 ± 8.15E-17	2.05E-11 ± 2.95E-12
XP06, 2.5 %, 1600 °C, 5 h	1.63E-15 ± 5.56E-17	1.25E-11 ± 4.46E-12
XP06, 1.0 %, 1600 °C, 5 h	3.13E-15 ± 2.31E-16	7.85E-11 ± 3.92E-11
XP06, 1.0 %, 1700 °C, 5 h	4.65E-15 ± 4.66E-16	5.43E-11 ± 3.60E-10
XP06, 1.0 %, 1750 °C, 5 h	4.89E-15	5.27E-11

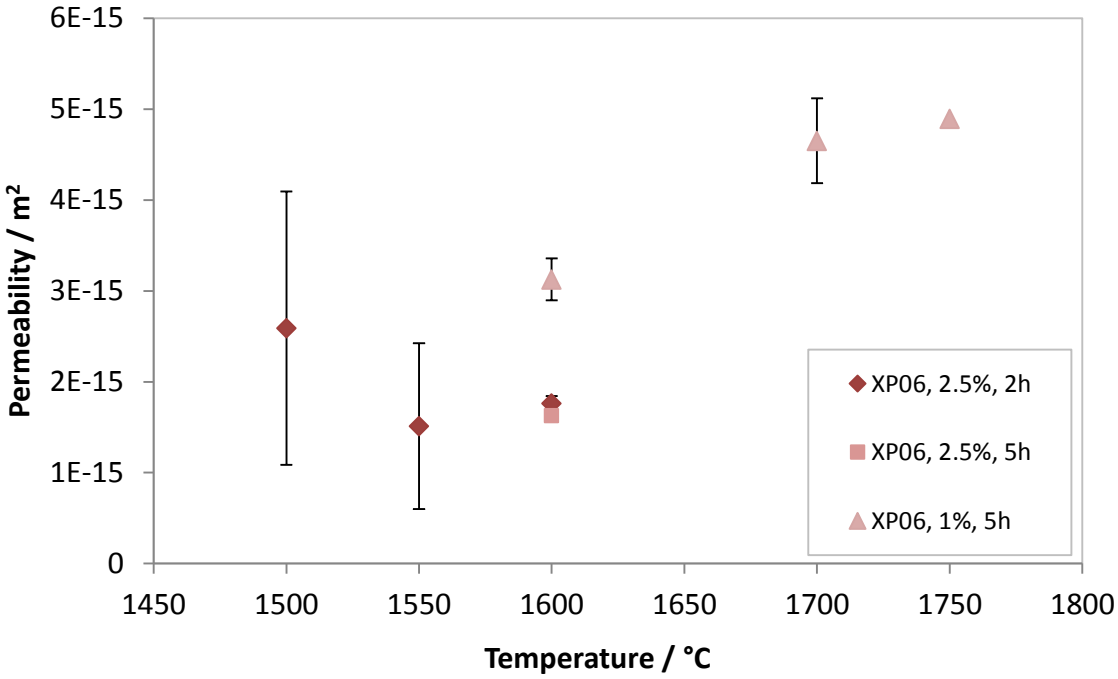

Figure 44: Influence of sintering temperature on the permeability of XP06 –samples with different holding time and SA contents

5.5.5. Characteristic strength of XP06 samples

Figure 45 shows the influence of different sintering temperatures, sintering aid contents and holding times on the characteristic strength of XP06 samples. The exact values can be seen in Table 16. With 2.5 % sintering aids and 2 h holding time, an increase in temperature from 1500 °C to 1600 °C results in an increase in characteristic strength. From 1500 °C to 1550 °C the strength roughly doubles, from 1550 °C to 1600 °C it triples.

Increasing the sintering time at 1600 °C from 2 h to 5 h makes no significant difference in the characteristic strength. Reducing the sintering aid content from 2.5 % to 1 % at the same

sintering temperature and holding time leads to a reduction of the characteristic strength. Increasing the temperature again, to 1700 °C, leads to a small increase in characteristic strength. Since the composition XP06, 1.0 %, 1750 °C, 5 h started to decompose, strength wasn't measured.

Table 16: Characteristic strength and Weibull parameter for XP06 with varied sintering aid content, sintering temperature and holding time, bracket values represent the confidence interval for 95 %

Probe	n	Weibull $\hat{m}$ (D_l – D_u)	σ_0 (C_l – C_u)
XP06, 2.5 %, 1500 °C, 2 h	20	3.9 (2.5 – 5.3)	34.9 (30.4 – 40.0)
XP06, 2.5 %, 1550 °C, 2 h	23	2.6 (1.7 – 3.4)	61.8 (50.8 – 74.9)
XP06, 2.5 %, 1600 °C, 2 h	23	2.0 (1.3 – 2.7)	185.4 (144.4 – 236.9)
XP06, 2.5 %, 1600 °C, 5 h	21	4.5 (2.9 – 6.0)	188.0 (166.9 – 211.4)
XP06, 1.0 %, 1600 °C, 5 h*	23	4.1 (2.7 – 5.4)	147.9 (130.8 – 166.9)
XP06, 1.0 %, 1700 °C, 5 h	23	8.0 (5.3 – 10.6)	163.1 (153.1 – 173.5)

** measured with the 100 kN cell used*

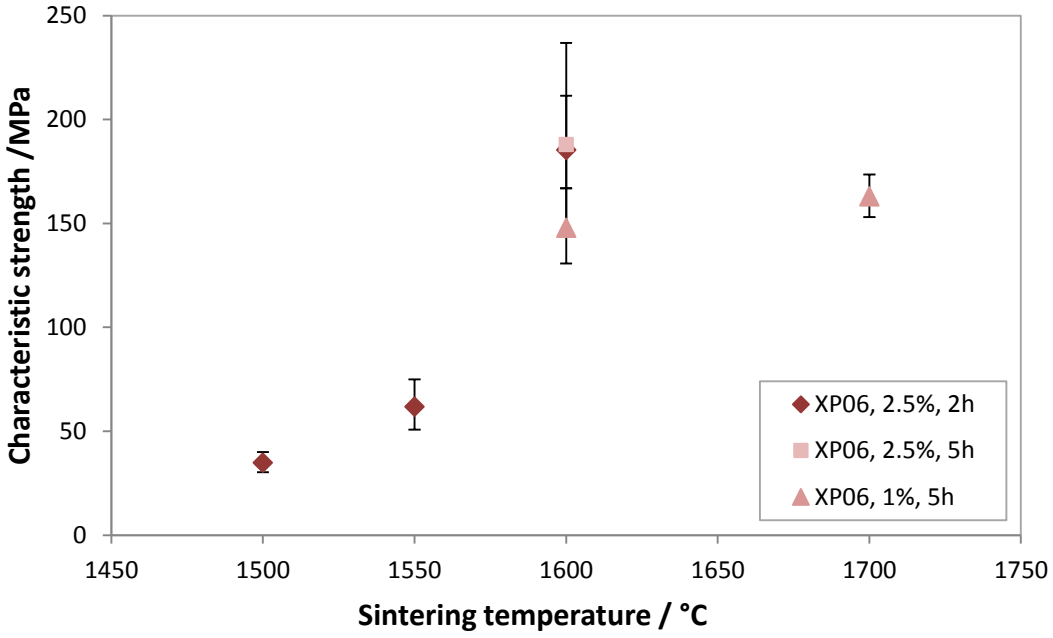

Figure 45: Influence of SA content, sintering temperature and holding time on the characteristic strength of XP06 –samples

5.5.6. Discussion of results for XP06 specimens

In Figure 46 a comparison of all samples with XP06 as Si_3N_4 source is shown. Starting with 2.5 % sintering aids and a holding time of 2 h, the temperature was increased from 1500 °C over 1550 °C to 1600 °C. The permeability of compositions sintered at 1500 °C and 1550 °C both showed low reproducibility. Porosity and the characteristic strength values of the same sample composition on the other hand had a high reproducibility and showed a decrease in porosity and an increase in characteristic strength. The median pore diameter stays on nearly the same level. Since the porosity had a high reproducibility it's most likely not the reason for low reproducibility of the permeability. The SEM pictures of the fracture surfaces look similar to the starting powder. The reason for the low reproducibility for the permeability is not known to this point.

An increase in sintering temperature from 1550 °C to 1600 °C leads to a comparable permeability, but with a lower decree of variation. The characteristic strength more than doubles and the porosity decreases. The morphology of the microstructure changes to anisotropic rod-like grains. The SEM images of the fracture surface suggest an increase in pore diameter. This observation is supported through the mercury intrusion results, which showed that the median pore diameter nearly doubled.

Changing the holding time from 2 h to 5 h leads to further increase of the median pore diameter. This again is consistent with the SEM picture, where it seems that the grains and the pore diameter grew in size. The porosity decreases on the other hand. The growth of the pore diameter seems to be enough to ensure that the permeability stays on the same level. The characteristic strength also stays on the same level, which could be explained with the grain growth.

Since previous experiments (see 5.4) showed that the reduction of sintering aid content leads to an increase in porosity and permeability, the next step was to reduce the sintering aids from 2.5 % to 1 %. The other parameters remained the same. This change leads, as predicted, to an increase in porosity and permeability.

The next test was conducted at a sintering temperature of 1700 °C with 1.0 % sintering aids and 5 h holding time, leading to a further increase of the median pore diameter and the permeability. The characteristic strength stays on the same level and the porosity decreases. With these process parameters two different phases are visible, one in grey and one in white.

The different colours could indicate that the sintering aids are not equally distributed.[4] To put this theory to the test EDX scans were conducted of both areas. There is no significant difference between the elemental distributions of the two areas. Yttrium wasn't found at all. Considering the low amount of 1 % of Y_2O_3 which leads to a Y content < 1 %, the contained percentage may be under the detection limit. An alternative explanation could be free silicon.[4]

Finally, the sintering temperature was increased to 1750 °C. As seen in Figure 43, this lead to a beginning decomposition of the samples.

In the literature, a higher sintering temperature was possible with applied N_2 pressure.[4] To observe the changes in the properties due to the decomposition all measurements except for characteristic strength and XRD were made. For this, the decomposed parts were removed. The measurements showed that everything nearly stays at the same level, which again shows the durability of the system. As seen in Table 14 the data shows an increase of the median pore diameter to 2 µm. Since the SEM picture in Figure 34 suggests a decrease, this is possibly because of the beginning decomposition of the sample. With the increase to 1750 °C the light grey phase, visible at 1700 °C, turns into a darker grey with no white circles.

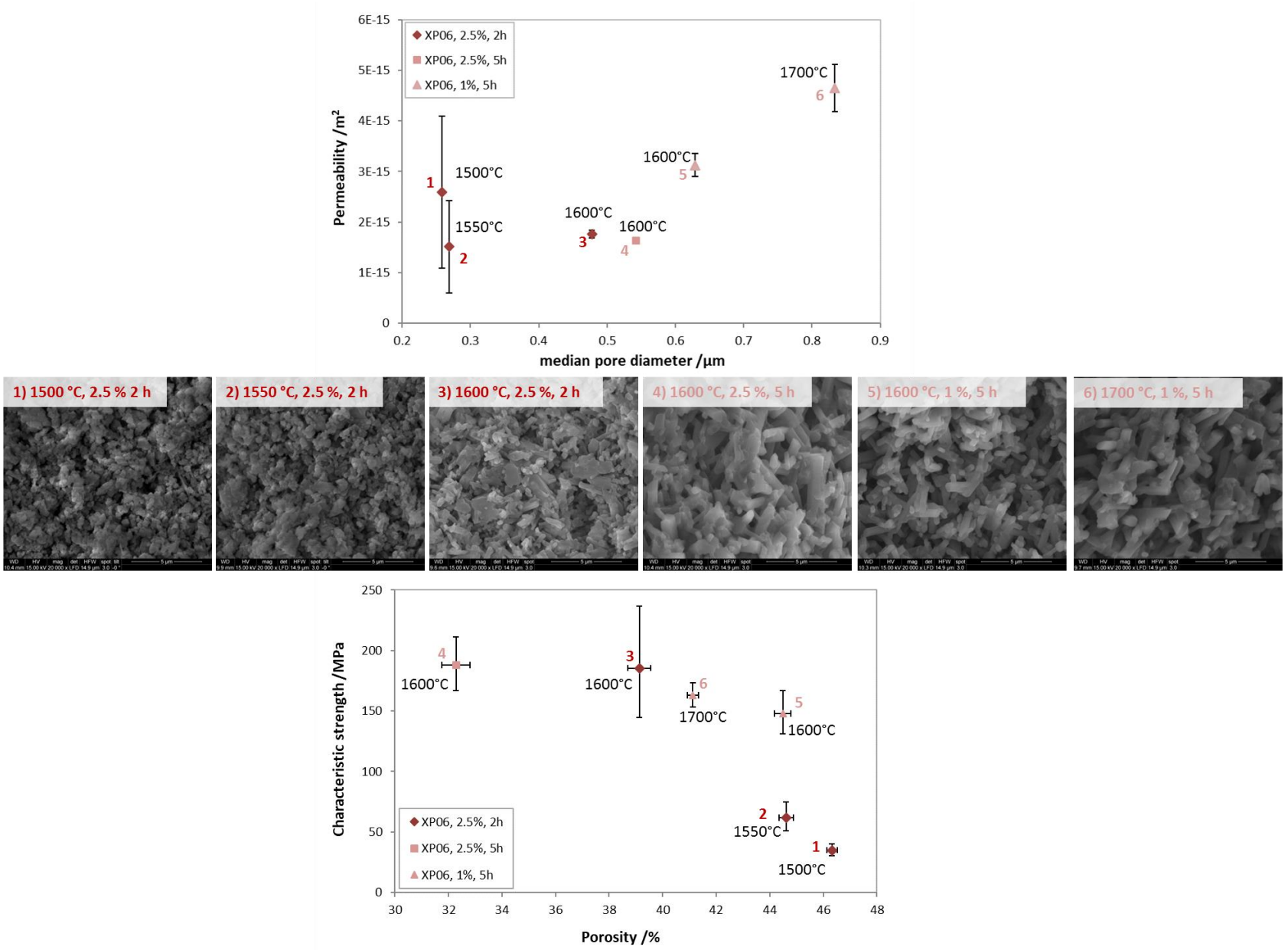

Figure 46: Influence of SA content, sintering Temperature and holding time on XP06 Samples

5.6. General Discussion

5.6.1. Density and porosity by water intrusion vs mercury intrusion porosimetry

The porosity of the sample was measured by water intrusion (EN 623-2) and mercury porosimetry. The mercury measurement provided two values for porosity. One was calculated via the intruded mercury and one was calculated using the skeleton density.

A comparison of these three values can be seen in Figure 47. The values achived are very similar. The only exception is the sample 10A11 (E03, 2.5 %, 1600 °C, 5 h). The reason for this is most likely the high density of the sample and the inaccessible porosity of 8.9%.

In this work, only the porosity determined by water intrusion was used. The advantage of revering to this measurement is, that for water intrusion every sample of each composition was measured. This made it possible to calculate an average and a standard deviation.

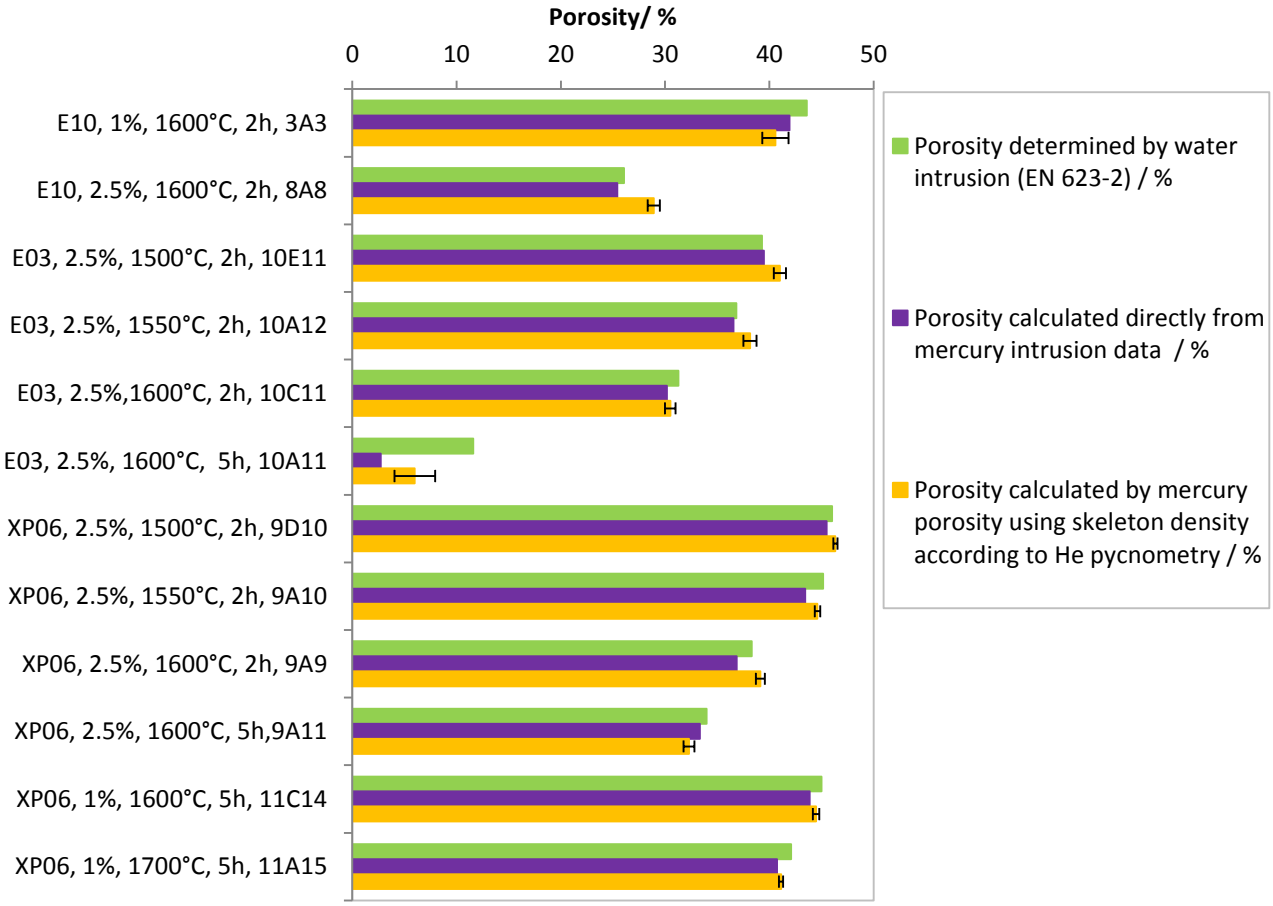

Figure 47: Comparison of the results of the different methods for the measurements of porosity

5.6.2. Variation of Si_3N_4 powder type

In this chapter the different types of powders are compared. The main differences between the three powders are the β – Si_3N_4 ratio and the particle size. E03 and E10 consist primarily of α – Si_3N_4, whereas XP06 has a β – Si_3N_4 content of 11.7%.
The particle size is comparable between XP06 and E03 (1.5 µm), whereas E10 has a particle size of around 1 µm diameter.

In Figure 48 and Figure 49, a comparison of specimens obtained from different powders can be seen. All other preparation parameters were kept constant. With the smallest particle size, E10 has the lowest median pore diameter and porosity. The increase of the particle size leads to a small increase in porosity and on increase of the median pore diameter. The permeability nearly doubles.

The samples made from XP06 had the highest porosity, permeability and median pore diameter. The characteristic strength of all samples stays at the same level. The fact that XP06 can maintain the same characteristic strength with increased porosity is most likely, due to the different microstructures. The anisotropic rod-like grains, only obtained in XP06, maintain stable while providing a greater median pore diameter. These different behaviours seem caused by the higher β – Si_3N_4 content of XP06. With a β – Si_3N_4 content, of 12 % rod-like grains start to form at 1600 °C. The XRD measurement shows that the sintered samples consist mostly of β – Si_3N_4.

With a holding time of 5 h another distinct difference between E03-samples and XP06-samples can be observed. While the porosity of the sample made of XP06 was reduced from 39.1 % to 32.3%, the porosity of the sample made of E03 drops from 30.5 % to 6.0 %. Again, the different β – Si_3N_4 contents in the starting powder with the resulting microstructure are the explanation.
The SEM images show that the microstructure compared to a sintering time of 2 h stayed nearly the same. Only the grain size increased slightly. The permeability and characteristic strength remained on the same level.
For E03 the microstructure changed extremely, now there are rod-like grains visible and the structure overall looks much denser, which leads to a strong decrease in permeability and a

strong increase in characteristic strength. XRD measurements showed that the β-Si_3N_4 content increased to 44 %.

As discussed before in chapter 5.3.6, the reduction of sintering aid content led to an increase in permeability and a decrease in characteristic strength. This is true for powders solely made up of α-Si_3N_4 and powders with a β-Si_3N_4 content of 12 %.

By increasing the holding time from 2 h to 5 h and decreasing the sintering aid content from 2.5 % to 1.0 % a higher permeability and the characteristic strength for XP06 samples were achieved.

Lastly, sintering temperature sets the samples apart. As discussed before, E03 samples densified from around 30 % porosity to 6 % at a holding time of 5 h at 1600 °C. Under the same conditions XP06-samples maintain their porosity and therefore the permeability stays on the same level.
Because of that behaviour XP06-samples were sintered at 1700 °C for 5 h with a sintering aid content of 1.0%. The samples confirmed the former observation and yielded a slightly less porous sample with a slightly better characteristic strength, a higher median pore diameter and a higher permeability.

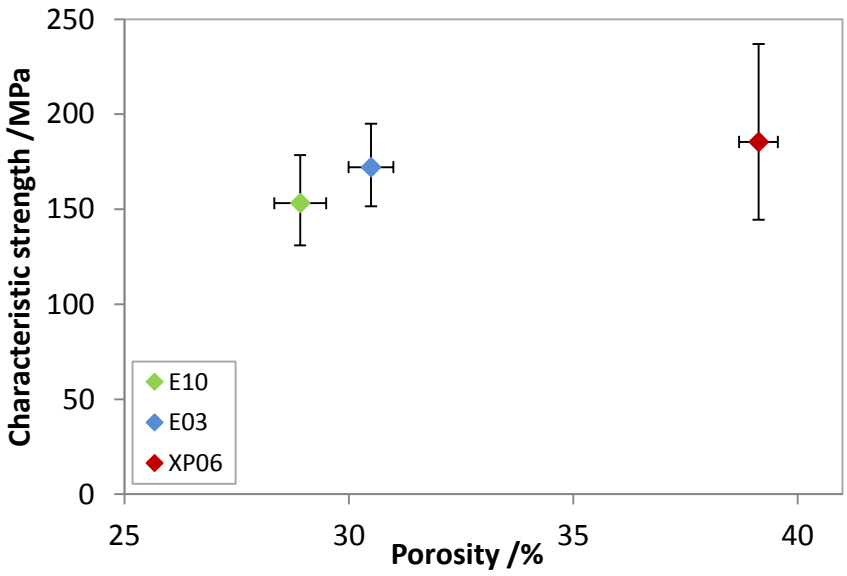

Figure 48: Comparison of characteristic strength and porosity of the different powder types (2 h at 1600 °C, with 2.5 % SA)

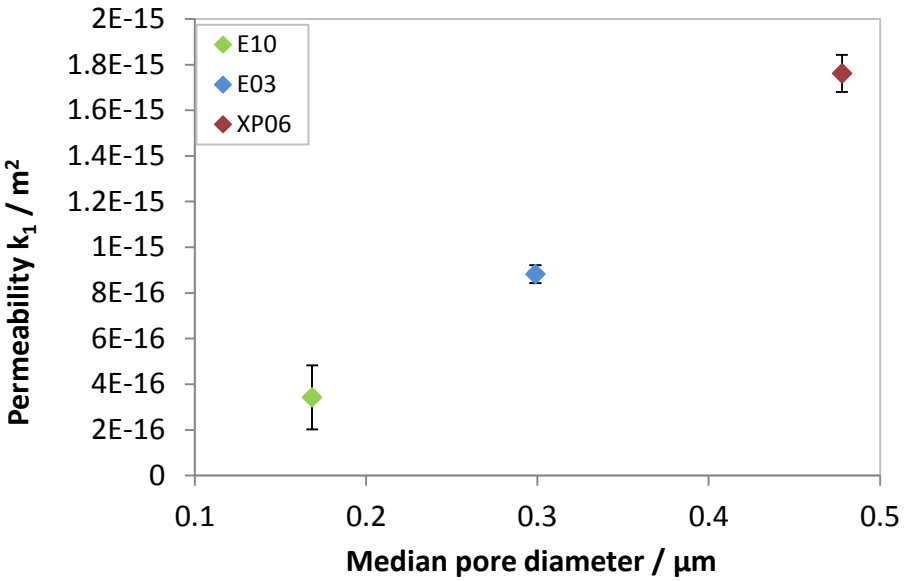

Figure 49: Comparison of permeability and porosity of the different powder types (2 h at 1600 °C, 2.5 % SA)

5.6.3. Comparison of the pore size distribution

Figure 50 features the pore size distribution determined via mercury porosimetry of four samples. In the figure three different samples with the same process parameters (2.5 % SA content, 1600 °C sintering temperature, 2 h holding time), except for the Si_3N_4 source are shown. The fourth sample features a completely different composition (1.0 % SA content, 1700 °C sintering temperature, 5 h holding time) with XP06 as Si_3N_4 source.

The pore size distributions of E10 and E03 appear very similar in shape, with E03 achieving the higher pore diameter. The shape of the pore size distribution of XP06 is slightly narrower than the one of E10 and E03 and features a higher pore diameter. It is interesting that the shape of the pore size distribution does not change, even if all process parameters are changed. At a sintering temperature of 1700 °C for 5 h with a SA content of 1.0 %, the only change is a shift of the distribution to higher pore diameters. This indicates that the pore structure is built up the same way.

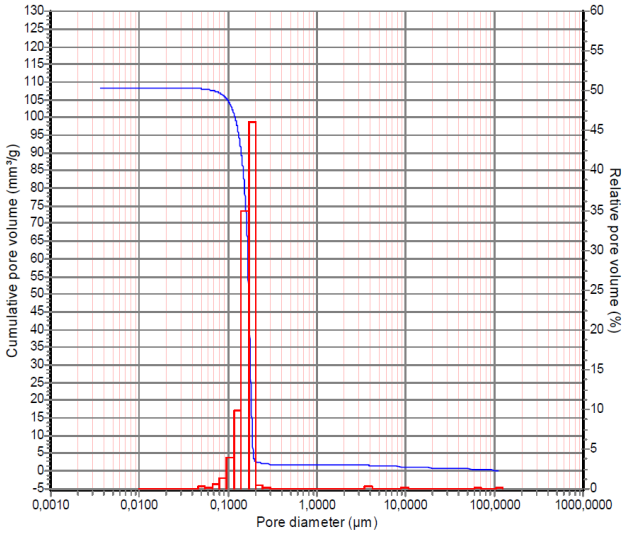

E10, 2.5 % SA, 1600 °C, 2 h, 8A8

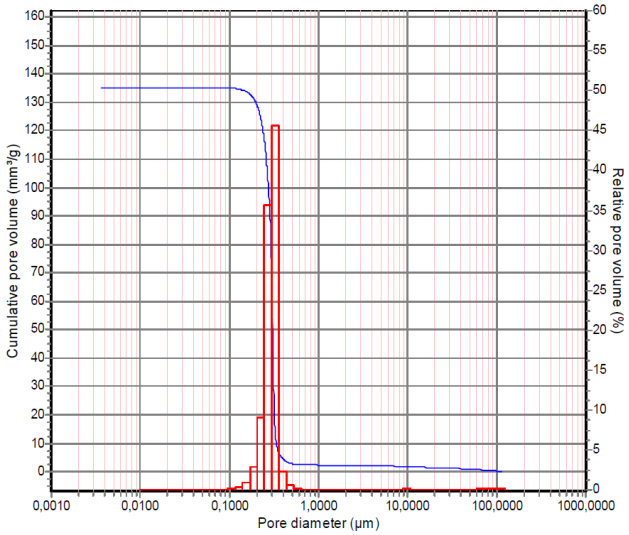

E03, 2.5 SA, 1600 °C, 2h 10C11

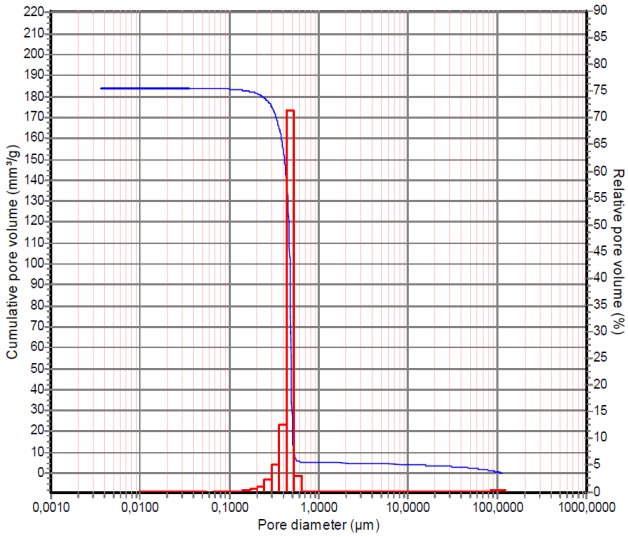

XP06, 2.5 % SA, 1600 °C, 2 h, 9A9

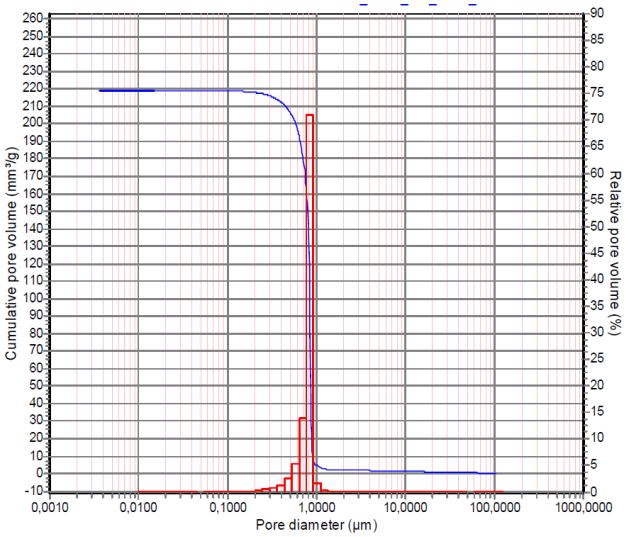

XP06, 1% SA, 1700 °C, 5 h, 11A15

Figure 50: Comparison of the pore size distribution of three samples with different Si3N4 sources and the final composition

5.6.4. Comparison of sample surfaces

The difference between the Si_3N_4 sources may be because of the different ways the pore structure is built up. As seen in Figure 51, the samples made from E10 and E03 are built up of equiaxed grains connected over necks. The particle size of the starting powder seems to make a sigificant difference in the pore size. The surface on the outside of the samples look like the fracture surface shown before. The surface on the outside of E10 and E03 samples look rougher than the inside, both featuring open porosity.

The XP06-samples are made from the rod-like elongated grains. Again, the fracture surface looks very similar to the surface on the outside and the inside. In contrast to the samples made from E03 and E10, the outside seems not rougher than the inside. A visible difference between fracture surface and the other two sides is the grain size. The outside and the inside features bigger grains for both XP06 with 2.5 % SA content at 1600 °C for 2 h and XP06 with 1.0 % SA content at 1700 °C for 5 h. Both out- and inside exhibits open porosity.

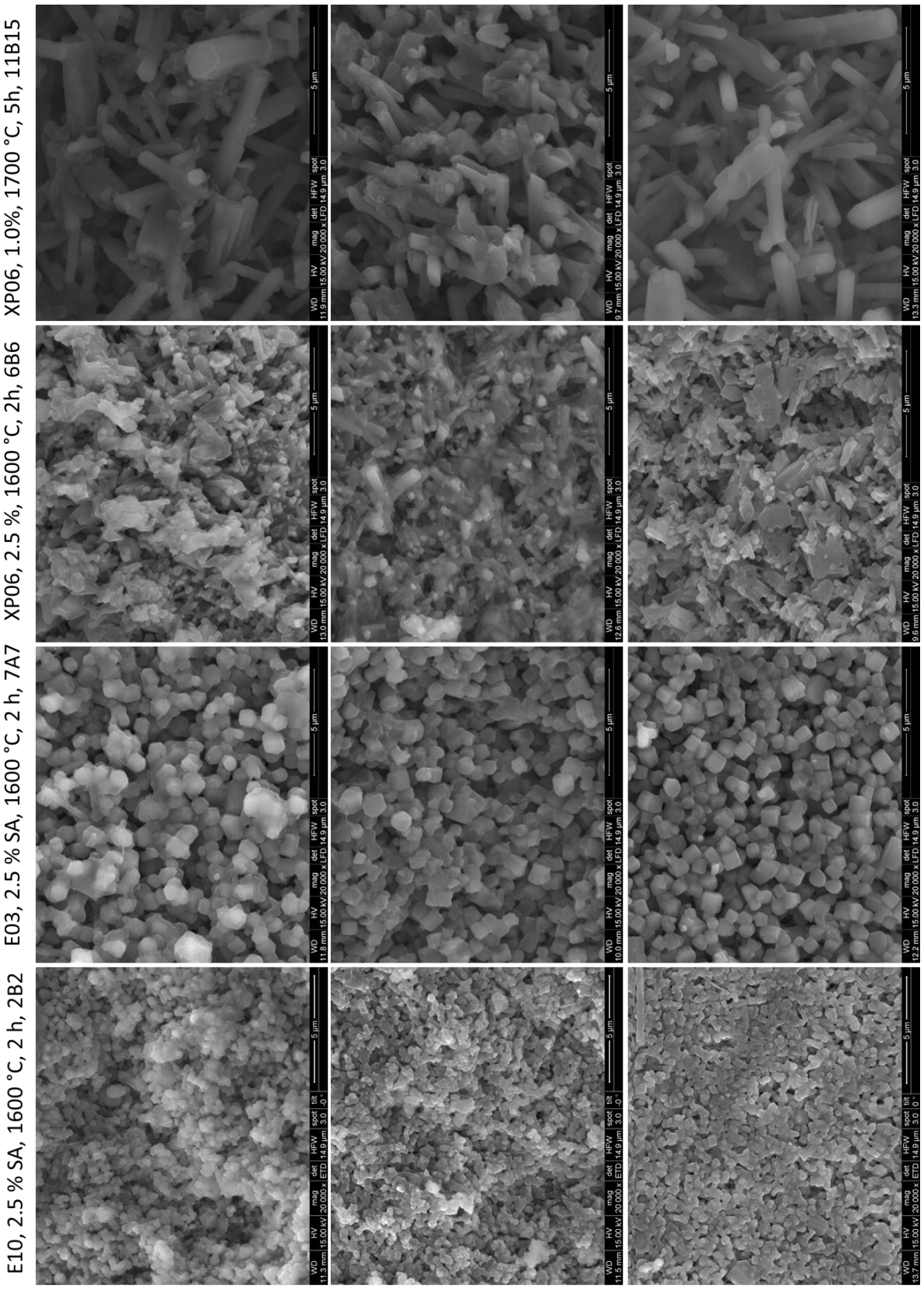

Figure 51: Comparison of SEM images of the outer tube surface, the fracture surface, the inner tube surface of four different samples

6. SUMMARY AND CONCLUSIONS

The aim was to manufacture tubular porous ceramic support structures with controlled open porosity. This structure should be used as a support material for silicon nitride layers with a finer porosity with a possible usage for membrane applications. The porosity was achieved via partial sintering and should be between 30 to 40 percent. The permeability should be maximised while the characteristic strength should remain sufficient for the application as membrane support.

Therefore, out of three different silicon nitride sources various compositions with different process parameter were generated and tested. The process parameters changed included sintering temperature, sintering aid content, holding time, particle size of the starting powder and α/β ratio in the Si_3N_4 source. As methods of investigation mercury porosimetry, helium pycnometry, water immersion and scanning electron microscopy were used. Furthermore, a test rig to measure permeability based on a European standard (DIN EN ISO 4022) was used. The starting composition contained E10 as Si_3N_4 source, 2.5 % of Al_2O_3 and Y_2O_3 as sintering aids, and was sintered at 1600 °C for 2 h.

Figure 52 - Figure 55 show the porosity, the permeability, the characteristic strength and the median pore diameter of all different compositions with increasing sintering temperature respectively.

A larger particle size of E03 compared to E10 increased the permeability, characteristic strength and the median pore diameter. Even better values could be achieved with the use of XP06 with a β - Si_3N_4 percentage of 11.7 %.

Originating from the starting composition the sintering aids were reduced in steps from 2.5 % to 0.2 % which led to an increase in porosity and median pore diameter. The permeability increased but had a low reproducibility at the lower SA contents of 0.5 % and 0.2 %.

The direct comparison of the powders discussed before showed that E03 with its higher particle size and XP06 with its higher particle size and higher β – Si_3N_4 content yielded better results in permeability while staying at the same level of characteristic strength. Because of that the different sintering temperature was only tested with E03 and XP06 samples.

For both powders, samples with 2.5 % sintering aids content and 2 h holding time in the sintering temperature range from 1500 °C to 1600 °C, were generated. With an increase of sintering temperature, the porosity of samples made from E03 decreases. Regarding the porosity, samples made from XP06 behaved in the same way, only at a higher level throughout the whole range. The characteristic strength increases for both tested Si_3N_4 sources. The permeability for E03 decreases with increasing sintering temperature, whereas for XP06 it stayed on the same level with increasing reproducibility. At 1600 °C, XP06 has a significantly higher permeability value.

For lower temperatures XP06 samples achieve smaller median pore diameters than E03 samples, but when reaching 1600 °C the median pore diameter doubles for XP06 samples, while the median pore diameter of E03 – samples stayed the same. The reason for this different behaviour seems to be the higher β – Si_3N_4 content of XP06-samples which leads to the formation of rod-like grains. This in turn leads to a different microstructure, which seem to favour permeability and characteristic strength. XRD measurements showed that after sintering at 1600 °C for 2 h samples made from XP06 consists nearly only of β – Si_3N_4.

By testing a different sintering time for samples made from XP06 and E03 another difference in behaviour occurs. The holding time was increased from 2h to 5 h while the sintering temperature of 1600 °C and the sintering aid content of 2.5 % remained the same in the beginning. The permeability for samples made from E03 was drastically reduced and the porosity dropped around 25 %.

The reason for this different behaviour lies in the change of the microstructure. The rod-like grains of the XP06 samples grew size and at the same time median pore diameter was increased. Because of that the permeability was able to stay on the same level even though the porosity decreased. Additionally, the characteristic strength increased.

For samples made from E03 it seems that the grains started to transform from α – Si_3N_4 to β – Si_3N_4 which in term leads to a densification and therefore to a reduction in permeability median pore diameter and porosity.

As mentioned above, the experiments with E10 showed that a reduction in sintering aid content leads to a higher permeability, median pore diameter, and porosity, with a decrease in characteristic strength. With these results in mind a reduction to 1 % for XP06 at 1600 °C for 5 h

was tested. As expected this resulted in a higher permeability, median pore diameter and porosity. However, in contrast to E10, the characteristic strength stayed the same. SEM images show that the microstructure for XP06 stays the same.

With the growth of the median pore diameter with increasing temperature observed at XP06 samples at the increase from 1550 °C to 1600 °C, the sintering temperature was further increased. The composition XP06 with 1 % SA content sintered for 5h at 1700 °C yielded an increased permeability, and the median pore diameter increased with a small decrease in porosity. The characteristic strength stayed on the same level. With this increase a light grey discolouration of the inner parts of the samples occurs. The reason for this is not clear.

Further increase of the sintering temperature to 1750 °C leads to beginning decomposition processes. However, it's worth noting that if the decomposed parts of the samples are removed and the remaining part of the sample is tested, the results stayed on the same level as the samples sintered at 1700 °C in terms of porosity and permeability. Also, the discolouration in the inner parts of the sample intensifies to a darker grey. If heated to higher temperature the samples decomposed completely.
Overall XP06 seems to be the best choice for the desired application as membrane support structure. The microstructure it forms above 1600 °C helps to achieve a high characteristic strength with an improved permeability.

It was possible to manufacture tubular porous ceramic support structures with controlled open porosity with reproducible parameters. Also compared to the starting composition with E10 as Si_3N_4 source with a sintering temperature of 1600 °C for 2 h and 2.5 % sintering aid content, an improvement in all characteristics was possible. The composition with XP06 as Si_3N_4 source with sintering temperature of 1700 °C for 5 h and 1.0 % sintering aid content showed the most promising results.

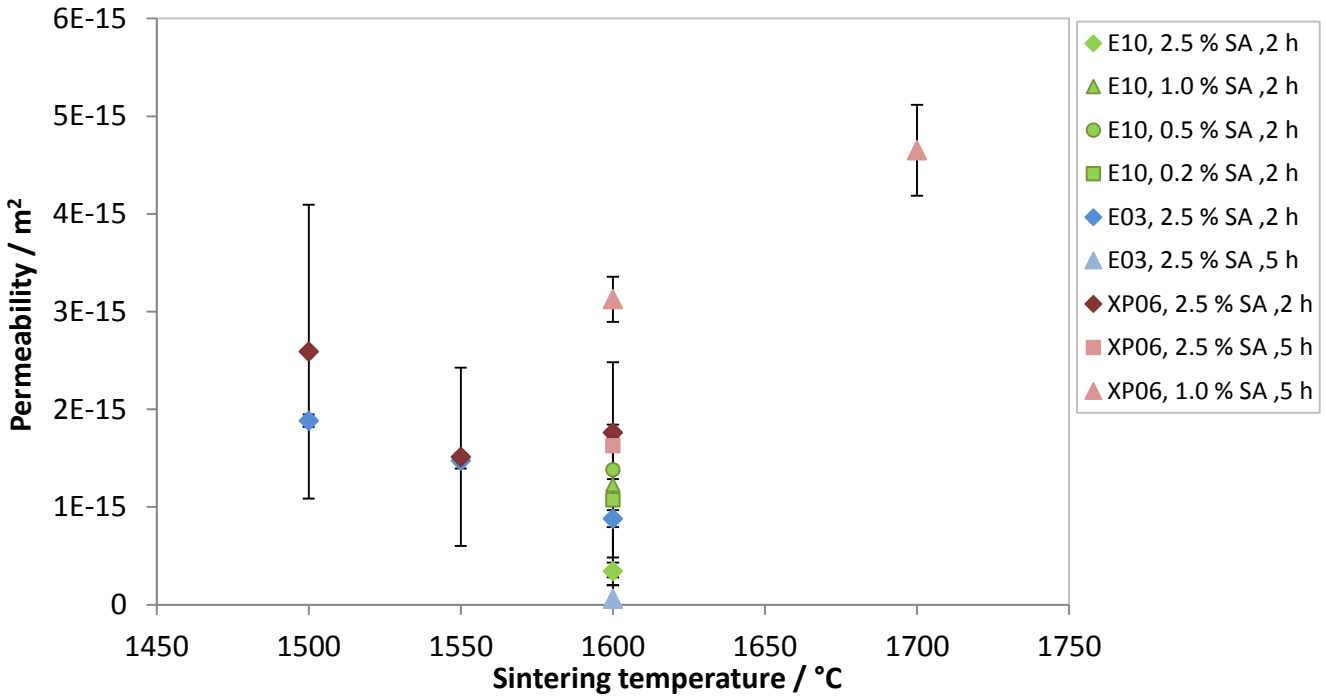

Figure 52: Influence of sintering temperature on the permeability of all sample compositions tested

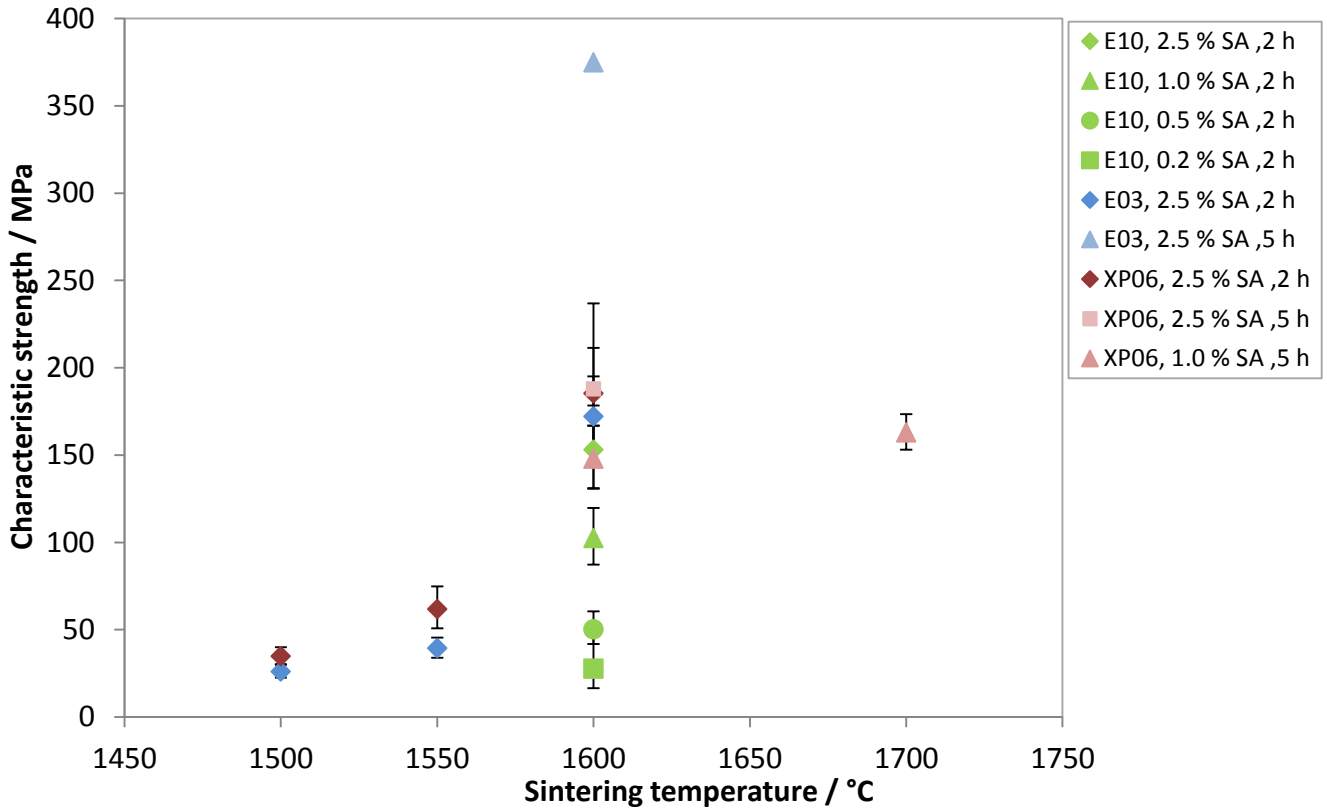

Figure 53: Influence of sintering temperature on the characteristic strength of all sample compositions tested

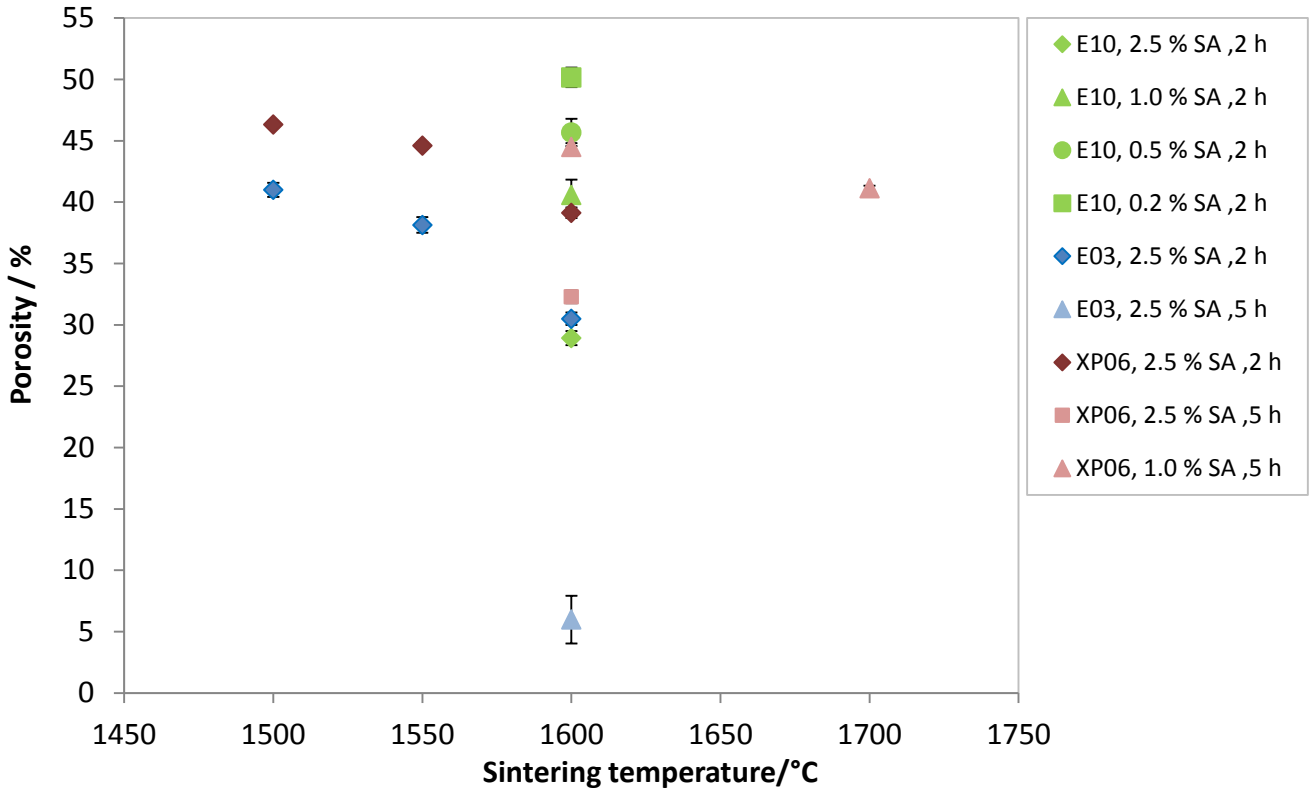

Figure 54: Influence of sintering temperature on the porosity of all sample compositions tested

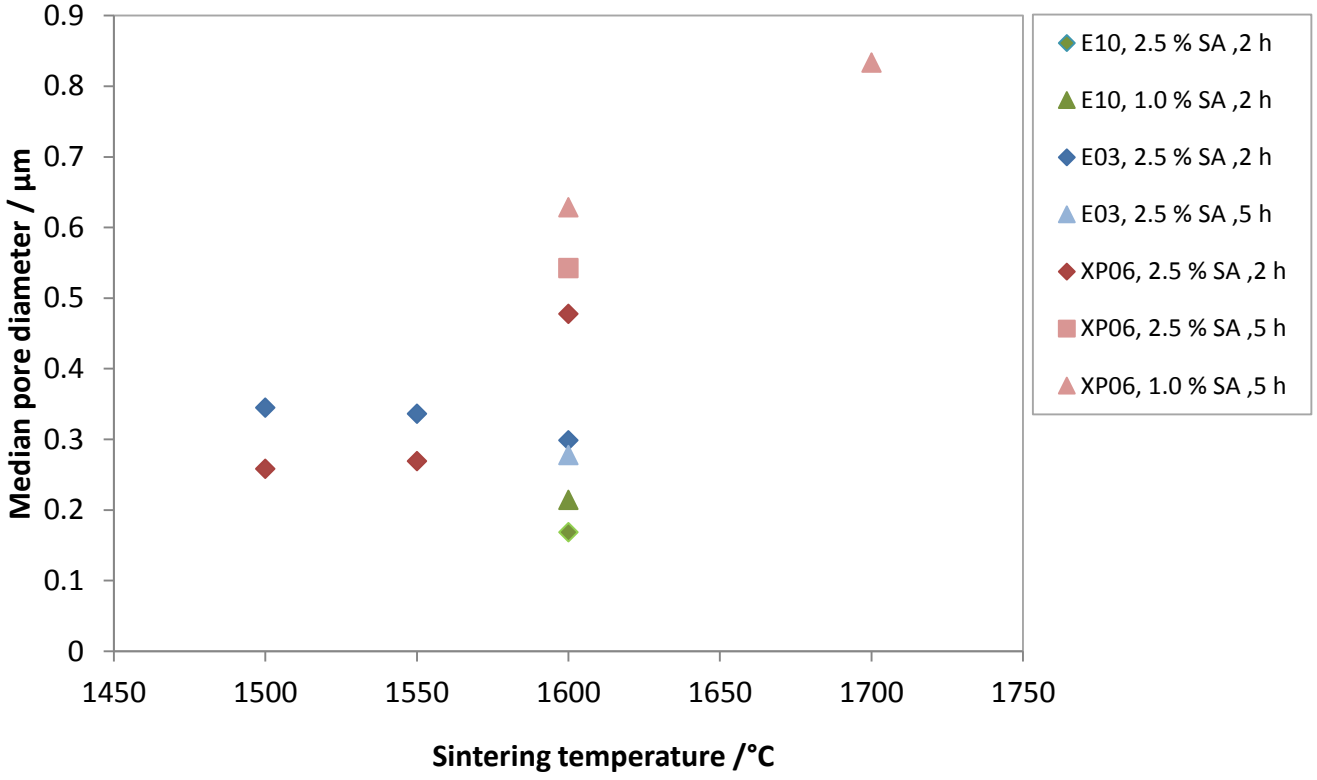

Figure 55: Influence of sintering temperature on the median pore diameter of all sample compositions tested

7. OUTLOOK

If the permeability proves to be high enough, a possible solution could be to reduce the sintering aid content further to 0.5 %. Since XP06 and E10 behave differently, this could lead to an increase in permeability and porosity, despite the problems described in chapter 5.3.6, which occur with a reduction of sintering aids under 1 %.

Another promising way of improving the permeability found in literature is the use of pore form agents as sacrificial fillers, In the work of Kalemata et. al, starch was used as a pore form agent in addition to the partial sintering.[17] They used uniaxial dry pressing as shaping technique and produced planar structures. The adaptation to slip casting with the complex tubular shape would require some work but seems promising.

To achieve a gradient in the pore size, slip-casting with two different slurries in one mould could be an easy solution.

8. REFERENCES

1. Elyassi, B., Sahimi, M. and Tsotsis, T.T., *Silicon carbide membranes for gas separation applications.* Journal of Membrane Science, 2007. **288**(1–2): p. 290-297.
2. Suwanmethanond, V., Goo, E., Liu, P.K.T., Johnston, G., Sahimi, M. and Tsotsis, T.T., *Porous Silicon Carbide Sintered Substrates for High-Temperature Membranes.* Industrial & Engineering Chemistry Research, 2000. **39**(9): p. 3264-3271.
3. Verweij, H., Lin, Y.S. and Dong, J., *Microporous Silica and Zeolite Membranes for Hydrogen Purification.* MRS Bulletin, 2006. **31**(10): p. 756-764.
4. Riley, F., *Structural Ceramics: Fundamentals and Case Studies*. 2009: Cambridge University Press.
5. Jansen, M., *High Performance Non-Oxide Ceramics II*. 2002: Springer. 167.
6. Konegger, T., Tsai, C.-C., Peterlik, H., Creager, S.E. and Bordia, R.K., *Asymmetric polysilazane-derived ceramic structures with multiscalar porosity for membrane applications.* Microporous and Mesoporous Materials, 2016. **232**: p. 196-204.
7. Brouczek, D. and Konegger, T., *Open-Porous Silicon Nitride-Based Ceramics in Tubular Geometry Obtained by Slip-Casting and Gelcasting.* Advanced Engineering Materials: p. DOI: 10.1002/adem.201700434.
8. Itaya, K., Sugawara, S., Arai, K. and Saito, S., *PROPERTIES OF POROUS ANODIC ALUMINUM OXIDE FILMS AS MEMBRANES.* Journal of Chemical Engineering of Japan, 1984. **17**(5): p. 514-520.
9. Deng, W., Yu, X., Sahimi, M. and Tsotsis, T.T., *Highly permeable porous silicon carbide support tubes for the preparation of nanoporous inorganic membranes.* Journal of Membrane Science, 2014. **451**: p. 192-204.
10. Mori, H., Mase, S., Yoshimura, N., Hotta, T., Ayama, K. and Tsubaki, J.I., *Fabrication of supported Si_3N_4 membranes using the pyrolysis of liquid polysilazane precursor.* Journal of Membrane Science, 1998. **147**(1): p. 23-33.
11. Dabir, S., Deng, W., Sahimi, M. and Tsotsis, T., *Fabrication of silicon carbide membranes on highly permeable supports.* Journal of Membrane Science, 2017. **537**: p. 239-247.
12. Colombo, P., Mera, G., Riedel, R. and Sorarù, G.D., *Polymer-Derived Ceramics: 40 Years of Research and Innovation in Advanced Ceramics.* Journal of the American Ceramic Society, 2010. **93**(7): p. 1805-1837.
13. Maarten Biesheuvel, P. and Verweij, H., *Design of ceramic membrane supports: permeability, tensile strength and stress.* Journal of Membrane Science, 1999. **156**(1): p. 141-152.
14. Gregorová, E. and Pabst, W., *Porosity and pore size control in starch consolidation casting of oxide ceramics—Achievements and problems.* Journal of the European Ceramic Society, 2007. **27**(2–3): p. 669-672.
15. Quinlan, M., Plucknett, K.P., Garrido, L. and Genova, L. *Compositional design of porous β-Si3N4 prepared by pressureless-sintering compositions in the Si-Y-Mg-(Ca)-O-N system*. in *Ceramic Engineering and Science Proceedings*. 2008.
16. Yang, J.-F., Zhang, G.-J., Kondo, N., Ohji, T. and Kanzaki, S., *Synthesis of Porous Si3N4 Ceramics with Rod-Shaped Pore Structure.* Journal of the American Ceramic Society, 2005. **88**(4): p. 1030-1032.

17. Kalemtas, A., Topates, G., Özcoban, H., Mandal, H., Kara, F. and Janssen, R., *Mechanical characterization of highly porous β-Si3N4 ceramics fabricated via partial sintering & starch addition.* Journal of the European Ceramic Society, 2013. **33**(9): p. 1507-1515.
18. Suttor, D. and Fischman, G.S., *Densification and Sintering Kinetics in Sintered Silicon Nitride.* Journal of the American Ceramic Society, 1992. **75**(5): p. 1063-1067.
19. Salmang, H. and Scholze, H., *Keramik*. 7 ed. 2007, Berlin Heidelberg: Springer-Verlag.
20. Lange, F.F., *Fracture Toughness of Si3N4 as a Function of the Initial α-Phase Content.* Journal of the American Ceramic Society, 1979. **62**(7-8): p. 428-430.
21. Topates, G., Mammitzsch, L., Petasch, U., Adler, J., Kara, F. and Mandal, H., *Microstructure–permeability relation of porous β-Si3N4 ceramics.* Journal of the European Ceramic Society, 2013. **33**(9): p. 1545-1551.
22. Salmang, H., Scholze, H. and Telle, R., *Keramik.* Keramik, 2007, Springer
23. Keramik, I.T. and Industrie, V.d.K., *Brevier Technische Keramik*. 2003: Fahner, Hans.
24. Hostaša, J., Silvestroni, L., Piancastelli, A., Sciti, D., Martino, D.D. and Esposito, L., *Slip Casting of a Si3N4-Based System.* International Journal of Applied Ceramic Technology, 2012. **9**(2): p. 246-258.
25. Available from. http://www.zschimmer-schwarz.com/DOLAPIX_A_88/simon/zschimmer-schwarz/media/site/downloads/merkblatt/1_K_K_EN_6581_20_1_100.pdf.
26. Innocentini, M.D.M. and Pandolfelli, V.C., *Permeability of Porous Ceramics Considering the Klinkenberg and Inertial Effects.* Journal of the American Ceramic Society, 2001. **84**(5): p. 941-944.
27. Hans Dieter Baehr, K.S., *Wärme- und Stoffübertragung*. 8 ed. 2013: Springer Vieweg.
28. Available from. http://www.peacesoftware.de/einigewerte/luft.html.
29. T. Konegger, T. Prochaska, R. Obmann: "Tubular open-porous polymer-derived ceramic structures with tailored permeability"; Poster: 9th International Conference on High Temperature Ceramic Matrix Composites (HTCMC-9) & Global Forum on Advanced Materials and Technologies for Sustainable Development (GFMAT 2016), Toronto, Canada; 06-26-2016 - 07-01-2016.
30. *DIN_EN_623-2 Hochleistungskeramik; Monolithische Keramik; Allgemeine und strukturelle Eigenschaften; Teil 2: Bestimmung von Dichte und Porosität; Deutsche Fassung:1993*. 1993, Beuth: Berlin.
31. Normung, D.D.I.f., *DIN EN 843-7, Hochleistungskeramik – Mechanische Eigenschaften monolithischer Keramik bei Raumtemperatur – Teil 7: C-Ring-Prüfungen;* 2010.
32. DIN, *DIN EN 843-5, Hochleistungskeramik – Mechanische Eigenschaften monolithischer Keramik bei Raumtemperatur – Teil 5: Statistische Auswertung*. 2007

APPENDIX:

A1 Temperature control at the hot press

The given temperatures in this work are the nominal adjusted temperatures on the hot press. As the temperature measurement was pyrometer controlled above 650 °C, it suffered from the usually occurring uncertainties known for such measurements.
The placement of the crucible in the hot-press and the adjustment of the point of measurement of the pyrometer, proves to be very important as a minor change leads to different results.
The heating performance and the process temperature control rings (PTCR-HTH 1450 – 1750 °C, Ferro) in the crucible served as a guideline if the adjusted temperature was reached or exceeded.
The PTCR have a known shrinkage over a given temperature range. The diameter was measured with calipers (micrometer-D, Schupp). With the diameter the corresponding temperature can be found in the PTCR table. If the holding time is higher than an hour, a correction of the obtained temperature is necessary. According to Schupp at a holding time of 2 h the temperature shown in the table must be reduced by 13 °C and for 5 h holding time it must be reduced by 45°C. All temperatures used in this discussion were already corrected.
It is important to note that the values obtained via PTCR are not meant for exact temperature measurement, they serve more as a guideline to see whether the temperature in subsequent runs stays the same.

In Figure 58 the nominal temperature compared to the heating power is shown. The temperature sometimes yielded in a different power level. Figure 56 shows the temperature and heating power during the course of one run at a sintering temperature of 1700 °C. Listed values for the heating power are taken from the constant area marked with 1 in Figure 56.

For example, at an adjusted temperature of 1600 °C the heating power ranged from 7 kW to 8 kW. According to PTCR results 7 kW represents a temperature of 1512 °C and 8.16 kW

represents a temperature of 1657 °C. That indicates that a heating power difference of 1 kW is equal to a temperature difference of 150 °C.

At an adjusted temperature of 1750 °C, the heating performance ranged between 8.15 kW and 11.4 kW. The unexpected high temperatures at 11.4 kW led to a complete decomposition of the samples to a point, where only a ball of silicon was left (see Figure 58, left picture D). On the other hand, 8.15 kW, also a value achieved with a nominal temperature of 1750 °C is on the power level of samples with a nominal temperature of 1600 °C.

Looking at the decomposed samples it seems that the top decomposed stronger than the bottom. This indicates that a temperature gradient is present in the crucible. To control that, two runs with two PTCR-Rings were run. As sintering temperature 1000 °C (PTCR-LTH, Ferro) and 1600 °C (PTCR-HTH, Ferro) with 2 h holding time were chosen. No powderbed was used. The chosen setting is shown in Figure 57. The difference between position A and B according to the PTCR was around 40 °C at a chosen high difference of ~4.5 cm.

Another problem was that the maximum temperature of the PTCR-HTH of 1750 °C was exceeded every time 1700 °C was adjusted.

As a counter measure various positions for the point of measurement were tested, but the unpredictability of the heating remained for higher temperatures.

The problem seems especially prominent at high temperatures and if the nominal temperature reaches the intended temperature. This might be because of the according adjustment of the pyrometer measuring point. Then it was close to the edge, which might be one of the reasons for the variation.

A possible solution would be holding the measurement at 900 °C and adjust the pyrometer by moving the measuring point to match the temperature. Admittedly, if the pyrometer measuring point proves to be the problem, this wouldn’t help.

Another possible solution could be a heating power controlled run.

In any case it is very recommend to control the heating power after every run. The exact values for the heating power according to the different sintering runs, can be found in Table 17.

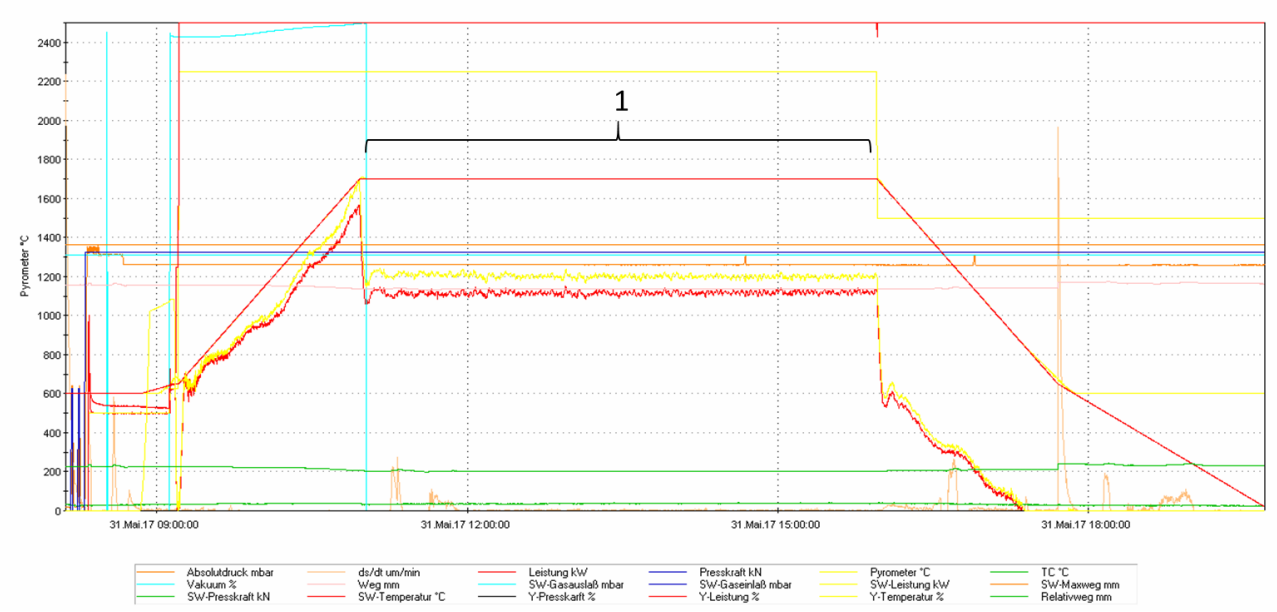

Figure 56: Temperature and heating power of the course of one run at 1700 °C, 1: area of constant heating power

Table 17: Values for the temperature of the PTCR rings for the control of the high difference

PTCR Typ	Lot. Nr.	$T_{nominell}$ °C	position	T_{Korr} °C
LTH	145	1100	B	1045
LTH	145	1100	A	1085
HTH	435	1600	B	1614
HTH	435	1600	A	1669

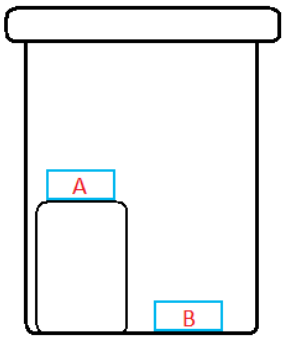

Figure 57: Placement of the PTCR rings for the control of the high difference (~4.5 cm)

Table 17: Heating power and adjusted temperature for all runs

run	Date	heating power kW	$T_{nominal}$ °C
1	16/11/2016	7.2	1600
2	24/11/2016	7.1	1600
3	16/12/2016	7.9	1600
4	19/12/2016	8.03	1600
5	21/12/2016	6.46	1550
6	22/12/2016	6.23	1500
7	12/01/2017	7.15	1600
8	17/01/2017	6.57	1550
9	19/01/2017	6.24	1500
10	20/02/2017	8.05	1600
11	21/03/2017	8.18	1600
12	04/04/2017	9.1	1700
13	26/04/2017	9.93	1800
14	08/05/2017	8.15	1750
15	08/06/2017	11.6	1750
16	29/06/2017	9.55	1750

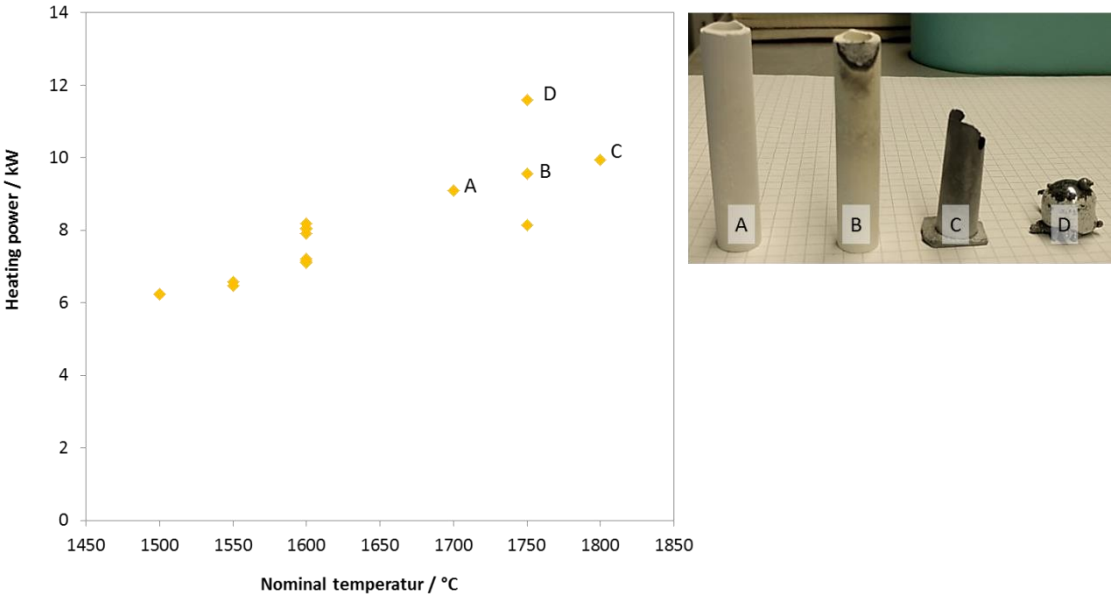

Figure 58: Heating power and the nominal temperature on the hot press

A2 Data overview

	T °C	run	SA m%	ρ_s kg/m^3	$\rho_{s\emptyset}$ kg/m^3	Π_a %	$\Pi_{a\emptyset}$ %	k_1 m^2	$k_{1\emptyset}$ m^2	k_2 m^2	$k_{2\emptyset}$ m^2
E10 2 h											
5C5	1600	1	0.2	3.161	3.205 ± 0.049	49.13	50.17 ± 0.81	1.43E-15	1.07E-15 ± 6.42E-16	7.50E-13	2.02E-12 ± .33E-12
5D5	1600	4	0.2	3.274		51.10		1.71E-16		2.44E-14	
5E5	1600	4	0.2	3.180		50.28		1.62E-15		5.29E-12	
4A4	1600	3	0.5	3.206	3.199 ± 0.006	44.80	45.68 ± 1.11	2.86E-15	1.38E-15 ± 1.10E-15	1.07E-11	4.01E-12 ± 4.79E-12
4D4	1600	1	0.5	3.201		47.24		1.06E-15		1.17E-12	
4E4	1600	3	0.5	3.191		45.00		2.22E-16		1.02E-13	
3A3	1600	1	1	3.163	3.192 ± 0.020	42.33	40.58 ± 1.25	1.11E-15	1.23E-15 ± 8.71E-17	1.68E-12	2.40E-12 ± 5.34E-13
3B3	1600	3	1	3.205		39.53		1.32E-15		2.56E-12	
3E3	1600	3	1	3.207		39.87		1.25E-15		2.96E-12	
8A8	1600	2	2.5	3.205	3.207 ± 0.010	28.85	28.92 ± 0.58	2.29E-16	3.43E-16 ± 1.40E-16	8.09E-14	1.23E-13 ± 3.14E-14
8B8	1600	7	2.5	3.197		28.77		2.89E-16		1.16E-13	
8C8	1600	7	2.5	3.197		29.30		3.08E-16		1.26E-13	
2B2	1600	1	2.5	3.211		29.69		6.18E-16		1.78E-13	
2C2	1600	3	2.5	3.224		27.97		2.70E-16		1.13E-13	
2D2	1600	3	2.5	3.214		27.71		7.44E-15		4.04E-13	

	T °C	run	SA m%	ρ_s kg/m^3	$\rho_{s\emptyset}$ kg/m^3	Π_a %	$\Pi_{a\emptyset}$ %	k_1 m^2	$k_{1\emptyset}$ m^2	k_2 m^2	$k_{2\emptyset}$ m^2
E03 2h											
10E11	1500	9	2.5	3.214	3.211 ± 0.004	40.14	41.00 ± 0.59	1.82E-15	1.88E-15 ± 6.41E-17	7.47E-12	5.61E-12 ± 1.08E-12
10D12	1500	9	2.5	3.204		41.37		1.84E-15		4.86E-12	
10E12	1500	9	2.5	3.212		40.81		1.89E-15		4.93E-12	
7E7	1500	9	2.5	3.215		41.68		1.99E-15		5.18E-12	
10A12	1550	8	2.5	3.212	3.212 ± 0.000	38.26	38.14 ± 0.63	1.50E-15	1.47E-15 ± 7.78E-17	5.22E-12	3.66E-12 ± 1.01E-12
10B12	1550	8	2.5	3.212		38.99		1.58E-15		3.63E-12	
10C12	1550	8	2.5	3.212		38.08		1.44E-15		3.37E-12	
7D7	1550	8	2.5	3.213		37.22		1.37E-15		2.43E-12	
7A7	1600	2	2.5	3.190		26.05		4.93E-16		4.00E-13	
10B11	1600	7	2.5	3.207	3.208 ± 0.001	30.59	30.50 ± 0.50	9.99E-16	8.82E-16 ± 8.76E-17	9.86E-13	8.56E-13 ± 8.58E-14
10C11	1600	7	2.5	3.209		31.11		9.31E-16		8.80E-13	
10D11	1600	7	2.5	3.209		30.56		7.81E-16		7.78E-13	
7B7	1600	7	2.5	3.205		29.72		8.16E-16		7.79E-13	
E03 5 h											
7C7	1600	10	2.5	2.960	2.903 ± 0.040	8.72	5.98 ± 1.95	3.44E-17	5.99E-17 ± 3.94E-17	5.63E-15	1.17E-14 ± 9.59E-15
10A11	1600	10	2.5	2.874		4.32		2.99E-17		4.15E-15	
10E10	1600	10	2.5	2.875		4.90		1.16E-16		2.52E-14	

	T °C	run	SA m%	ρ_s kg/m^3	$\rho_{s\emptyset}$ kg/m^3	Π_a %	$\Pi_{a\emptyset}$ %	k_1 m^2	$k_{1\emptyset}$ m^2	k_2 m^2	$k_{2\emptyset}$ m^2
XP06 2h											
9C10	1500	6	2.5	3.208	3.206 ± 0.003	46.31	46.32 ± 0.20	1.73E-15	2.59E-15 ± 1.50E-15	2.83E-12	3.34E-12 ± 5.03E-13
9D10	1500	6	2.5	3.206		46.11		5.18E-15		4.14E-12	
9E10	1500	6	2.5	3.209		46.23		1.51E-15		3.01E-12	
6C6	1500	6	2.5	3.200		46.65		1.94E-15		3.39E-12	
9D9	1550	5	2.5	3.209	3.207 ± 0.001	44.45	44.61 ± 0.27	1.78E-15	1.51E-15 ± 9.12E-16	3.77E-12	2.60E-12 ± 1.49E-12
9E9	1550	5	2.5	3.206		44.28		1.42E-15		3.50E-12	
9A10	1550	5	2.5	3.208		44.99		1.56E-16		4.54E-14	
6D6	1550	5	2.5	3.208		44.72		2.70E-15		3.08E-12	
6B6	1600	2	2.5	3.214		41.48		1.76E-15		5.04E-12	
9A9	1600	4	2.5	3.215	3.220 ± 0.005	38.87	39.13 ± 0.43	1.86E-15	1.76E-15 ± 8.15E-17	2.47E-11	2.05E-11 ± 2.95E-12
9B9	1600	4	2.5	3.222		38.94		1.66E-15		2.11E-11	
9C9	1600	4	2.5	3.216		38.84		1.70E-15		1.65E-11	
6A6	1600	4	2.5	3.227		39.88		1.83E-15		1.97E-11	

	T °C	run	SA m%	ρ_s kg/m^3	$\rho_{s\emptyset}$ kg/m^3	Π_a %	$\Pi_{a\emptyset}$ %	k_1 m^2	$k_{1\emptyset}$ m^2	k_2 m^2	$k_{2\emptyset}$ m^2
XP06 5h											
9A11	1600	10	2.5	3.067	3.072 ± 0.009	31.60	32.28 ± 0.53	1.70E-15	1.63E-15 ± 5.56E-17	1.83E-11	1.25E-11 ± 4.46E-12
9B11	1600	10	2.5	3.064		32.36		1.62E-15		1.17E-11	
9C11	1600	10	2.5	3.084		32.89		1.57E-15		7.53E-12	
11A14	1600	11	1	3.203	3.200 ± 0.003	44.10	44.49 ± 0.31	3.45E-15	3.13E-15 ± 2.31E-16	2.42E-11	7.85E-11 ± 3.92E-11
11B14	1600	11	1	3.197		44.75		3.05E-15		5.87E-11	
11C14	1600	11	1	3.202		44.83		2.82E-15		1.10E-10	
11D14	1600	11	1	3.197		44.29		3.18E-15		1.21E-10	
11A15	1700	12	1	3.125	3.141 ± 0.032	41.11	41.13 ± 0.20	4.66E-15	4.65E-15 ± 4.66E-16	1.63E-10	5.43E-11 ± 3.60E-10
11B15	1700	12	1	3.096		41.26		5.38E-15		2.07E-10	
11C15	1700	12	1	3.176		41.33		4.49E-15		-5.49E-10	
11E13	1700	12	1	3.165		40.81		4.09E-15		3.97E-10	
15G2	1750	15		3.163	3.176 ± 0.008	39.65	40.47 ± 0.73	4.89E-15		5.27E-11	
15H2	1750	15		3.186		40.63					
15I2	1750	15		3.178		40.03					
15J2	1750	15		3.179		41.57					

Overview of mercury measurement

	Si_3N_4 source	T °C	Holding time t [h]	SA content m%	d_{median} µm	d_{modal} µm	Πa^1 %	Πa^2 %	$\rho_{apparent}$ kg/m³
8A8	E10	1600	2	2.5	0.17	0.17	26.1	25.4	3.143
3A3	E10	1600	2	1.0	0.21	0.22	43.6	41.9	3.143
10E11	E03	1500	2	2.5	0.35	0.35	39.3	39.5	3.199
10A12	E03	1550	2	2.5	0.34	0.34	36.8	36.6	3.191
10C11	E03	1600	2	2.5	0.30	0.30	31.3	30.2	3.197
7A7	E03	1600	2	2.5	0.29	0.29	24.9	25.9	3.232
10A11	E03	1600	5	2.5	0.28	0.22	11.6	2.71	2.899
9D10	XP06	1500	2	2.5	0.26	0.27	46.0	45.5	3.179
9A10	XP06	1550	2	2.5	0.27	0.28	45.2	43.4	3.147
6B6	XP06	1600	2	2.5	0.36	0.37	40.9	40.2	3.207
9A9	XP06	1600	2	2.5	0.48	0.47	38.3	36.9	3.172
9A11	XP06	1600	5	2.5	0.54	0.53	34.0	33.3	3.180
11C14	XP06	1600	5	1.0	0.63	0.63	45.0	43.9	3.146
11A15	XP06	1700	5	1.0	0.83	0.81	42.1	40.7	3.137
15G2	XP06	1750	5	1.0	2.00	1.82	44.2	40.5	3.010

[1] Porosity calculated by mercury porosity using skeleton density according to He pycnometrie / %
E10: 3.171 ± 0.021 g/cm³, E03: 3.187 ± 0.009 g/cm³, XP06: 3.246 ± 0.043 g/cm³
[2] Porosity calculated directly from mercury intrusion data / %